THE ROLE OF TEMPORAL CHANGES OF THE ZONAL WIND ON THE EXCITATION OF LARGE SCALE TRANSIENTS

by

ARLINDO MORAES DA SILVA, JR.

M. S., Physics,
Pontificia Universidade Catolica do Rio de Janeiro,
Brazil
(1984)

Submitted to the Department of
Earth, Atmospheric, and Planetary Sciences
in partial fulfillment of the requirements
for the degree of

Doctor of Philosophy in Meteorology

at the

Massachusetts Institute of Technology

March, 1989

Signature of Author _____
Center for Meteorology and Physical Oceanography
March, 1989

Certified by _____
Richard S. Lindzen
Professor of Meteorology
Thesis Supervisor

Accepted by _____
Thomas Jordan
Chairman, Departmental Committee on Graduate Students

THE ROLE OF TEMPORAL CHANGES OF THE ZONAL WIND ON THE EXCITATION OF LARGE SCALE TRANSIENTS

by

ARLINDO MORAES DA SILVA, JR.

Submitted to the Department of Earth, Atmospheric,
and Planetary Sciences on March, 1989
in partial fulfillment of the requirements for the degree of
Doctor of Philosophy in Meteorology.

ABSTRACT

The main objective of this thesis is to investigate how temporal changes in the zonal mean flow affect stationary waves in the northern hemisphere winter. More specifically, we assess the dependence of stationary waves on the zonally averaged zonal flow, the time scale associated with the transition of stationary waves from one steady configuration to another, and determine the nature of the transients excited in the process.

To accomplish this goal we used a barotropic and a baroclinic model. In the barotropic calculation we stressed wind changes that cause stationary wave changes of large meridional scales with some structure in the tropics, changes which are favorable for the excitation of ultralong Rossby waves. In the baroclinic calculation we restricted ourselves to wind changes in the subtropics which have been shown by Nigam and Lindzen (1989) to be very important for stationary waves in mid- and high-latitudes. For such changes, no excitation of Rossby waves was found.

Despite the limitations of the barotropic model, some aspects of the observed ultralong Rossby waves were present in the calculation. In particular, the dominance of the 16-day waves was suggested.

Confirming the results of Nigam and Lindzen (1989), we found that small changes in the subtropical jet can cause significant changes in the stationary wave response. We found a very fast establishment of the new steady

solution (4-5 days), both in the troposphere and in the stratosphere. The exception is for a northward shift of the subtropical jet, in which case the establishment of the new stationary solution in the stratosphere occurs on a longer time scale, which is mainly determined by dissipation.

Thesis Supervisor: Richard S. Lindzen
Title: Professor of Meteorology

Acknowledgements

The author most gratefully thanks his advisor, Prof. Richard Lindzen, for his guidance, help and lively discussions throughout the past four and a half years. Critical discussions with Profs. Randy Dole, Brian Farrell and Glenn Flierl, as well as fellow student Rob Black, were also most helpful.

Special thanks goes to my good friend and colleague Dan Marchesin down in Brazil for encouraging me in my scientific education and introducing me to the field of meteorology. Additional thanks to Steve Cohn and Dick Dee from Courant Institute for their help and advice, especially with the numerical work of this thesis.

Diana Spiegel deserves a special thank you for her patience and willingness to answer my numerous questions concerning the use of the computational facilities here at MIT. Thanks also to Herb Houston at NASA/Goddard for his promptness in solving all problems concerning the MIT/Goddard connection. I also acknowledge Dave Krowitz for

his help with the port of my code to the Alliant.

And last but not least, I thank Ellen, my wife, for proofreading the manuscript and for two and a half years of dedication and patience.

Contents

List of Figures

List of Tables

Chapter 1

Introduction

In the last few years many studies (Lin, 1982; Jacqmin and Lindzen, 1985; Nigam et al., 1986,1988; Chen and Trenberth, 1988a,b; Nigam and Lindzen, 1988, among others) have been devoted to the modelling of stationary waves in the northern hemisphere winter, each one with a different degree of success. By and large, these models reproduce the horizontal and vertical structure of the waves, at least the major features. A considerable degree of effort has been dedicated to identify the relative importance of the different forcing mechanisms involved: heating, topography and transient eddies. In addition, the sensitivity of the solution to variations in the basic state has also been examined (Nigam and Lindzen, 1989). All of these studies have been concentrated on the steady solution of a linearized and forced atmosphere, or on a long term climatology of General Circulation Models (GCMs). In this

work we examine how stationary waves make a transition from one steady configuration to another during a finite interval of time.

The main objective of this thesis is to investigate how temporal changes in the zonal mean flow affect stationary waves in the northern hemisphere winter. More specifically, we assess the dependence of stationary waves on the zonally averaged zonal flow, the time scale associated with the transition of stationary waves from one steady configuration to another, and the nature of the transients excited in the process.

Recently, Nigam and Lindzen (1989) have shown that small changes in the subtropical jet can cause significant changes in the stationary wave pattern, both in the troposphere and the stratosphere. These anomalous stationary waves are expected to play a significant part in the low frequency variability of the northern hemisphere. For example, a shift of the subtropical jet of only about 6 degrees equatorward gives an increase in stationary waves in the troposphere of about 120 meters. In chapter 6 we explore the potential of anomalous stationary waves to explain the persistent anomaly cases of Dole (1982).

Transients are generally associated with the establishment of a new stationary solution. When changes in forcing or basic state occur in a time scale short enough (compared to wave frequency and dissipation), a new stationary wave is not immediately established. The difference

between the asymptotic stationary wave and the solution in a finite time is often referred to as transients. The nature of the transients depends on the scale of the difference in stationary waves. For large scale changes in the stationary solution (long zonal and meridional scales), westward propagating ultralong Rossby waves are expected to be excited. For changes in stationary solution of shorter scales, excitation of quasi-stationary transients is more likely. We will see that transient ultralong Rossby waves are more easily excited when wind changes are mostly in the tropics. Wind changes associated with a shift of the subtropical jet are very important for the stationary waves in mid- and high-latitudes in the northern hemisphere, but the transients in this case are quasi-stationary.

The approach adopted in this thesis is simple and is designed with two goals in mind. First, we should be able to study the establishment of a new stationary solution. Second, transients, meaning that part of the solution which is not associated with forcing, are to be unambiguously defined. We therefore consider the following initial value problem: 1) Start with the stationary solution associated with a particular basic state; 2) in a specified time interval change the basic state to a different configuration; and 3) after this transition period analyze the transients excited in the process. The establishment of the new stationary solution can be analyzed by looking at the difference between the solution at the time t minus the initial condition. A more detailed description of this approach will be given in chapter 3.

Outline of the thesis

This thesis is organized as follows:

Chapter 2 gives a background on stationary waves, Rossby waves and persistent anomalies. This is not a comprehensive review, but rather a collection of remarks relevant to this research.

Chapter 3 presents a simple theory for the adjustment of the stationary waves and describes the approach of this thesis. We start by introducing the formalism of linear waves with a time dependent basic state, using the barotropic vorticity equation. We then extend the results to a general linear atmosphere. After that, we introduce a measure for the transients generated from the adjustment of the stationary solution, and derive a simple formula for the ultralong Rossby waves and quasi-stationary transients.

Chapter 4 describes the details of the barotropic and baroclinic models used in this thesis. We document the model equations, basic state, forcing dissipation and numerical procedure. We also introduce the model diagnostics to be used in the subsequent chapters: quasi-geostrophic index of refraction and Plumb's wave flux.

Chapter 5 is concerned with changes in stationary solution and the excitation of transients in a barotropic model. It shows the sensitivity of the stationary waves, how stationary waves get reestab-

lished following a change in wind, and the parametric dependence of the transients. In this chapter, we concentrate on a particular kind of transients: the ultralong Rossby waves. It is shown that transient Rossby waves are excited when wind changes are in the tropics.

Chapter 6 extends the calculation of Chapter 5 to a baroclinic atmosphere. It is shown that transient Rossby waves are not excited in this model, at least when the wind changes are shifts of the subtropical jet. This chapter emphasizes the three-dimensional structure of the transients, as well as the reestablishment of stationary waves. A comparison with persistent anomalies is also made.

Chapter 7 summarizes the main results of the previous chapters and present the concluding remarks. It also discusses the limitations of our calculation and the remaining problems.

Chapter 2

Background

This chapter presents some theoretical and observational background on stationary waves, Rossby waves and blocking and persistent anomalies. It is not intended to be a comprehensive review of the subject, but rather to point out to the unfamiliar reader aspects relevant to our research.

2.1 Stationary waves

As discussed out in the introduction, stationary waves and their variability are central for the concepts to be developed in this thesis. In this section we will look at some of the main properties of the observed stationary waves in the Northern Hemisphere winter, as well as some modelling and theoretical studies. We will not attempt to review the

subject here, but rather present the main points that will be relevant to rest of this work. A review of observed stationary waves can be found in Derome (1979) and Wallace (1983). Theory and modelling have been reviewed by Held (1982). Some recent papers on the subject are Jacqmin and Lindzen (1985), Nigam et al. (1986,1988), Chen and Trenberth (1988), Nigam and Lindzen (1989) and Randel (1989).

From the observational point of view, stationary waves are defined as the monthly or seasonal mean atmospheric circulation with the zonal mean removed. Even though the trend in the literature is to concentrate on the geopotential height field, a comprehensive description of stationary waves should include winds, and temperature fields. The main points about the observed stationary waves that we want to stress are:

- Stationary waves are large scale features. On the northern hemisphere the most important contributions come from zonal wavenumbers one, two, and three. In fig. 2.1 we show the northern hemisphere climatological mean January distribution of stationary wave geopotential height at 200mb based on the atlas of Crutcher and Meserve (1970). Notice the lows downstream of the Tibetan plateau and the Rocky mountains, suggestive of wave trains excited by these mountain ranges. Plumb (1985) developed a tri-dimensional wave flux in order to ascertain the geographical origin of climatological stationary waves. His flux at 500mb and

150mb is shown in fig. 2.2. Even though there are questions about the validity of this approach, the results from his calculation do confirm the notion that the waves in the northern hemisphere are forced within the northern hemisphere. In particular it suggests that the tropics may act as a sink for waves excited in mid- and high-latitudes.

- The vertical structure of stationary waves have an almost equivalent barotropic structure. We show in fig. 2.3 the longitude-height cross-section of stationary wave geopotential height for the winter season. As can be seen from this illustration there are also distinct westward tilts in the troposphere, and at 45N the geopotential height tends to peak around 300mb. These westward tilts are generally associated with upward propagating disturbances[1] and correspond to a northward heat flux. The vertical structure of the stationary waves can be further analyzed with diagrams of amplitude and phase as depicted in fig. 2.4- 2.6, from van Loon et al. (1972). Notice that features with short meridional scale are restricted to levels below 15 km, tilts are more prominent in the troposphere, and only zonal wavenumbers 1 and 2 reach the stratosphere.

- In order to illustrate the interannual variability of stationary

[1]Wallace (1983) discusses the pitfalls of these interpretation when both topographic and thermal forcing are present. In essence, a wave with *westward* tilt when added to another wave with *no* vertical tilt can result in a wave with *eastward* tilt, simply because phases are not additive.

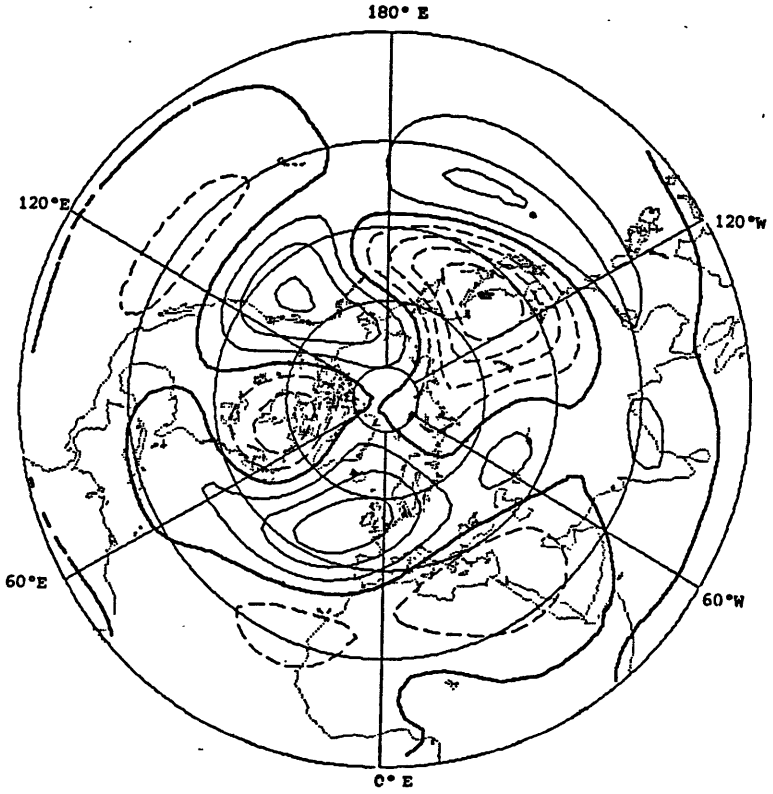

Figure 2.1: Nothern hemisphere climatological mean January distribution of stationary wave geopotential height at 200mb. Contour interval is 60 meters, zero contour is thickened and negative contour dashed (from Crutcher and Meserve, 1970).

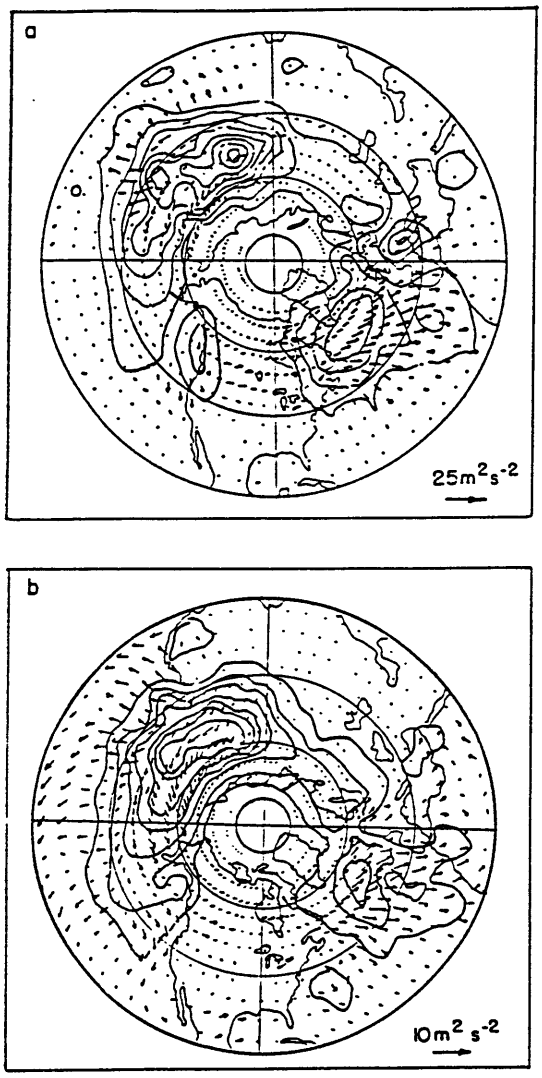

Figure 2.2: Observed stationary-wave flux at a) 500 and at b) 150 mb (After Plumb, 1985).

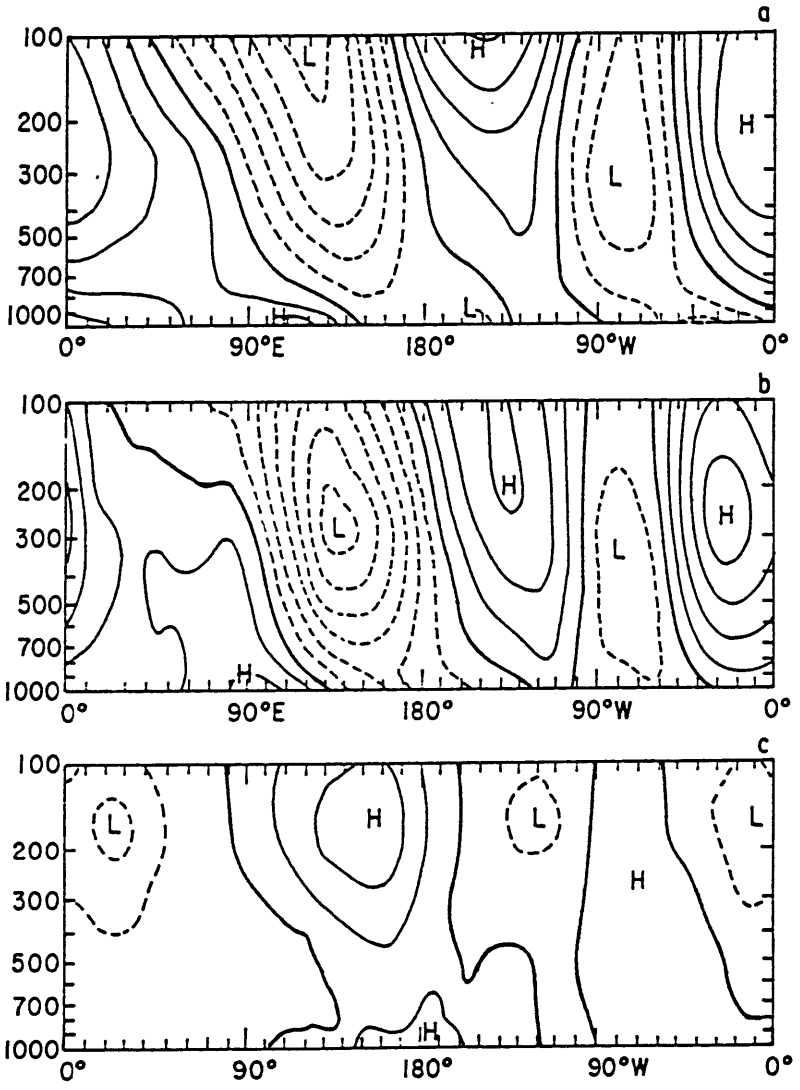

Figure 2.3: Longitude height cross section of stationary wave geopotential height for the winter season: a) 60N, b) 45N, and c) 25N (from Wallace, 1983, adapted from Lau, 1979).

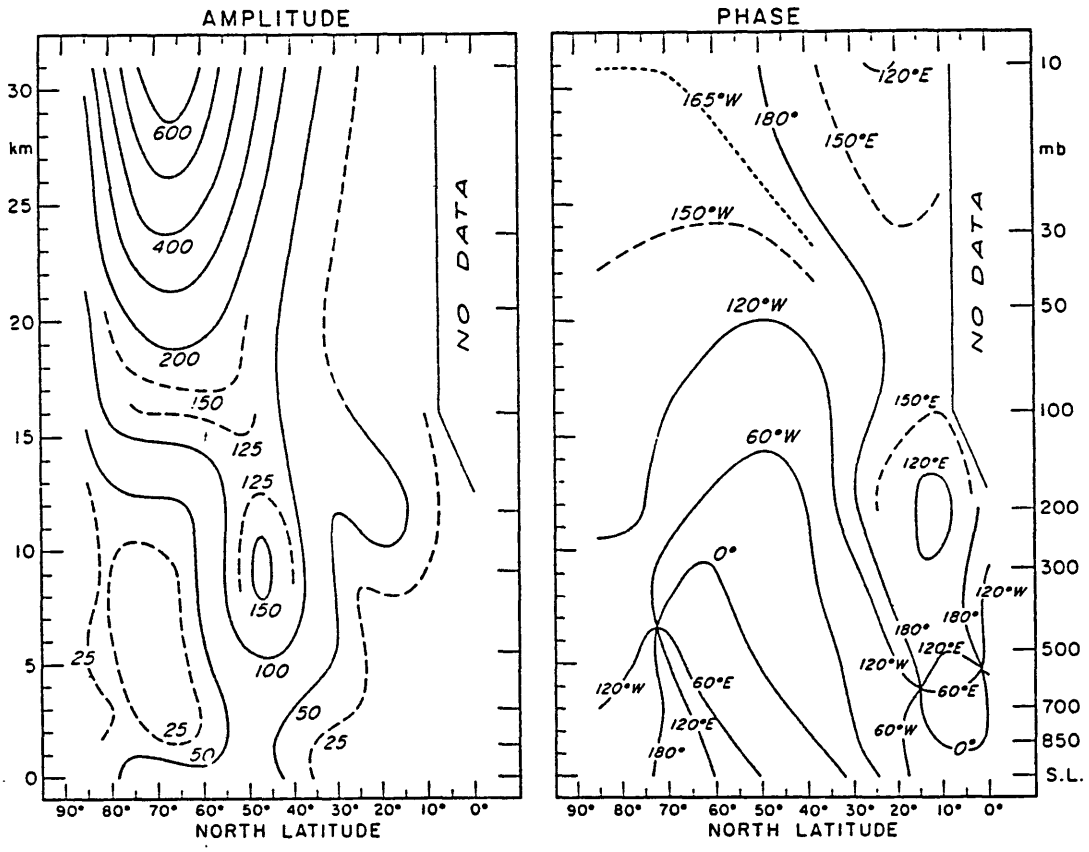

Figure 2.4: Latitude-height cross-section of stationary zonal wavenumber 1 amplitude (meters) and phase (longitude of ridge) in January, average over the years 1964-1970 in the troposphere and over 1965-1969 in the stratosphere (after van Loon et al., 1973)

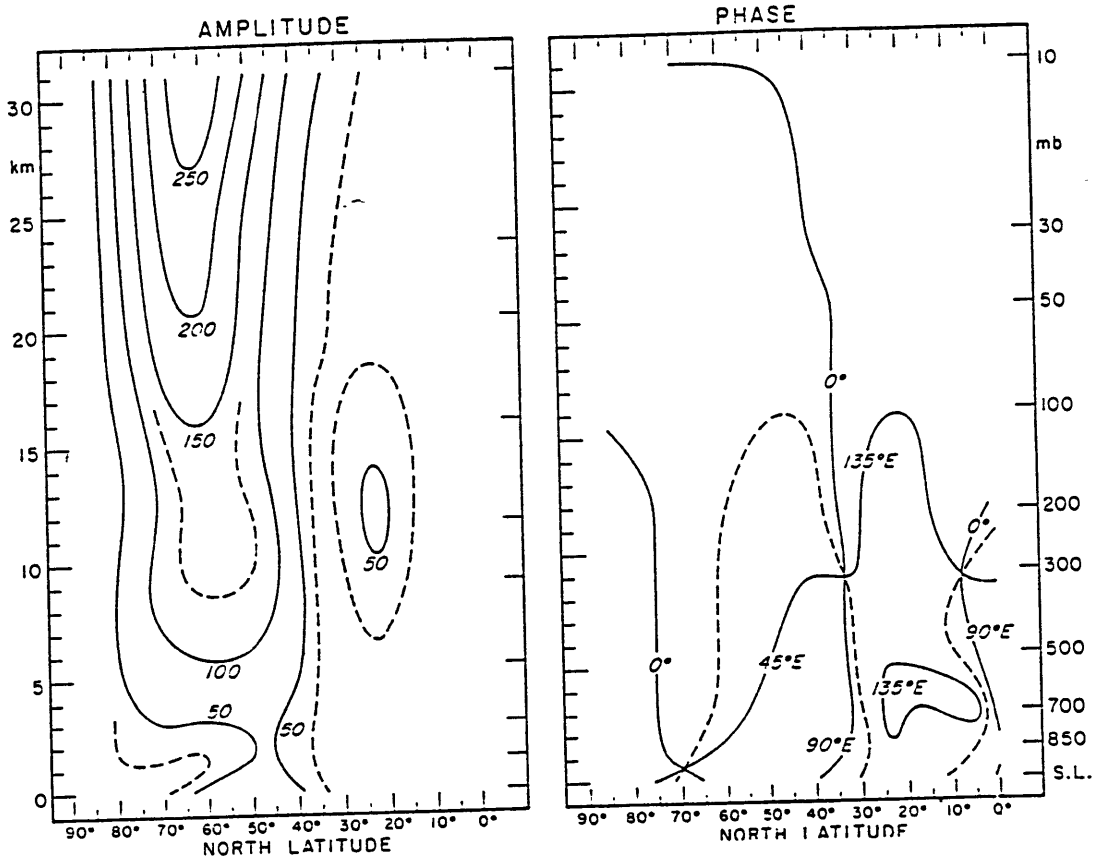

Figure 2.5: As in fig. 2.4 but for zonal wavenumber 2.

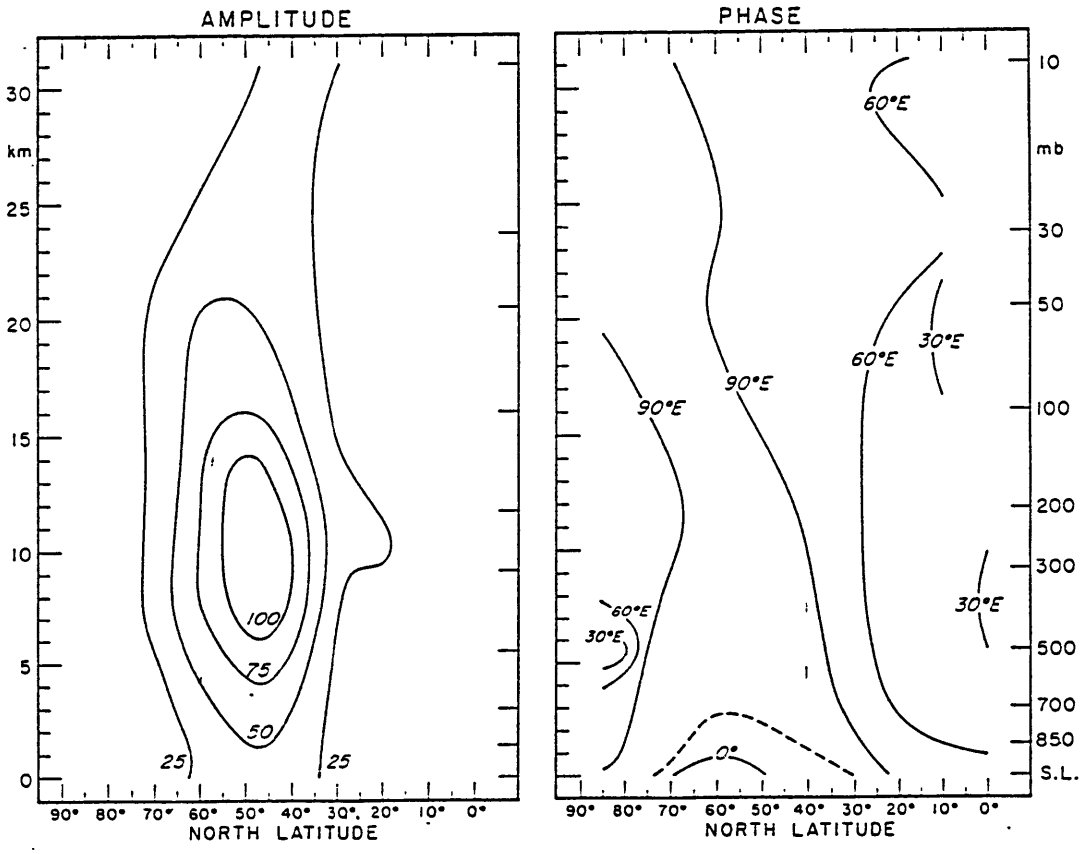

Figure 2.6: As in fig. 2.4 but for zonal wavenumber 3.

waves, we consider a case in which the stationary waves were particularly high. Figure 2.7 shows amplitude and phase of wavenumber one stationary wave during January 1958 (after Muench, 1967), a month not included in the data set of fig. 2.4. Comparing 2.7 with the climatological waves of fig. 2.4, we see that the most noticeable difference is in the amplitude of the wave, which is roughly 50% higher in January 1958 than in the average of several years. There are also differences in the phase of the wave: the amphidromic point at 700mb in the subtropics is located more to the south in January 1958, and the phase lines in mid- and high-latitudes are almost horizontal in January 1958, contrary to the climatology which shows another amphidromic point about (75N,500mb).

- Of particular interest for the mechanism proposed in this thesis is the relationship between the zonal flow and the stationary waves. As a matter of illustration, we show in fig. 2.8 the climatological zonal flow for the period December-February (from Newell et al., 1972). Comparing with the climatological zonal wavenumber one wave of figure 2.4, we see that the wave amplitude at the upper troposphere is located about 15 degrees to the North of the subtropical jet. In the stratosphere, the wave amplitude maxima tend to coincide with the maxima in zonal wind. As discussed in chapter 6, this relationship is consistent with the notion of waves excited in the lower troposphere, propagating upward with an

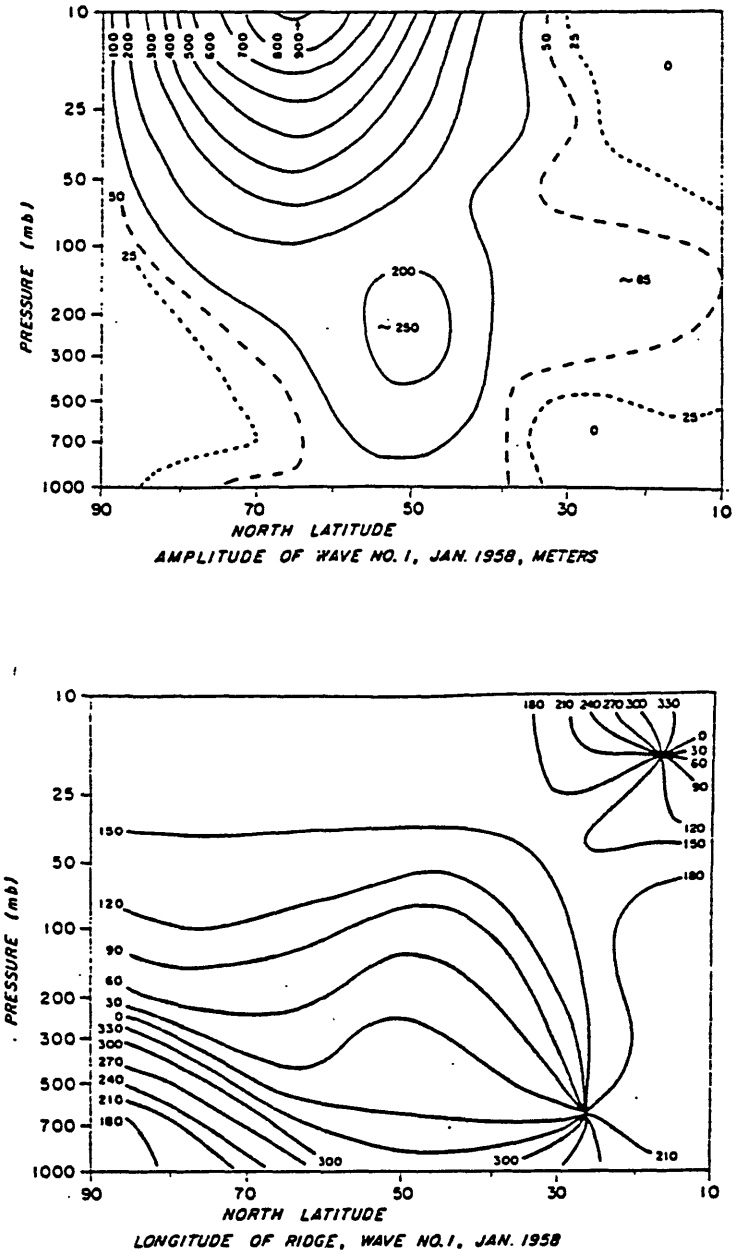

Figure 2.7: Latitude-height cross-section of stationary zonal wavenumber 1 amplitude (meters) and phase (longitude of ridge) for January 1958 (after Muench, 1967).

index of refraction determined by the zonal wind.

The modelling of stationary waves starts with the classical paper of Charney and Eliassen (1949). In this paper, they consider the barotropic vorticity equation in a beta-plane channel, forced by topography, and linearized about a westerly zonal flow. The solutions obtained with this model have the same scale as the forcingv and the potential for resonance. Despite the simplicity of the model, there is a striking agreement with the observed 500 mb geopotential height. The theory of resonant stationary waves was further developed by Tung and Lindzen (1979a,b) and Tung (1979). Later studies, using more comprehensive models (e.g., Jacqmin and Lindzen, 1985) found no indication of resonant stationary waves with a two-dimensional basic state in spherical geometry.

Barotropic models on the sphere have also had some success explaining the horizontal distribution of stationary waves (e.g., Grose and Hoskins, 1979). Not only do barotropic models of stationary waves not provide any information about vertical propagation, they also have some peculiar behavior. As indicated by EP-flux calculations either from observations (e.g. Edmon et al., 1980) or from tri-dimensional modeling (e.g. Jacqmin and Lindzen, 1985), most of the wave activity generated in the troposphere tends to propagate upward rather then meridionally[2]. In a barotropic model, having only one layer, all

[2]Recall that the vertical component of the EP vectors is proportional to the wave

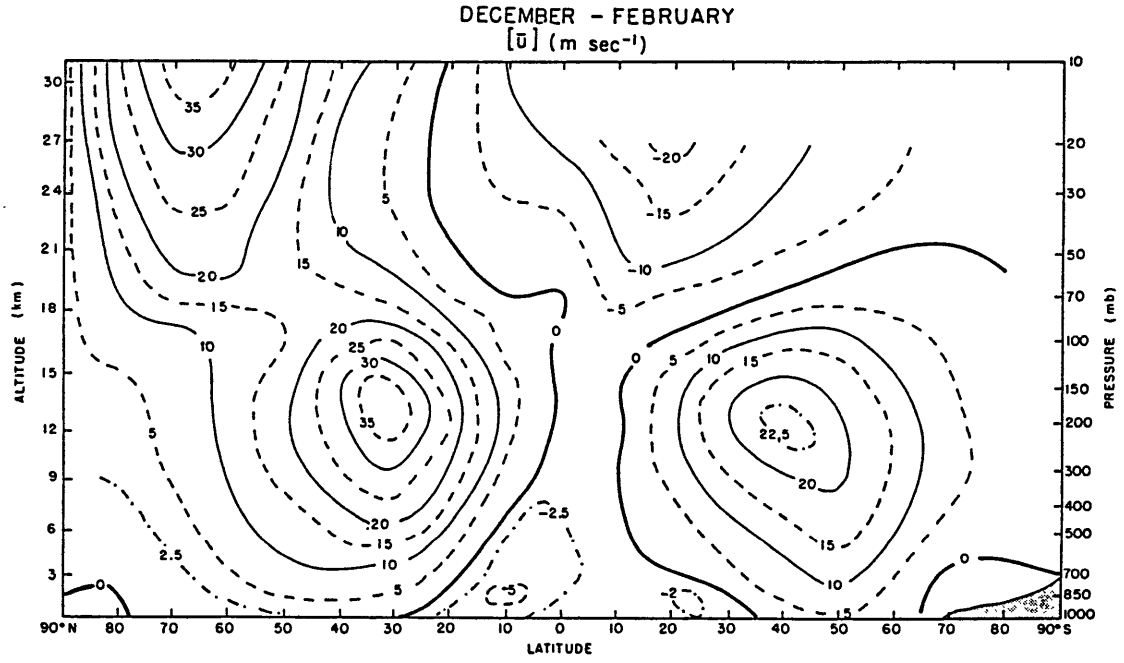

Figure 2.8: Latitude-height section of the mean zonal wind (m/s) for the period December-February (after Newell et al., 1972).

the wave activity generated in this layer has to propagate horizontally. One of the implications of this horizontal confinement is that the waves behave differently to changes in the zonal flow than do waves in a tri-dimensional model (see chapter 5).

In this thesis we will model stationary waves with a steady primitive equation model on the sphere; the basic state zonal wind is taken from observations. The validity of linear models of this sort have been investigated by Nigam et. al. (1986,1988), who compared results of the linear model with the climatology of a companion GCM. Of course, the stationary waves of the two models were not identical, but they were qualitatively and quantitatively close, and both linear model and GCM reproduced the main features of the atmosphere. A comparison of the several linear models (including ours) with the observed waves will be presented in chapter 6.

2.2 Rossby waves

Since the original work of Rossby and collaborators (1939), many papers have been devoted to the study of large-scale atmospheric disturbances, both theoretically and observationally. Reviews of the subject are presented by Madden (1979) and Salby (1984a). Among these distur-

heat flux, while the meridional component is proportional to the wave momentum flux. The vectors tend to most point upward simply because for stationary waves the heat flux contribution is greater then the northward momentum flux contribution.

bances, ultralong planetary-scale waves have been extensively reported and identified as normal modes of a model atmosphere. Even though the modeling of these normal modes has been considered in many works (Kasahara, 1980; Salby, 1981a,b, among others), the mechanism of excitation of these waves has not been addressed in great detail.

In this work, we will be concerned mostly with the westward propagating ultralong Rossby waves, namely, those disturbances with zonal wavenumber less than 4 and with a meridional wavenumber less than 4, on the sphere. Following Daley and Williamson (1985), we will refer to the observed mode by its approximated period, e.g. 5-day wave, 16-day wave, etc., and to the theoretically derived mode by the symbol H_s^ℓ, where s/ℓ is the zonal/meridional wavenumber (e.g., $s = 1, 2, 3, \ldots$ $\ell = 1, 2, 3\ldots$).

The gravest modes of the atmosphere are relatively robust and may be captured even by the simplified model of an isothermal atmosphere linearized about a state of rest. In such a model, the equations decouple into a vertical structure equation, and a horizontal structure equation which is formally similar to the Laplace Tidal Equations (LTE). The vertical structure equation, for an unbounded atmosphere, has only one solution, the so-called Lamb's wave (Lamb, 1932), whose amplitude increases with height and has no vertical phase tilt. This vertical structure traps most of the energy in the troposphere, and the troposperic structure is by and large independent of the basic state and

dissipation in the upper levels (Bretherton,1969). The solutions of the horizontal structure equation are the Hough functions (Hough, 1898), which consist of eastward and westward gravity modes and the Rossby (rotational) manifold. The introduction of realistic basic state and dissipation does not alter these results in a substantial way. In particular, the meridional Hough mode structure, as well as the external barotropic structure, remain valid throughout the troposphere (Salby, 1981a,b.) The main modifications are: 1) realistic mean winds reduce the frequency of the Rossby modes, especially for higher meridional wavenumbers; 2) the variation of the mean winds with time causes the modes to have a band of frequencies rather than a single discrete frequency. At least in the troposphere, the modes considered here do not have critical lines (where the phase speed is equal to the zonal wind) and are consequently stable.

On the observational side, many studies (reviewed in Madden, 1979 and Salby, 1984) have provided strong evidence for the existence of external normal modes in the atmosphere. Two kinds of data analysis have been presented in the literature, which will be referred to as *global* and *local* analysis. The former consists of a theoretical-observational approach in which the data are projected onto theoretically derived global normal modes, with a minimum of temporal filtering. In this category are the works of Eliassen and Machenhauer (1965), Ahlquist (1982, 1985), Lindzen et al. (1984), and Daley and Williamson (1985). This approach captures the episodic nature of these waves but is inca-

pable of resolving their sometimes localized nature. On the other hand, the *local* analysis consists of decomposing the data into zonal Fourier components and using sophisticated time series analysis to determine the periods and structures of the waves. In these studies, there is no *a priori* introduction of any latitudinal dependence; however, heavy filtering is used to select the frequencies of interest. This kind of analysis is represented mainly by the work of Madden and collaborators (for a complete list of reference see Madden, 1979 and Salby, 1984a). The local analysis in general does not adequately determine the episodic nature of the waves, since it overestimates the lifetime due to the sharp filtering (Madden, 1983), but it can determine any possible spatial confinement of these waves.

In this thesis we will use a global approach to analyze the transient Rossby waves in our model. It is worthwhile to mention that in the presence of shear the eigenvectors of the linear model are no longer orthogonal and the concept of bi-orthogonality should be used (e.g. Held, 1985; Farrell, 1988). To illustrate the effects of this loss of orthogonality we show in fig. 2.9 the time evolution of the amplitude and phase of the spectral coefficient in terms of Hough functions from the linear barotropic model to be described in chapter 4. In this run, we initialize the model with the 16-day wave multiplied by a Gaussian envelope to render it negligible outside (30S,30N); the basic state in this case has easterlies in the tropics. We clearly see that the wave propagates with the predicted phase speed while the amplitude vacillates in time. This

same behavior is apparent in the observed amplitude and phase of the 16-day wave of Lindzen et al. (1984), reproduced in fig. 2.10. Since there is no clear choice for the right basic state in the atmosphere, and since for the gravest modes there is very little difference between the Hough functions and the *real* eigensolution (Kasahara,1980), we will use the Hough function in our analysis. It should be borne in mind that vacillation of the sort exemplified above does not represent excitation and dissipation of the mode, but rather an artifact of our analysis.

The importance of the external Rossby modes in the atmospheric circulation is another point that has not been considered in detail. Several authors (e.g. Lindzen et al., 1982; Madden, 1983; Hirooka, 1986) have proposed a mechanism for the influence of transient Rossby waves on the mean flow, through interference with the quasi-stationary waves. The possible role of these waves in the stratospheric sudden warming has also been suggested (Palmer, 1981; Hirooka and Hirota, 1985). Lindzen et al. (1984) pointed out that the total Rossby wave field may contribute substantially to persistent anomalies.

Studies that account for the excitation of ultralong Rossby waves include a one-dimensional model (Hirota, 1971) with regularly oscillating mean winds and a two-dimensional model on a beta plane (Madden, 1975; Garcia and Geisler, 1981) forced by stochastic noise. None of these studies accounts for the global nature of these waves, nor has a mechanism for the origin of the forcing. Recently, Salby and Gar-

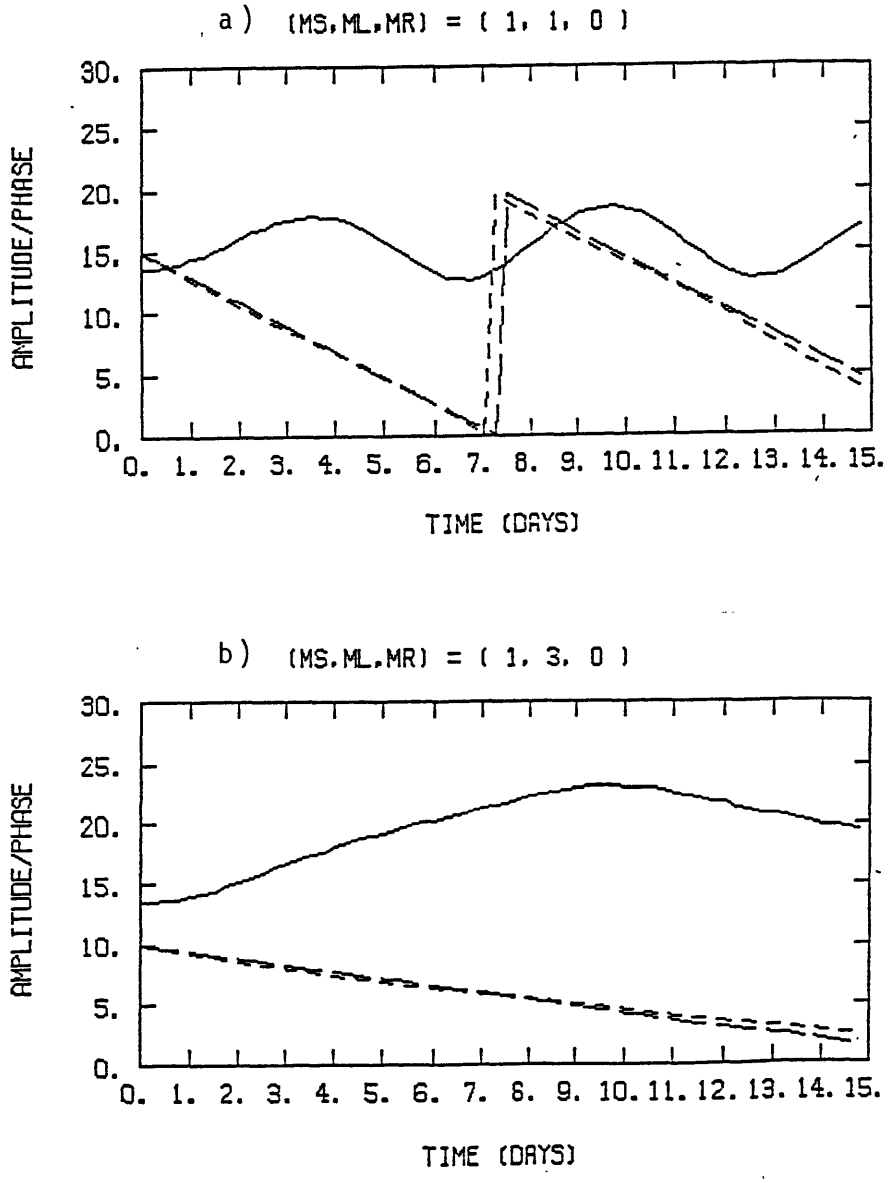

Figure 2.9: Amplitude and phase of ultralong Rossby waves obtained with the barotropic model initialized with a restricted 16-day wave (see text for details). Amplitude (full line) and phase (short dashed line) as a function of time for : a) 5-day wave, and b) 16-day wave. Also shown is the theoretically predicted phase (long dashed-line).

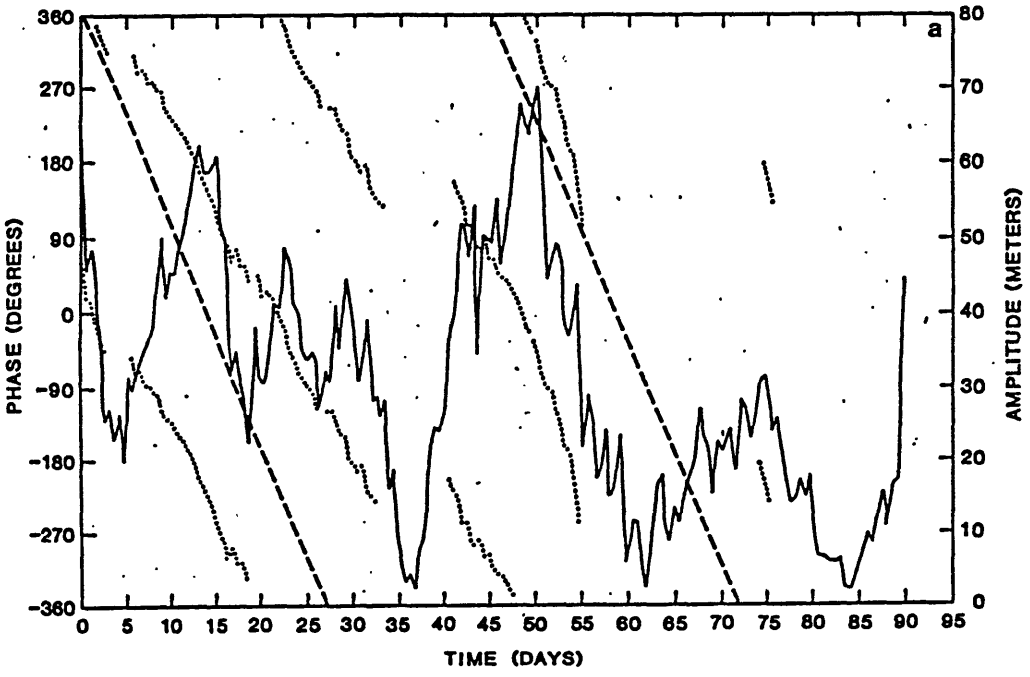

Figure 2.10: Observed amplitude and phase of the 16-day wave with zonal wavenumber 3 (from Lindzen et al., 1984).

cia (1987) and Garcia and Salby (1987), have computed the transient response to localized episodic heating in the tropics. In this linear primitive equation model the basic state is assumed constant in time and episodic heating is prescribed. For fast heating (occurring in a time interval of about 5 days) they found that the 5-day wave dominates the westward propagating disturbances, while for slow heating (occurring in a time interval of about 30 days) the westward propagating response is dominated by disturbances with very low phase speeds (much slower than the 16-day wave). The predominance of the 5-day wave for fast heating is consistent with Hamilton (1985), who observed a very high correlation between the 5-day wave and the eastern Pacific sea surface temperatures.

2.3 Blocking and persistent anomalies

Low frequency phenomena in the atmosphere have received increased attention in the last few years. The term is generally used to refer to atmospheric motion with time scales of about two weeks and longer, though there is no strict definition. Sometimes persistence of a blocking pattern for one week has been cast as such. Lindzen (1986) discuss the notion of persistence, noting that atmospheric oscillations like ultralong Rossby waves (e.g., 16-day wave) may contribute substantially to the overall persistent pattern. In this section we will briefly consider two low frequency phenomena that have been widely studied in the last

decade: *blocking* and *persistent* anomalies.

The definition of persistent anomalies we use here is the same introduced by Dole (1982). It simply states that an anomaly is persistent if it meets a duration and amplitude criterion: for a key grid point the anomalous geopotential height has to persist for T days above a threshold value of M meters. Typical values of the threshold parameters are (T,M) = (10 days,100 meters), and the key grid points correspond roughly to the north Pacific (PAC) and north Atlantic (ATL) storm track regions and to Northern Soviet Union (NSU). There is no standard definition of blocking. The most common criteria involve a persistence of a split jet or blocked flow for about 1-2 weeks (e.g., Rex, 1950). There is great diversity of criteria, even though in one way or another they reproduce some common features.

Many studies (e.g. Malguzzi and Malanotte-Rizzoli, 1985a,b,1987; Malanotte-Rizzoli and Hancock, 1987) have regarded blocking and persistent anomalies as the same phenomenon and approached them theoretically from an identical framework. There is considerable evidence that persistent anomalies as in Dole (1982) do not always correspond to a blocking configuration. Taking for example Dole's Atlantic case, only the positive composite anomalies when added to the climatology give a blocked flow. The negative counterpart, instead, corresponds to a high index flow. Despite this fact, positive and negative anomalies have a certain degree of symmetry, suggesting perhaps that they have a com-

mon mechanism or share the same basic physics. One should also be cautious when comparing persistent anomalies and blocking cases. For example, in a preliminary study we found that *none* of Dole's (1982) persistent anomaly composites (Pacific, Atlantic and Northern Soviet Union, with threshold (T,M)=(10 days, 100 meters)) meets the blocking criterion of Lejenas and Doos (1987)[3]. Given the above remarks, it seems prudent not to consider blocking and persistent anomalies as necessarily the same phenomenon. Due to persistent anomaly large scale and time evolution similar to stationary Rossby waves, we will be most concerned with persistent anomalies in this thesis.

On the theoretical side, low frequency phenomena have been approached in different ways. Multiple equilibria (Charney and DeVore, 1979, among others), local nonlinear theories (Malguzzi and Malanotte-Rizzoli, 1985a,b,1987), bi-modality (Hansen and Sutera, 1984), instabilities of the mean flow (Simmons et al., 1983; Pierrehumbert, 1986), resonant Rossby waves (Tung and Lindzen, 1979a,b; Tung, 1979), instabilities of the tri-dimensional mean flow (Frederiksen and Webster,1989 and references therein), are examples of those approaches. Some problems with the above theories are discussed by Lindzen (1986). The perspective adopted in this thesis is that anomalous stationary waves, primarily associated with an anomalous basic state, may contribute significantly to the persistent anomaly picture. As stationary waves

[3]Lejenas and Doos (1987) define a blocking event for a particular longitude whenever the difference between the 500mb geopotential height at 40N and 60N is negative, irrespective of the duration of the event.

have a tri-dimensional structure, these anomalies are not restricted to the troposphere, and as we shall see in chapter 6, the largest scales can reach the stratosphere. This prediction is clear in opposition to local nonlinear theories which assume that blocking (and for that matter persistent anomalies) is trapped in the stratosphere. Extension of Dole's (1982) analysis to the stratosphere is in progress (Dole, personal communication) and will help resolve this question.

Chapter 3

A simple theory of the adjustment mechanism

In this chapter we develop a theory for transients excited when a temporal change occurs in the zonally averaged zonal wind. The wind changes we will be interested in are not a simple oscillation in place. Rather, in the barotropic and baroclinic calculations of chapters 5 and 6, the changes will be in wind structure, which chiefly determines the path taken by stationary waves. However, as a conceptual model we start with the barotropic vorticity equation linearized around a spatially constant zonal wind which is allowed to depend on time. After presenting this approach and discussing transient and stationary waves in this simplified model, we extend the results to a general linear atmosphere in section 3.2. Application to ultralong Rossby waves and quasi-stationary transients then follows, and the transient efficiency

function is introduced.

3.1 An example: the barotropic vorticity equation

The barotropic vorticity equation in the presence of topography, when linearized around a spatially constant zonal wind $U(t)$, becomes (Charney and Eliassen, 1949)

$$\left(\frac{\partial}{\partial t}+U(t)\frac{\partial}{\partial x}+r\right)\nabla^2\Psi+\beta\frac{\partial\Psi}{\partial x}=-U(t)\frac{f_o}{H_o}\frac{\partial h_S}{\partial x} \tag{3.1}$$

where H_o is the mean depth of the fluid and h_S the topographic height, and r is a constant damping coefficient. The notation is otherwise conventional and symbols may be found in appendix A. Let the initial condition of eq. (3.1) be denoted

$$\Psi(x,y,t=0)=\Psi_o(x,y) \tag{3.2}$$

For a β-plane channel geometry both solution and forcing can be represented as

$$\begin{aligned} F(x,y,t) &\equiv -U(t)\frac{f_o}{H_o}\frac{\partial h_S}{\partial x} \\ &= Re\sum_{k,\ell} f_{k\ell}(t)e^{ikx}sin\ell y \end{aligned} \tag{3.3}$$

$$\Psi(x,y,t) = Re\sum_{k,\ell} A_{k\ell}(t)e^{ikx}sin\ell y \tag{3.4}$$

$$\Psi_o(x,y) \;=\; Re\sum_{k,\ell} A_{o_{k\ell}} e^{\imath kx} sin\ell y \tag{3.5}$$

Substituting these expressions in 3.1 and using the orthogonality of the $e^{\imath kx}sin\ell y$'s we find an ordinary differential equation for the time dependent coefficients

$$\begin{cases} \dot{A_{k\ell}} + \mathcal{L}A_{k\ell} = f_{k\ell} \\ A_{k\ell}(t=0) = A_{o_{k\ell}} \end{cases} \tag{3.6}$$

where $\dot{A}$ means the time derivative of A and $\mathcal{L}$ is given by

$$\mathcal{L}(t) \equiv \imath k\left(U(t) - \frac{\beta}{k^2+\ell^2}\right) + r \tag{3.7}$$

We start by assuming that U does not depend on time. In this case we can unambiguously partition the solution into a transient and stationary part[1]

$$A(t) = A_T(t) + A_S \tag{3.8}$$

where the stationary part A_S is simply

$$A_S = \mathcal{L}^{-1} f \tag{3.9}$$

and the transient part satisfies the equation

$$\begin{cases} \dot{A_T} + \mathcal{L}A_T = 0 \\ A_T(0) = A_o - A_S \end{cases} \tag{3.10}$$

[1]From now on we drop the subscript $k\ell$ denoting the horizontal wavenumber.

whose solution is

$$\begin{aligned} A_T(t) &= e^{-\mathcal{L}t} A_T(0) \\ &= e^{-rt} e^{-ik(U-c_o)t} A_T(0) \\ &\equiv \mathcal{U}_o(t,0) A_T(0) \end{aligned} \tag{3.11}$$

where c_o is the Rossby wave phase speed

$$c_o = \frac{\beta}{k^2 + \ell^2}. \tag{3.12}$$

It is apparent that in the limit $t \to \infty$ the transient part A_T vanishes due to the dissipative term r:

$$\lim_{t\to\infty} A_T(t) = 0 \tag{3.13}$$

Now let us consider the case where $\mathcal{L}$ and f depend on time. In order to facilitate the analysis, we consider an idealized situation in which the wind varies only for $0 < t < \tau$. In addition, we take the initial condition to be the stationary solution associated with the wind at time zero, namely

$$A(t=0) = A_o = \mathcal{L}^{-1} f(0). \tag{3.14}$$

During the transition period, let us define the quantity

$$A_F(t) = \mathcal{L}^{-1} f(t) \tag{3.15}$$

which is analogous to the stationary solution 3.9. In terms of A_F, we can define another quantity A_1 such that

$$A(t) = A_F(t) + A_1 \tag{3.16}$$

Substituting (3.16) into (3.6) we find the equation satisfied by A_1

$$\begin{cases} \dot{A}_1 + \mathcal{L}(t)A_1 = -\dot{A}_F \\ A_1(t=0) = 0 \end{cases} \tag{3.17}$$

To solve (3.17) we first find the homogeneous solution A_H by setting the RHS to zero. The homogeneous solution can be easily found:

$$\begin{aligned} A_H(t) &= \exp\left(\int_0^t \mathcal{L}(t')dt'\right) A_H(0) \\ &= \exp\left[-\imath k\left(c_o t + \int_0^t U(t')dt'\right)\right] A_H(0) \\ &\equiv \mathcal{U}_o(t,0)A_H(0) \end{aligned} \tag{3.18}$$

The particular solution is found using the method of variation of parameters. We set $A_P = \mathcal{U}_o(t,0)B(t)$ and upon substitution into (3.17) obtain

$$\begin{aligned} A_P &= -\int_0^t \mathcal{U}_o(t,0)\mathcal{U}_o(0,t')\dot{A}_F dt' \\ &= -\int_0^t \mathcal{U}_o(t,t')\dot{A}_F dt' \end{aligned} \tag{3.19}$$

where we have used the property $\mathcal{U}_o(t,0)\mathcal{U}_o(0,t') = \mathcal{U}_o(t,t')$, which follows from eq. (3.18). The final solution takes the form

$$A(t) = A_F(t) - \int_0^t \mathcal{U}_o(t,t')\dot{A}_F dt' \tag{3.20}$$

The split between transient and stationary (*forced*) solution is ambiguous during this transition period, since both $A_F(t)$ and the second term on the RHS are both changing with time. The key quantity to be analyzed during this transition period is the departure from the initial

condition. This quantity, loosely called *anomaly* field in chapters 5 and 6, will allow us to investigate the establishment of the new stationary solution and how the information that the wind is changing in one location can propagate to other regions. After the transition period τ the partition between stationary (forced) and transient (*free*) waves are again well defined, namely

$$A(t) = A_S + A_T(t) \tag{3.21}$$

where

$$A_S = A_F(\tau) \tag{3.22}$$

$$A_T = -\mathcal{U}_o(t,\tau)\int_0^\tau \mathcal{U}_o(\tau,t')\dot{A_F}dt' \tag{3.23}$$

The interpretation of (3.17) is evident: the *traveling* component (*transient* when dissipation is present) is equal to the summation (in the integral sense) of the instantaneous adjustments of the *quasi-stationary* solution (more precisely, the instantaneous *steady* solution, eq. 3.22), represented by $\delta\dot{A}_F = -\dot{A}_F dt'$, propagated from the instant $t' < \tau$ to the instant $t > \tau$. It should be noted that the time variation of A_F can arise either from $\mathcal{L}$ or f, or both. In particular, it will be seen in chapter 5 that time variation in f (flow over topography) may give a much smaller contribution compared to time variation in $\mathcal{L}$ (time variation of the zonal flow in the interior of the layer.) Notice that the forcing of the traveling component does not require the presence of the

same time scale in the RHS forcing; it may occur in the presence of *stationary* forcing alone.

The transient efficiency function

The *transient efficiency function* ξ is defined as the percentage ratio between the transients right at $t = \tau$ and the differences in stationary solution[2]

$$\xi = 100 \left| \frac{\int_0^\tau \mathcal{U}_o(\tau, t') \dot{A}_F dt'}{A_F(\tau) - A_F(0)} \right| \tag{3.24}$$

Approximated formulas for this quantity will be derived in sections 3.3 and 3.4 for ultralong Rossby waves and quasi-stationary Rossby waves. A comparison with the results of the barotropic and baroclinic models will be performed in chapters 5 and 6.

The expressions derived in this section could be used to compute exactly the excited transients and the changes in stationary solution, given a simple analytical expression for $U(t)$. However, in a model like this, with a spatially uniform basic state, changes in the forced waves would be global and mostly associated with the local response to forcing, rather than to propagation. The perspective adopted in this work is that local changes in wind alter the path taken by stationary waves, with transients being generated in the process. Therefore, we

[2]This quantity is generally evaluated at maximum and minimum stationary wave centers, so that the vanishing of the denominator is not of physical interest.

do not explore the specifics of this model. It was used here only as a conceptual model to develop a formalism which is generalized below.

3.2 A more general case

This section extends the results of the previous section to a general linear atmosphere, which can be barotropic or baroclinic. The steps (and even notation) are kept close to the example above in order to facilitate the comparison.

The (linear) equations for traveling and forced waves in the atmosphere may be written as

$$\begin{cases} \left(\frac{\partial}{\partial t} + \mathcal{L}\right) \mathbf{W}(\mathbf{x};t) = \mathbf{F}(\mathbf{x},t) \\ \mathbf{W}(\mathbf{x},t=0) = \mathbf{W}_o(\mathbf{x}) \end{cases} \tag{3.25}$$

where $\mathcal{L}$ is a linear operator that depends explicitly on time

$$\mathcal{L} = \mathcal{L}(\mathbf{x},t) \tag{3.26}$$

$\mathbf{W}$ is a vector representing the dependent variables, $\mathbf{F}$ is any (RHS) forcing that may apply (possibly but not necessarily a function of time) and $\mathbf{x}$ is a vector containing the spatial coordinates (latitude, longitude and vertical coordinates.) Let us define

$$\mathbf{W}_F = \mathcal{L}^{-1}\mathbf{F}(\mathbf{x},t). \tag{3.27}$$

$\mathbf{W}_F$ corresponds to the *steady* solution when $\mathcal{L}$ and $\mathbf{F}$ are taken as independent of time. In terms of $\mathbf{W}_F$ the solution of (3.25) may be written as

$$\mathbf{W}(\mathbf{x},t) = \mathcal{U}_o(t,0)\,[\mathbf{W}_o(\mathbf{x}) - \mathbf{W}_F(\mathbf{x},0)] + \mathbf{W}_F(\mathbf{x},t) + \mathbf{W}'(\mathbf{x},t) \quad (3.28)$$

where $\mathcal{U}_o(t,0)$ is the evolution operator (or propagator)[3] associated with (3.25) when $F = 0$, namely, the free problem

$$\begin{cases} \left(\frac{\partial}{\partial t} + \mathcal{L}\right)\mathcal{U}_o(t,0)\mathbf{Q}_o = 0 \\ \\ \mathcal{U}_o(0,0)\mathbf{Q}_o(\mathbf{x}) = \mathbf{Q}_o(\mathbf{x}) \end{cases} \quad (3.29)$$

with $\mathbf{Q}_o(\mathbf{x})$ being any possible initial condition. At this point we assume that $\mathcal{L}$ is such that $\mathcal{U}_o$ has the following properties (Reed and Simon, 1975, sec. x.12):

$$\begin{cases} \text{i)} & \mathcal{U}_o(t,s) & = \mathcal{U}_o(t,r)\mathcal{U}_o(r,s) \\ \text{ii)} & \mathcal{U}_o^{-1}(t,s) & = \mathcal{U}_o(s,t) \\ \text{iii)} & \mathcal{U}_o(t,t) & = I \text{ (identity operator)} \end{cases} \quad (3.30)$$

for any time r, s, t. Eq. (3.28) can be viewed as a definition of $\mathbf{W}'$. Substituting (3.28) into (3.25), and using (3.27), (3.29) we obtain the equation satisfied by $\mathbf{W}'$:

$$\begin{cases} \left(\frac{\partial}{\partial t} + \mathcal{L}\right)\mathbf{W}' = -\frac{\partial}{\partial t}\mathbf{W}_F \\ \\ \mathbf{W}'(\mathbf{x}, t=0) = 0 \end{cases} \quad (3.31)$$

[3]When $\mathcal{L}$ is independent of time $\mathcal{U}_o$ is simply

$$\mathcal{U}_o(t,s) = e^{-i\mathcal{L}(t-s)}$$

A solution for (3.31) can easily be found using the method of variation of parameters. Now let us write

$$\mathbf{W}'(\mathbf{x},t) = \mathcal{U}_o(t,0)\mathbf{Y}(\mathbf{x},t). \tag{3.32}$$

With the aid of (3.29), we can show

$$\left(\frac{\partial}{\partial t} + \mathcal{L}\right)\mathbf{W}' = \mathcal{U}_o(t,0)\left[\frac{\partial \mathbf{Y}}{\partial t}\right] = -\frac{\partial}{\partial t}\mathbf{W}_F \tag{3.33}$$

which in turn implies

$$\mathbf{Y}(\mathbf{x},t) = -\int_0^t \mathcal{U}_o(0,t')\left[\frac{\partial \mathbf{W}_F}{\partial t}\right] dt' \tag{3.34}$$

where we have used the formal property (3.30-iii). Eq. (3.34) is a well known result for the solution of inhomogenous differential equations (Coddington and Levinson, 1955, pg. 74). Substituting (3.32) into (3.28) we find

$$\mathbf{W}(\mathbf{x},t) = \mathcal{U}_o(t,0)\left[\mathbf{W}_o(\mathbf{x}) - \mathbf{W}_F(\mathbf{x},0) + \mathbf{Y}(\mathbf{x},t)\right] + \mathbf{W}_F(\mathbf{x},t) \tag{3.35}$$

As before, we consider the idealized problem in which $\mathcal{L}$ and $\mathbf{F}$ depend on time only for $t < \tau$, where τ is the transition period. In addition, we also assume the initial condition to be

$$\mathbf{W}_o(\mathbf{x}) = \mathbf{W}_F(\mathbf{x},0) \tag{3.36}$$

For $t > \tau$ we can write (3.35) as

$$\mathbf{W}(\mathbf{x},t) = \mathbf{W}_T(\mathbf{x},t) + \mathbf{W}_S(\mathbf{x}) \tag{3.37}$$

The traveling component $\mathbf{W}_T$ is given by

$$\mathbf{W}_T(\mathbf{x},t) = -\int_0^t \mathcal{U}_o(t,t') \left[\frac{\partial \mathbf{W}_F(\mathbf{x},t')}{\partial t'}\right] dt' \tag{3.38}$$

where we have used (3.34),(3.35) and the formal property (3.30i). The stationary component $\mathbf{W}_S$ is simply

$$\mathbf{W}_S(\mathbf{x}) = \mathbf{W}_F(\mathbf{x},\tau) = \mathcal{L}^{-1}\mathbf{F}(\mathbf{x},\tau) \tag{3.39}$$

The expressions above generalize similar expressions obtained with the barotropic vorticity equation in the last section. Next, we apply them to ultralong Rossby waves and quasi-stationary transients.

3.3 Application to ultralong Rossby waves

Eq. (3.38) can be used to derive an approximate formula for the amplitude of the transient ultralong Rossby waves. Let us assume that the propagation of these modes is insensitive to the variations in the zonal flow, in the following sense

$$\mathcal{U}_o(t,t')\mathbf{H}(\mathbf{x}) \approx \exp\left[-(r+\imath\sigma)(t-t')\right]\mathbf{H}(\mathbf{x}) \tag{3.40}$$

where $\mathbf{H}(\mathbf{x})$ denotes the mean spatial structure of the mode, σ its average frequency and r is the linear damping parameter. As shown in Kasahara (1980) the meridional structure of these waves is fairly insensitive to the basic wind. However, climatological periods for individual

seasons can depart from the annual average by approximately 10% . Since the changes in wind to be considered here are modest and we are only interested in the qualitative understanding of the role of parameters, we will ignore this effect. Furthermore, for $t > \tau$ assume $\mathcal{L}$ to have a complete set $\{\mathbf{H}_n\}$ of eigenvectors such that

$$\mathcal{L}\mathbf{H}_n = -(r_n + \imath\sigma_n)\mathbf{H}_n(\mathbf{x}) \tag{3.41}$$

(the discrete index n above is introduced only to simplify the notation; part of the spectrum of $\mathcal{L}$ may be continuous; n labels zonal as well as meridional wavenumbers.) The eigenvectors $\{\mathbf{H}_n\}$ are assumed to be orthonormal[4]

$$\langle \mathbf{H}_n, \mathbf{H}_{n'} \rangle \equiv \int \mathbf{H}_n^*(\mathbf{x})\mathbf{H}_{n'}(\mathbf{x})d\mathbf{x} = \delta_{nn'} \tag{3.42}$$

The particular solution $\mathbf{W}_F$ is assumed to have the simple time dependence

$$\mathbf{W}_F(\mathbf{x},t) = \begin{cases} \mathbf{W}_F(\mathbf{x},0) + \frac{t}{\tau}\Delta\mathbf{W}_F(\mathbf{x}) & \text{if } 0 < t \leq \tau \\ \mathbf{W}_F(\mathbf{x},0) + \Delta\mathbf{W}_F(\mathbf{x}) & \text{if } \tau \leq t \end{cases} \tag{3.43}$$

Eq. (3.43) can be interpreted as a Taylor expansion of $\mathbf{W}_F(\mathbf{x},t)$ around $t = 0$, where only the first order term is retained and finite differences are used to evaluate the derivative. Using (3.38) and (3.43) we can compute the traveling component at $t = \tau$

$$\mathbf{W}_T(\mathbf{x},\tau) \;=\; \frac{1}{\tau}\int_0^\tau \mathcal{U}_o(\tau,t')\Delta\mathbf{W}_F(\mathbf{x})dt'$$

[4]In reality, in the presence of shear the eigenvectors of $\mathcal{L}$ are no longer orthogonal (e.g. Held, 1985). However, orthogonality is approximately true among the gravest modes. We assume (3.42) for the sake of mathematical simplicity.

(3.44)

$$= \sum_n \langle \mathbf{H}_n, \mathbf{W}_T \rangle \mathbf{H}_n \equiv \sum_n \alpha_n \mathbf{H}_n \tag{3.45}$$

The α_n are the spectral coefficients of the excited transients. Similarly, we may expand

$$\Delta \mathbf{W}_F = \sum_n \langle \mathbf{H}_n, \Delta \mathbf{W}_F \rangle \mathbf{H}_n \equiv \sum_n \beta_n \mathbf{H}_n \tag{3.46}$$

which allows us to rewrite (3.45) as

$$\mathbf{W}_T(\mathbf{x}, \tau) = -\frac{1}{\tau} \sum_n \beta_n \int_0^\tau \mathcal{U}_o(\tau, t') \mathbf{H}_n dt' \tag{3.47}$$

For the gravest modes we assume (3.40), and the integral in (3.47) can be easily evaluated, given

$$\alpha_n = \xi_n^{RW} \beta_n \tag{3.48}$$

where

$$\xi_n^{RW}(r_n \tau_n, \sigma_n \tau_n) = -\frac{1 - \exp[-(r_n + \imath \sigma_n)\tau]}{(r_n + \imath \sigma_n)\tau} \tag{3.49}$$

The function ξ^{RW} is analogous to the transient efficiency function defined in section 3.1. It represents the effects of propagation and attenuation on the transients generated by the adjustments of the quasi-stationary solution, for the ultralong Rossby modes. The relevant parameters are the wave period ($2\pi/\sigma$) and the dissipative time scale (r^{-1}), both normalized by the transition period (τ). Figure 3.1 shows ξ^{RW} as a function of the normalized wave period and the dissipative

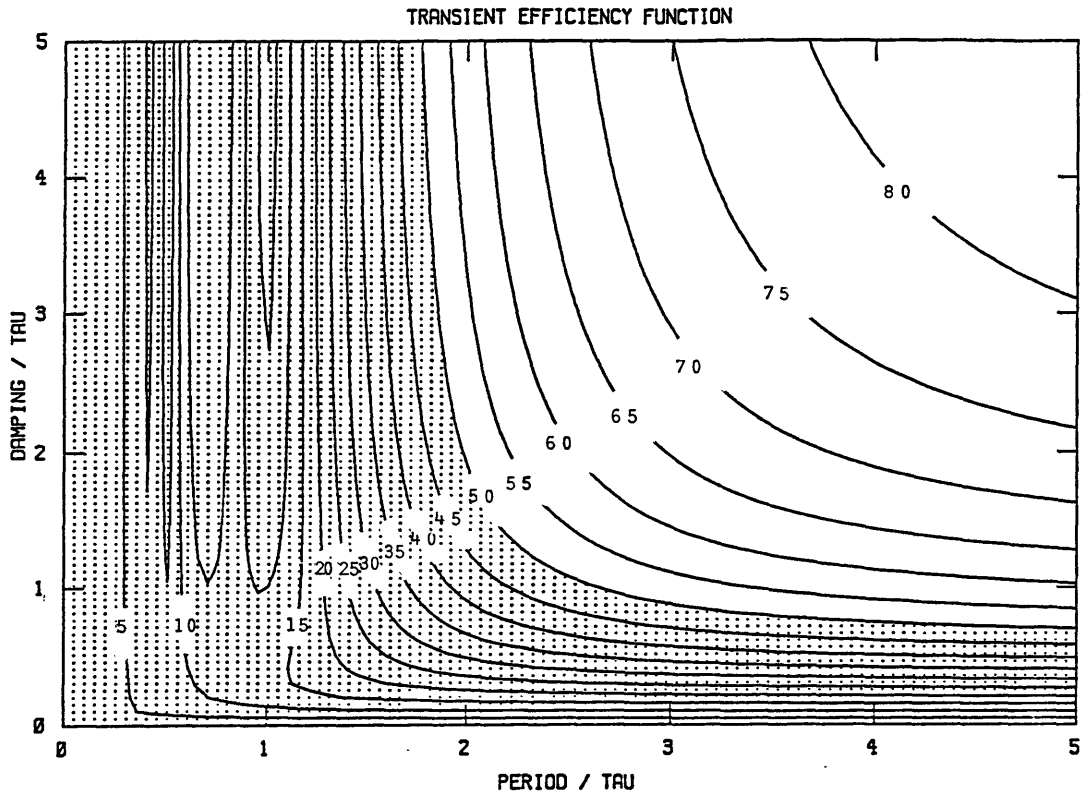

Figure 3.1: Approximate transient efficiency function for ultralong Rossby waves (eq. 3.49). The horizontal axis is the wave period $(2\pi/\sigma)$ divided by τ and the vertical axis is the damping time scale $(1/r)$ divided by τ. Regions where the transient efficiency function is smaller that 50% are shaded.

time scale. Regions where ξ^{RW} is less than 0.5 are shaded. Two asymptotic limits are also shown in fig. 3.2, where we set either σ or r to zero and plot ξ^{RW} as a function of the other parameter. From this figures we see that the effect of σ (propagation of transients) is important only for wave periods shorter than the transition period. The reason for such behavior in this particular case is clear: as transients become *available* through the adjustment of the stationary solution, they start to propagate zonally. If the transition period contains exactly an integral number of wave periods destructive interference will occur. This relation between wave period and transition period is particular to the time dependence we assumed for $\mathbf{W}_F$, though this interference mechanism may be extended to the more general case. Notice that in the absence of damping we need $\tau < (2\pi/\sigma)$ in order to efficiently excite transients. The effect of damping is straightforward: transients are attenuated as they become available. It also introduces irreversibility in the sense that perfectly destructive interference cannot occur when $r \neq 0$. It is interesting to notice that for small $(r + \imath\sigma)\tau$ the quantity ξ^{RW} is independent of τ. In chapter 5 we compare ξ^{RW} with the numerically obtained transient efficiency function. The agreement is quite good.

3.4 Application to quasi-stationary transients

Anticipating the results of the baroclinic calculation of chapter 6, we consider the case where transients are quasi-stationary. The criterion for quasi-stationarity is that the period of the disturbances is much longer than the transition period τ. In this case, we expect propagation to have a minor effect on the amplitude of the excited transients. Dissipation, therefore, is the major player. For simple Rayleigh friction, the dissipative limit of the transient efficiency function (eq. 3.49) is given by

$$\xi^{dissip}(r\tau) = -\frac{1 - e^{-r\tau}}{r\tau} \tag{3.50}$$

The amplitude of this function is depicted in fig. 3.2 as a function of the normalized damping time scale. Notice that for damping time scales longer than the transition period the efficiency is greater than 75%, and goes to zero as $r\tau$ approaches zero. In section 6.5 we compare ξ^{dissip} with the numerically determined transient efficiency function on a baroclinic model. The agreement is good provided we keep in mind the non-uniformity of the damping parameter.

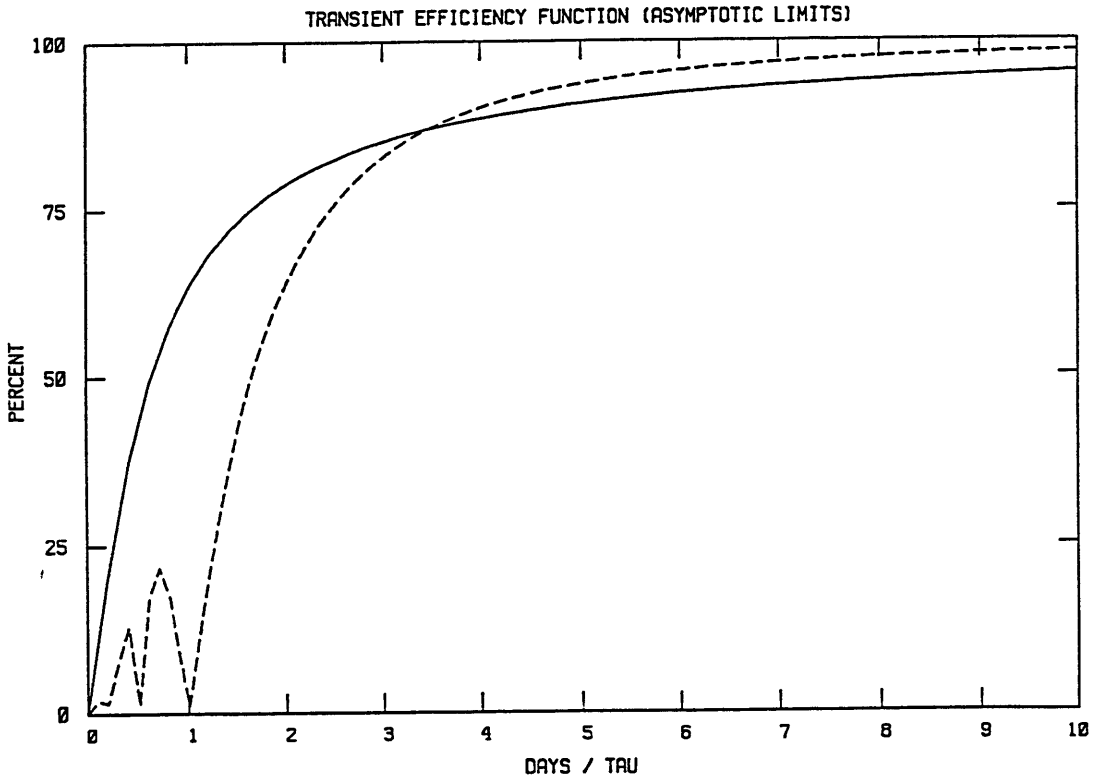

Figure 3.2: Asymptotic limits of the approximate transient efficiency function for ultralong Rossby waves (eq. 3.49). Full line: the dissipationless limit ($r = 0$). Dashed line: the quasi-stationary transient (or dissipative) limit, where $\sigma = 0$. The horizontal axis is either the wave period or the damping time scale, both divided by τ.

3.5 On the propagation of information

In this section we examine how the *information* of local changes in wind propagates from one location to another. On a switch-on initial value problem with fixed basic state and zero initial condition, disturbances propagate away from a localized forcing with their group velocity[5]. As mentioned before, the perspective adopted in this thesis is that transients can be excited even when the external forcing is kept fixed, the changes in the medium (operator $\mathcal{L}$) being the key factor. We argue that, despite the mathematically different formulations, the *information* that the medium has locally changed is communicated to other regions as in the switch-on problem; the information propagates with the group velocity.

To illustrate this process, let us assume that the dynamics is determined by an operator whose dependence on time is as follows:

$$\mathcal{L}(\mathbf{x},t) = \mathcal{L}_o(\mathbf{x}) + \epsilon\mathcal{L}_1(\mathbf{x},t) \tag{3.51}$$

where $\mathcal{L}_o$ does not depend on time and ϵ is a small parameter. Furthermore, let us take the RHS forcing to be independent of time and the initial condition to be the stationary solution associated with $\mathcal{L}_o$,

[5]Of course, we are assuming a well behaved medium such that WKB theory applies. For the largest scales it is often difficult to justify mathematically the WKB validity. However, comparison with numerical results has shown that even in such cases the notion of an index of refraction and wave theory based on the WKB theory can be a very useful diagnostic (e.g., Karoly and Hoskins, 1982.

namely

$$\begin{cases} \left(\frac{\partial}{\partial t} + \mathcal{L}\right) \mathbf{W}(\mathbf{x};t) = \mathbf{F}(\mathbf{x}) \\ \mathbf{W}(\mathbf{x}, t=0) = \mathcal{L}_o^{-1}\mathbf{F}(\mathbf{x}) \end{cases} \tag{3.52}$$

We proceed to perform a formal expansion in powers of the *small* parameter ϵ, viz.

$$\mathbf{W} = \mathbf{W}_o + \epsilon \mathbf{W}_1 + O(\epsilon^2) \tag{3.53}$$

Substituting (3.53) into (3.52) and collecting terms, we find to order zero

$$\mathbf{W}_o = \mathcal{L}_o^{-1}\mathbf{F} \tag{3.54}$$

To order ϵ the equation is

$$\begin{cases} \left(\frac{\partial}{\partial t} + \mathcal{L}_o\right) \mathbf{W}_1 = -\mathcal{L}_1 \mathbf{W}_o = -\mathcal{L}_1 \mathcal{L}_o^{-1}\mathbf{F} \\ \mathbf{W}_1(\mathbf{x}, t=0) = 0. \end{cases} \tag{3.55}$$

Hence, the anomaly field defined in section 3.1 reads

$$\mathbf{W}_a = \mathbf{W}(\mathbf{x},t) - \mathbf{W}(\mathbf{x},0) \tag{3.56}$$

$$= e^{\mathcal{L}_o t} \int_o^t e^{\mathcal{L}_o t'} (-\epsilon \mathcal{L}_1 \mathbf{W}_o)\, dt' \tag{3.57}$$

Eq. (3.57) states that at first order in ϵ the anomaly field is equivalent to a forced initial value problem with the effective forcing

$$\mathbf{F}_{eff} = -\epsilon \mathcal{L}_1 \mathbf{W}_o = -\epsilon \mathcal{L}_1 \mathcal{L}_o^{-1}\mathbf{F} \tag{3.58}$$

In addition, in the cases to be considered in this thesis, the operator $\mathcal{L}_1$ will be local, i.e. associated with local changes in wind. Therefore,

the effective forcing in (3.58) will also be localized. Analogously to the switch-on initial value problem, *information* will propagate from the effective forcing region according to the group velocity. This result is confirmed by the numerical simulations of chapter 5 and 6.

3.6 Discussion

In this chapter we have developed a framework to study the transients excited when a change in stationary waves takes place. We have introduced a measure of the excited transients and deduced a simple formula to predict them. In doing so, we have isolated the relevant parameters: wave period and dissipative time scale normalized by the transition period. This simple theory will serve as a guideline to the numerical investigations of chapters 5 and 6.

Chapter 4

Model Development

4.1 Introduction

In this chapter we describe the barotropic and baroclinic models that are used as tools throughout this thesis. They constitute linear versions of the shallow water equations and primitive equations on the sphere. For each model, there is a time-dependent and steady state version, which are highly consistent with each other. Model equations, forcing, dissipation and numerics are among the items discussed below. The first section deals with the barotropic model while the second present the details of the baroclinic model.

4.2 The barotropic model

In this section we described the shallow water equations over the sphere, linearized about a basic state slowly varying in time. This model will be used in chapter 5 to study the transients excited by the mechanism described in chapter 3. Even though the waves of interest are essentially in geostrophic balance, no geostrophic scaling is assumed. The reason for this lies in the fact that the adjustments we want to study occur in the tropics, where geostrophy breaks down. On the other hand, the design of the experiments minimizes the excitation of gravity waves.

4.2.1 Model equations

The nonlinear shallow water equations over the sphere may be written as (see Appendix A for symbols):

$$\begin{cases} \frac{\partial h}{\partial t} + \frac{1}{a\cos\phi}\left[\frac{\partial}{\partial\lambda}(h-h_S)u + \frac{\partial}{\partial\phi}(h-h_S)v\cos\phi\right] & = h_T - rh \\ \frac{Du}{Dt} - \left(f + \frac{u}{a}\tan\phi\right)v + \frac{g}{a\cos\phi}\frac{\partial h}{\partial\lambda} & = -ru \\ \frac{Dv}{Dt} + \left(f + \frac{u}{a}\tan\phi\right)u + \frac{g}{a}\frac{\partial h}{\partial\phi} & = -rv \end{cases} \tag{4.1}$$

where the linear damping parameter r is composed of a constant part and a part depending on latitude, viz.

$$r = r_c + r_t e^{-(\phi/\phi_t)^2}$$

$$\equiv \quad r_c + r_{trop}(\phi) \tag{4.2}$$

The function $r_{trop}(\phi)$ will be referred to as *tropical* damping. The symbol D/Dt has its usual meaning in barotropic models

$$\frac{D}{Dt} \equiv \frac{\partial}{\partial t} + \frac{u}{a\cos\phi}\frac{\partial}{\partial\lambda} + \frac{v}{a}\frac{\partial}{\partial\phi}$$

Now, consider the linearization around a basic state slowly varying in time

$$\begin{cases} U_o = U_o(\phi, t) \\ V_o = 0 \\ H_o = H_o(\phi, t) \end{cases} \tag{4.3}$$

In order for the basic state to satisfy approximately the shallow water equations we require

$$\left(f + \frac{u_o}{a}\tan\phi\right) + \frac{g}{a}\frac{\partial H_o}{\partial\phi} = 0 \tag{4.4}$$

Write

$$\begin{cases} u = U_o + \quad u' \\ v = \quad\quad v' \\ h = H_o + \quad h' \end{cases} \tag{4.5}$$

Neglecting quadratic terms in the perturbations as well as $\partial U_o/\partial t$ and $\partial H_o/\partial t$ eqs. (4.1) become (dropping primes)

$$\left(\frac{\partial}{\partial t} + \frac{\partial}{\partial\lambda}\mathbf{A} + \frac{\partial}{\partial\phi}\mathbf{B} + \mathbf{C} + \mathbf{D}\right)\mathbf{W} = \mathbf{F} \tag{4.6}$$

where $\mathbf{W} = [\ h\ u\ v\ ]^T$ and

$$\mathbf{F} = \left(\frac{U_o}{a\cos\phi}\frac{\partial h_S}{\partial\lambda} + h_T\right)\begin{bmatrix} 1 \\ 0 \\ 0 \end{bmatrix}. \tag{4.7}$$

A, B, C, and **D** are the 3x3 matrices defined below:

$$\mathbf{A} = \frac{1}{a\cos\phi}\begin{bmatrix} U_o & H_o & 0 \\ g & U_o & 0 \\ 0 & 0 & U_o \end{bmatrix} \tag{4.8}$$

$$\mathbf{B} = \frac{1}{a}\begin{bmatrix} 0 & 0 & H_o \\ 0 & 0 & 0 \\ g & 0 & g \end{bmatrix} \tag{4.9}$$

$$\mathbf{C} = \begin{bmatrix} 0 & 0 & -\frac{H_o}{a}\tan\phi \\ 0 & 0 & -\left(f + \frac{U_o}{a}\tan\phi\right) \\ 0 & f + \frac{2U_o}{a}\tan\phi & 0 \end{bmatrix} \tag{4.10}$$

$$\mathbf{D} = \begin{bmatrix} r & 0 & 0 \\ & r & \frac{1}{a}\frac{\partial U_o}{\partial\phi} \\ 0 & 0 & r \end{bmatrix} \tag{4.11}$$

The partition of the operator between matrices **C** and **D** at this point is completely arbitrary, and the choice made in (4.10)-(4.11) is based on the properties of the numerical scheme to be discussed in the subsection *Numerics*, below.

4.2.2 Model input

Basic state

The zonal wind is taken as changing slowly in time from an initial field U_1 to another U_2, in a characteristic time interval τ , centered at $t = t_*$. Namely,

$$U_o(\phi, t) = \alpha_1(t)U_1(\phi) + \alpha_2(t)U_2(\phi) \tag{4.12}$$

where

$$\alpha_1(t) = \frac{1}{2}\left[1 - \tanh\left(\frac{t-t_*}{2\tau}\right)\right]$$
$$\alpha_2(t) = \frac{1}{2}\left[1 + \tanh\left(\frac{t-t_*}{2\tau}\right)\right] \tag{4.13}$$

The height $H_o(\phi, t)$ is found by integrating the balance equation (4.4), imposing $H_o = 10$km at the equator. The reference zonal winds U_1 and U_2 are specified in terms of the prototype wind

$$U(\phi) = \left[A \sin^2(2f(\phi)) - B\right] \cos\phi \tag{4.14}$$

where

$$f(\phi) = \begin{cases} \phi & \text{if } |\phi| > \phi^* \\ \left[1 + \frac{\epsilon}{\tilde{\phi}}(\tilde{\phi} - \phi)\right]\phi & \text{if } |\phi| < \phi^* \end{cases} \tag{4.15}$$

with $\tilde{\phi} = \text{sign}(\phi)\phi$. In (4.15) ϕ^* is a reference latitude and ϵ is related to the position of the critical line. Thus, U_1 and U_2 are specified in terms of the parameters (A, B, ϕ^*, ϵ). Figure 4.1 shows U_1 and U_2 corresponding to $(A, B, \phi^*, \epsilon) = (35, 0, 0.8, 0)$ and $(A, B, \phi^*, \epsilon) = (40, 5, 0.8, -1)$. Observe that changes of U_o are restricted to latitudes within $\pm$ 45 degrees. These two zonal winds define the *control* basic states which will be used in most of chapter 5.

Topography

The topography is calculated using the spherical harmonic expansion given by Sankar-Rao (1965). Only zonal wave numbers 1, 2, and 3

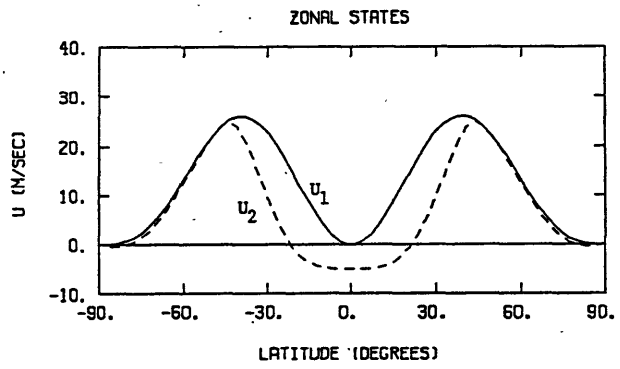

Figure 4.1: Zonal winds (in m s^{-1}) for the parameters (A, B, ϕ^*, ϵ) = (35,0,0.8,0), full line, and (A, B, ϕ^*, ϵ), dashed line.

are included. Figure 4.2 shows the amplitude of the topographic forcing (short dashed line) for these wavenumbers, where the meridional wavenumber extends up to $\ell = 14$[1]. The Sankar-Rao representation is a smoothed version of the Fourier decomposition of topography at 5 degrees latitude intervals given by Peixoto et al. (1964).

Thermal forcing

The meridional structure of the thermal forcing for zonal wavenumbers 1,2 and 3 is taken from Jacqmin and Lindzen (1985) and interpolated in terms of associated Legendre functions. The resulting function is multiplied by a Gaussian envelope in order to render it negligible out-

[1]The horizontal structure of the topography will be shown in connection with the baroclinic model.

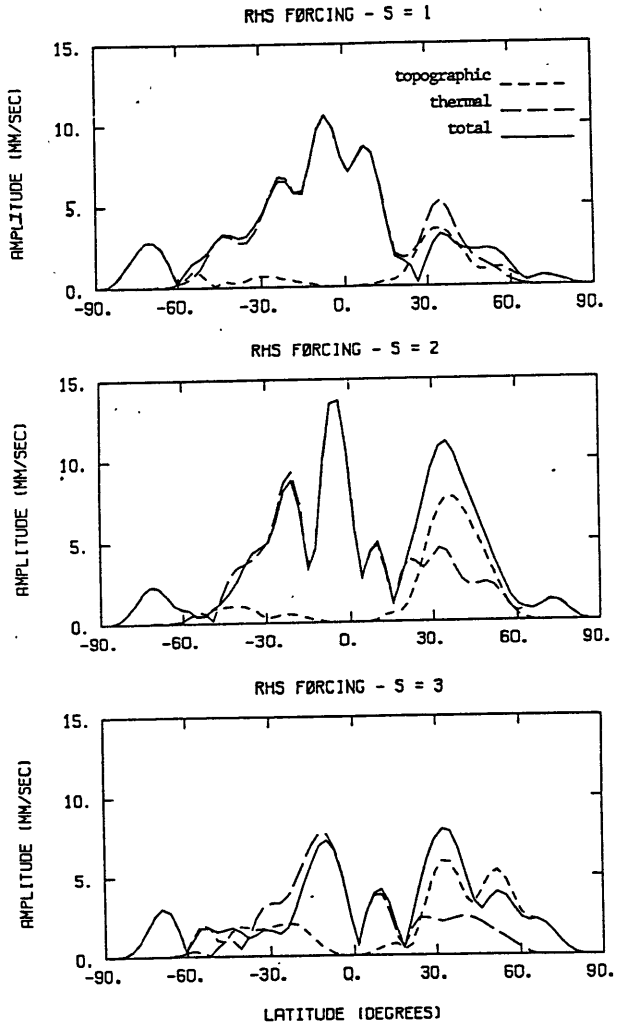

Figure 4.2: Amplitude of the right-hand side forcing [Eq. 4.7] for zonal wavenumvers 1, 2 and 3 (in mm s^{-1}): topographic forcing computed with zonal wind U_1 (see fig. 4.1), short dashed line; thermal forcing, long dashed line; amd total forcing (topographic + thermal), full line.

side (60S, 60N). This forcing is related to latent heat release and was computed from rainfall data. The maximum divergence associated with the waves (zonal wavenumbers 1,2, and 3) corresponds to a rainfall rate of approximately 5mm/day. In figure 4.2[2] we show the amplitude of the thermal forcing (long dashed line) in units mm/sec, for each zonal wavenumber. For comparison, the total forcing (full line) is also shown. The forcing in the tropics is predominantly thermal.

Initial condition

The initial condition is taken as the stationary solution associated with the initial zonal wind U_1 , i. e.,

$$\left(\frac{\partial}{\partial\lambda}\mathbf{A}+\frac{\partial}{\partial\phi}\mathbf{B}+\mathbf{C}+\mathbf{D}\right)\mathbf{W}_S=\mathbf{F} \tag{4.16}$$

With topographic forcing only, a constant (r_c) 15-day linear damping is used. When thermal forcing is included, a 5-day tropical damping (r_{trop}) is added within (-20N, 20N). This damping is introduced in order to reduce the amplitude of disturbances excited at the tropics. Presumably, part of these disturbances would propagate vertically in a baroclinic model (see chapter 6); also, thermal forcing is inevitably associated with cumulus friction. The numerical algorithm to compute $\mathbf{W_S}$ is described next.

[2]The horizontal structure of the thermal forcing will be shown in connection with the baroclinic model.

4.2.3 Numerics

Time dependent model

The linearized shallow water equations (4.6) are integrated in time using a fully implicit finite-difference scheme (Cohn et al., 1985, hereafter referred to as C), which is second order accurate in time and fourth order accurate in space. Detailed analysis of stability and accuracy may be found in C and Augenbaum et al. (1985 a, b). It proved to be necessary to apply a Shapiro Filter (Shapiro, 1970) in order to eliminate some small scale eddies at the polar latitudes. The filter was applied to the increments $\Delta\hat{h}$, $\Delta\hat{v}$, Δh, Δv (see C for notation) rather than to **W** itself, in a way which does not alter the order of accuracy of the scheme. The resolution used in the experiments is as follows

$$\begin{aligned} \Delta\lambda &= 5.6 \text{ degrees} \\ \Delta\phi &= 2.8 \text{ degrees} \\ \Delta t &= 30 \text{ minutes} \end{aligned}$$

for a time span of 30 days. Notice that in this implementation we did not use a spectral method for the zonal direction.

The code was tested using a *prescribed solution* technique (Marchesin, 1984; Dee and da Silva, 1986) in which the right hand side of the differential equation is modified in such a way that the exact solution of the initial value problem is known. Knowing the exact solution, the

truncation error of the numerical scheme can be studied in detail. In particular, the scheme was verified to be second order accurate in time and fourth order accurate in space, as expected.

Stationary Solution

The stationary solution $\Delta \mathbf{W}_S$, satisfying eq. (4.16), is computed using a fourth order semi-spectral method. The approximation in the latitudinal direction is consistent with the scheme used to integrate the time dependent model. In the longitudinal direction a spectral method is used, which differs from the finite difference scheme of the time dependent model. The stationary solution defined this way was taken as the initial condition and verified to be sufficiently close to the stationary solution of the time dependent model for the time interval considered in section 4. Next, we briefly described the procedure to obtain the stationary solution.

Writing the forcing and dependent variables as[3]

$$\mathbf{W}_S = Re\left[\sum_s \mathbf{W}^{(s)}(\phi)e^{is\lambda}\right] \tag{4.17}$$

$$\mathbf{F} = Re\left[\sum_s \mathbf{F}^{(s)}(\phi)e^{is\lambda}\right] \tag{4.18}$$

[3]The subscript S denoting *stationary* has been dropped and the superscript (s) labels the zonal wavenumber.

the equation satisfied by the complex field $\mathbf{W}^{(s)}$ are easily shown to be

$$\left(\frac{\partial}{\partial\lambda}\mathbf{B}+\mathbf{E}^{(s)}\right)\mathbf{W}^{(s)}=\mathbf{F}^{(s)} \tag{4.19}$$

where

$$\mathbf{E}^{(s)}=\mathbf{C}+\mathbf{D}+is\mathbf{A} \tag{4.20}$$

Using again a fourth order Pade derivative formula to approximate , the discrete version of (4.19) becomes

$$\left[\frac{\mu\delta}{\Delta\phi}\mathbf{B}+\left(I+\frac{\delta^2}{6}\right)\mathbf{E}^{(s)}\right]\mathbf{W}^{(s)}=\left(I+\frac{\delta^2}{6}\right)\mathbf{F}^{(s)} \tag{4.21}$$

where $\Delta\phi$ is the mesh size in the latitudinal direction and μ, δ are the grid operators defined below

$$\begin{aligned}\mu\mathbf{W}_j&=\frac{1}{2}\left(\mathbf{W}_{j+\frac{1}{2}}+\mathbf{W}_{j-\frac{1}{2}}\right)\\ \delta\mathbf{W}_j&=\mathbf{W}_{j+\frac{1}{2}}-\mathbf{W}_{j-\frac{1}{2}}\end{aligned} \tag{4.22}$$

Eq. (4.21) corresponds to a complex block-tridiagonal linear system of equations, and is solved using a standard Gaussian elimination technique.

The use of a spectral method in the zonal direction breaks the symmetry which allows us to consider the domain as double periodic in the time dependent model. For this reason, boundary conditions at the polar regions are required. For the particular grid considered

$$\phi_j=-\frac{\pi+\phi}{2}+j\Delta,\ j=1,...,J \tag{4.23}$$

the boundary conditions were specified as follows

$$\begin{aligned} \mathbf{W}_{j=0} &= \mathbf{S}\mathbf{W}_{j=1} \\ \mathbf{W}_{j=J+1} &= \mathbf{S}\mathbf{W}_{j=J} \end{aligned} \tag{4.24}$$

where **S** is the 3x3 matrix

$$\mathbf{S} = (-1)^s \begin{bmatrix} 1 & 0 & 0 \\ 0 & -1 & 0 \\ 0 & 0 & -1 \end{bmatrix} \tag{4.25}$$

Observe that no accuracy is lost at the boundaries. These conditions are derived by constructing each zonal component on the bi-dimensional grid and transposing the arrays in such a way that the domain appear to be periodic in the meridional direction. As mentioned in C, the sign of the wind components must be reversed on those elements in an *eastern* hemisphere.

The latitudinal mesh size was taken to be

$$\Delta\phi = 2.8 \text{ degrees} \tag{4.26}$$

based on grid refinements experiments. This value of $\Delta\phi$ is consistent with Nigam's (1986, fig. 3b) calculations for a quasi-geostrophic model using a second order accurate difference formula. Notice that this resolution and the dissipation used (r = 1/20 days) ensures that the critical line is absorptive. The code was further tested using the stationary solution as an initial condition for the time dependent model with a steady zonal wind.

Construction of Hough harmonics

The spectral analysis of the transients is performed using Hough modes as the basis functions, rather than the adjoint normal modes of the numerical model. This procedure is consistent with the way atmospheric data have been examined, as discussed in the *background* chapter. Amplitude and phase of the spectral coefficients are defined as in Lindzen et al. (1984).

The Hough harmonics used in the spectral decomposition analysis were computed using the software package described in da Silva and Dee (1985). In this implementation, expansion coefficients for the Hough functions, in terms of associated Legendre functions, are precomputed and stored on a disk file, which serves as a data basis for all the experiments. In all runs the equivalent depth was set equal to 10km.

4.3 The baroclinic model

4.3.1 Introduction

This section describes the stationary and time-dependent primitive equation model to be used in chapter 6. The models are designed with the following points in mind:

- The stationary waves should be properly resolved vertically and meridionally, so that their sensitivity to small changes in wind can be studied. Also, dissipation and resolution should be such that critical lines are absorptive;
- The models should be global (opposed to hemispheric) in order to allow inter-hemispheric propagation of transients, should this be the case;
- For economy, emphasize the troposphere and lower stratosphere (top of the model at 10 mb);
- The time-dependent and stationary models should be as compatible as possible, in order to make possible a clear definition of transients and a steady solution.

The details of implementation are given below.

4.3.2 Model equations

We start from the hydrostatic nonlinear primitive equations in sigma coordinates, on the sphere, in the presence of linear dissipation:

$$\frac{du}{dt} - \left(f + \frac{u}{a}\tan\phi\right)v + \frac{1}{a\cos\phi}\left(\frac{\partial\Phi}{\partial\lambda} + c_p\theta\frac{\partial p^\kappa}{\partial\lambda}\right) + ru = X \quad (4.27)$$

$$\frac{dv}{dt} + \left(f + \frac{u}{a}\tan\phi\right)u + \frac{1}{a}\left(\frac{\partial\Phi}{\partial\phi} + c_p\theta\frac{\partial p^\kappa}{\partial\phi}\right) + rv = Y \quad (4.28)$$

$$\frac{d\Pi}{dt} + \frac{\Pi}{a\cos\phi}\left[\frac{\partial u}{\partial \lambda} + \frac{\partial}{\partial \phi}(v\cos\phi)\right] + \Pi\frac{\partial \dot{\sigma}}{\partial \sigma} = 0 \quad (4.29)$$

$$\frac{d\theta}{dt} + \gamma\theta = p^{-\kappa}\frac{Q}{c_p} \quad (4.30)$$

$$\frac{\partial \Phi}{\partial \sigma} = -c_p\theta\frac{\partial p^{\kappa}}{\partial \sigma} \quad (4.31)$$

where

$$\Pi = \frac{p - p_{top}}{\sigma} \quad (4.32)$$

and

$$\frac{dA}{dt} = \frac{\partial A}{\partial t} + \frac{u}{a\cos\phi}\frac{\partial A}{\partial \phi} + \frac{v}{a}\frac{\partial A}{\partial \phi} + \dot{\sigma}\frac{\partial A}{\partial \sigma} \quad (4.33)$$

Most of the symbols above have their conventional meteorological meaning. For a complete list of symbols, see Appendix A. The exception is the potential temperature, that is defined here as

$$\theta = p^{-\kappa}T \quad (4.34)$$

The boundary conditions are the usual constraint of no flow across the boundaries

$$\dot{\sigma} = 0, \quad \text{at} \quad \sigma = 0, 1 \quad (4.35)$$

In order to minimize reflection from the upper boundary a sponge layer is specified in the uppermost levels. The above equations are linearized around a zonally symmetric basic state

$$u = U_o(\phi, \sigma, t) + u'$$

$$v = V_o(\phi,\sigma,t) + v'$$

$$\dot{\sigma} = \dot{\Sigma}_o(\phi,\sigma,t) + \dot{\sigma}'$$

$$\Pi = \Pi_o(\phi,\sigma,t) + \Pi'$$

$$\theta = \Theta_o(\phi,\sigma,t)\theta'$$

$$\Phi = \Phi_o + \Phi'$$

For wave-like perturbations of the form

$$u' = u'_s(\phi,\sigma)e^{\imath s\lambda}, \text{ etc...} \tag{4.36}$$

the *dimensional* time-dependent form of the linear equations is[4]

$$\frac{\partial u}{\partial t} + \frac{V_o}{a}\frac{\partial u}{\partial \phi} + \dot{\Sigma}_o\frac{\partial u}{\partial \sigma} + \left(\imath\frac{U_o s}{a\cos\phi} - \frac{V_o}{a}\tan\phi + r\right)u - \left(f + \frac{U_o}{a}\tan\phi\right)v - \frac{1}{a}\frac{\partial U_o}{\partial \phi}v + \frac{\partial U_o}{\partial \sigma}\dot{\sigma} + \frac{\imath s}{a\cos\phi}(\Phi + G_o\Theta_o)\Pi = X \tag{4.37}$$

$$\frac{\partial v}{\partial t} + \frac{V_o}{a}\frac{\partial v}{\partial \phi} + \dot{\Sigma}\frac{\partial v}{\partial \sigma} + + \left(f + \frac{2U_o}{a}\tan\phi\right)u + \left(\imath\frac{U_o s}{a\cos\phi} + \frac{1}{a}\frac{\partial V_o}{\partial \phi + r}\right)v + \frac{\partial V_o}{\partial \sigma}\dot{\sigma}\frac{1}{a}\frac{\partial \Phi}{\partial \phi} + G_o\Theta_o\frac{\partial \Pi}{\partial \phi} = Y \tag{4.38}$$

[4]To simplify the notation, from now on we omit the subscript s denoting the zonal wave number and the prime denoting a perturbation quantity.

$$\frac{\partial\theta}{\partial t} + \frac{V_o}{a}\frac{\partial\theta}{\partial\phi} + \dot{\Sigma}_o\frac{\partial\theta}{\partial\sigma} + \frac{1}{a}\frac{\partial\Theta_o}{\partial\phi}v + \frac{\partial\Theta_o}{\partial\sigma}\dot{\sigma} + \left(\imath\frac{U_o s}{a\cos\phi} + \gamma\right)\theta + H_o\dot{\Sigma}_o\frac{\partial\Theta_o}{\partial\sigma}\Pi = Q_o Q \tag{4.39}$$

$$\frac{\partial\Pi}{\partial t} + \Pi_o\frac{\partial\dot{\sigma}}{\sigma} + \imath\frac{U_o s}{a\cos\phi}\Pi + \frac{\Pi_o}{a\cos\phi}\left(\frac{\imath s}{a\cos\phi}u + \frac{\partial}{\partial\phi}v\cos\phi\right) = 0 \tag{4.40}$$

$$\frac{\partial\Phi}{\partial\sigma} = R_o\theta + S_o\Theta_o\Pi \tag{4.41}$$

The quantities G_o, R_o, S_o, H_o and Q_o are functions only of the basic state variable Π_o and will appear throughout this thesis. They are defined below.

$$P_o = \Pi_o\sigma + p_{top} \tag{4.42}$$

$$G_o = RP_o^{\kappa-1}\sigma \tag{4.43}$$

$$R_o = c_p\frac{\partial P_o^{\kappa}}{\partial\sigma} \tag{4.44}$$

$$S_o = -R\frac{\partial}{\partial\sigma}\sigma P_o^{\kappa-1} \tag{4.45}$$

$$H_o = \frac{\kappa\sigma}{P_o} \tag{4.46}$$

$$Q_o = \frac{P_o^{-\kappa}}{c_p} \tag{4.47}$$

(4.48)

The time-dependent model is solved numerically with the equations in their dimensional form as given above. However, the stationary model requires the equations to be in non-dimensional form in order to avoid an ill-conditioned matrix [5]. Therefore we non-dimensionalize the equations using the following factors:

$$(x_*, y_*) = a(x, y)$$

$$t_* = \Omega^{-1} t$$

$$(u_*, v_*) = \Omega a(u, v)$$

$$\sigma_* = \Omega \sigma$$

$$\theta_* = \frac{\Omega^2 a^2}{R \Pi_o^\kappa} \theta$$

$$\Phi_* = \Omega^2 a^2$$

$$\Pi_* = \Pi_o \Pi$$

[5] An early implementation had the equations in dimensional form which indeed gave a poorly conditioned matrix.

In the above equations the subscript $*$ denotes a dimensional quantity. The stationary, non-dimensional form of eqs. 4.37 — 4.41 is therefore given by

$$V_o\frac{\partial u}{\partial \phi} + \dot{\Sigma}_o\frac{\partial u}{\partial \sigma} + \left(\imath\frac{U_o s}{\cos\phi} - V_o\tan\phi + r\right)u - (2\sin\phi + U_o\tan\phi)\,v - \frac{\partial U_o}{\partial \phi}v + \frac{\partial U_o}{\partial \sigma}\dot{\sigma} + \frac{\imath s}{\cos\phi}(\Phi + G_o\Theta_o\Pi) = X \tag{4.49}$$

$$V_o\frac{\partial v}{\partial \phi} + \dot{\Sigma}\frac{\partial v}{\partial \sigma} + (2\sin\phi + 2U_o\tan\phi)\,u\left(\imath\frac{U_o s}{\cos\phi} + \frac{\partial V_o}{\partial \phi} + r\right)v + \frac{\partial V_o}{\partial \sigma}\dot{\sigma} + \frac{\partial \Phi}{\partial \phi} + G_o\Theta_o\frac{\partial \Pi}{\partial \phi} = Y \tag{4.50}$$

$$V_o\frac{\partial \theta}{\partial \phi} + \dot{\Sigma}_o\frac{\partial \theta}{\partial \sigma} + \frac{\partial \Theta_o}{\partial \phi}v + \frac{\partial \Theta_o}{\partial \sigma}\dot{\sigma} + \imath\left(\frac{U_O s}{\cos\phi} + \gamma\right)\theta + H_o\dot{\Sigma}_o\frac{\partial \Theta_o}{\partial \sigma}\Pi = Q_o Q \tag{4.51}$$

$$\frac{\partial \dot{\sigma}}{\sigma} + \imath\frac{U_o s}{\cos\phi}\Pi + \frac{1}{\cos\phi}\left(\imath s u + \frac{\partial}{\partial \phi}v\cos\phi\right) = 0 \tag{4.52}$$

$$\frac{\partial \Phi}{\partial \sigma} = R_o\theta + S_o\Theta_o\Pi \tag{4.53}$$

The non-dimensional form of the auxiliary quantities G_o, R_o, etc.., reads

$$P_o = \sigma + \frac{p_{top}}{\Pi_o}$$

$$G_o = P_o^{\kappa-1}\sigma$$

$$R_o = -P_o^{\kappa-1}$$

$$S_o = -P_o^{\kappa-1}\left(1+\frac{\kappa-1}{P_o}\sigma\right)$$

$$H_o = \kappa P_o^{-(\kappa+1)}\sigma$$

$$Q_o = P_o^{-\kappa}$$

Even though it is not apparent from eqs. 4.49-4.50, the topographic forcing enters the momentum equations. It can easily seen if we write the hydrostatic equation in integral form

$$\Phi = \Phi_T - \int_\sigma^1 (R_o\theta + S_o\Theta_o\Pi)\,d\sigma \tag{4.54}$$

$$\equiv \Phi_S + \tilde{\Phi} \tag{4.55}$$

where Φ_S denotes the topographic height multiplied by the gravity constant, properly non-dimensionalized. Upon substitution into the momentum equations we get

$$V_o\frac{\partial u}{\partial\phi} + ... + \frac{\imath s}{\cos\phi}\left(\tilde{\Phi} + G_o\Theta_o\Pi\right) = -\frac{\imath s}{\cos\phi}\Phi_T \tag{4.56}$$

$$V_o\frac{\partial v}{\partial\phi} + ... + \frac{\partial\tilde{\Phi}}{\partial\phi} + G_o\Theta_o\frac{\partial\Pi}{\partial\phi} = -\frac{\partial\Phi_T}{\partial\phi} \tag{4.57}$$

In order to facilitate comparison with other studies, the fields are expressed in terms of the log-σ coordinates described in section 4.3.4 be-

low. In addition, we will show the geopotential height in p-coordinates, which is not the same quantity in σ-coordinates. We use the simple transformation

$$\Phi_{pressure} = (\Phi_{sigma} + G_o \Theta_o \Pi) \tag{4.58}$$

to perform the conversion. It should be noted that the geopotential height in pressure coordinates as given above is the quantity in approximate geostrophic balance with the zonal and meridional winds.

Model basic state, forcing, dissipation, as well the numerics, will be presented in the following sections.

4.3.3 Model inputs

Basic state

Even though the models were designed to allow a meridional circulation, the results presented in this thesis will not use this feature. Therefore, we set

$$V_o = \dot{\Sigma}_o = 0 \tag{4.59}$$

We specify the zonal wind U_o and compute the basic state potential temperature using the thermal wind relation. From the v-momentum

equation and the hydrostatic equation one has [6]

$$\frac{1}{a}\frac{\partial \Phi_o}{\partial \phi} = -\left(f + \frac{U_o}{a}\tan\phi\right) U_o \tag{4.60}$$

$$\Theta_o = \frac{1}{R_o}\frac{\partial \Phi_o}{\partial \sigma} \tag{4.61}$$

Integrating eq. 4.60 with respect to ϕ and substituting in 4.61 we find the expression of Θ_o in function of U_o

$$\Theta_o = \frac{1}{R_o}\frac{\partial}{\partial \sigma}\left[-\int_{-\pi/2}^{\phi}\left(f + \frac{U_o}{a}\tan\phi'\right) U_o d\phi' + \chi(\sigma)\right] \tag{4.62}$$

$$= \Theta_U(\sigma,\phi) + \chi(\sigma) \tag{4.63}$$

The integration constant $\chi(\sigma)$ is determined by specifying the basic state temperature at 45N

$$\chi(\sigma) = \Theta_o(\sigma, \phi = 45N) - \Theta_U(\sigma, \phi = 45N) \tag{4.64}$$

The stationary model produced poor simulations when the basic state potential temperature was specified exactly as above. After some sensitivity experiments, it was determined that Θ_o should be specified only as a function of σ on a thin boundary layer near the surface (below 750mb). The time dependent model showed a higher sensitivity on the static stability parameter $-\partial\Theta_o/\partial\sigma$, which in turn made the model numerically unstable after day 1 of integration. In order to handle this limitation in the time dependent model we set the static stability parameter entering the thermodynamic equation to its value at 45N. The stationary solution showed negligible sensitivity to this choice. In fig.

[6] In this subsection we will use the *dimensional* form of the equations.

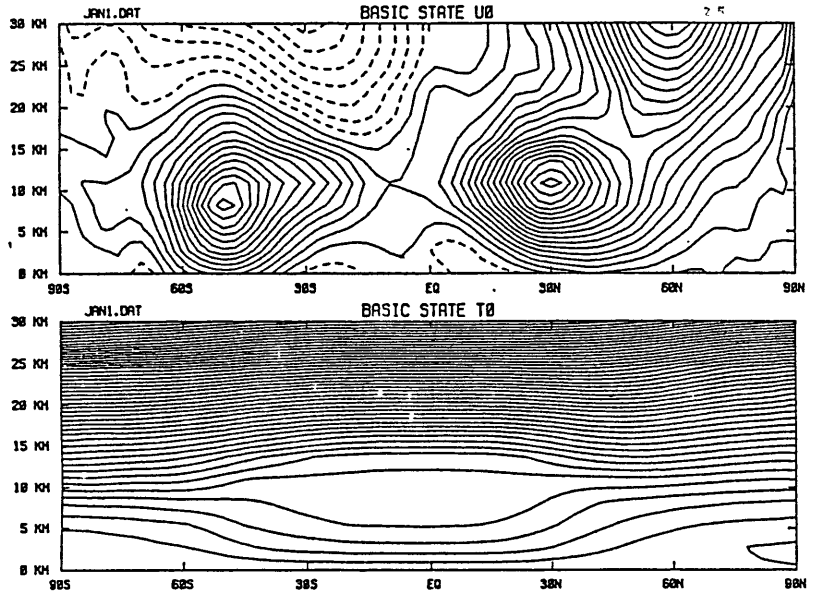

Figure 4.3: Baroclinic model basic state zonal wind (contour interval: 2.5 m/sec) and potential temperature (countour interval: 3.6 K), as a function of latitude and height.

4.3 we show the control basic state fields computed as above. The zonal wind is the monthly average for January '79 plotted from the FGGE level III-b gridded data prepared by the the ECMWF (Bengstsson et al, 1982). Most basic states considered in this thesis will be taken as a perturbation superimposed on this control case. They will be presented in the sections where they are discussed. The time-dependence of the basic state zonal wind is specified as in the barotropic model (see eq. 4.12).

Topography

The topography is calculated as in the barotropic model. Figure 4.4 shows the topographic height with the zonal mean removed. On the northern hemisphere, the most prominent feature is the Tibetan plateau with the Rocky mountains and Greenland being of secondary importance. The southern hemisphere topography is dominated by Antarctica at very high latitudes. The major features in the subtropics are the Andes and the African plateau. Notice that at this zonal truncation, the Andes are reduced to about 700 meters, much less than the 1800 meters of Antarctica.

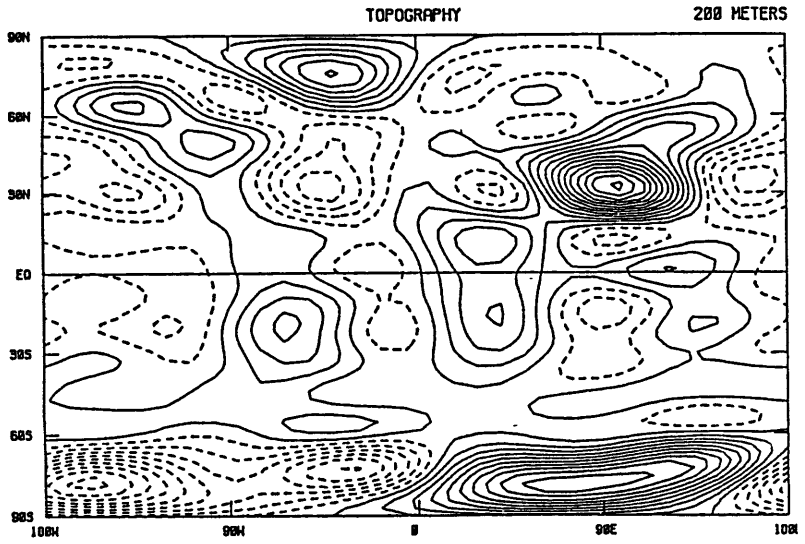

Figure 4.4: Topographic height in meters with zonal mean removed (contour interval: 200 meters).

Heating

The meridional structure of the thermal forcing for each zonal wavenumber is again taken from Jacqmin and Lindzen (1985) and interpolated to our grid using cubic splines. The vertical structure of the heating is specified as a single function of altitude, given in fig. 4.5. This vertical structure is typical of tropical latitudes and it is not very appropriate for mid- and high-latitudes, where the depth of the heating field should be decreased to about 6 km. The horizontal distribution of the thermal forcing for the entire globe is depicted in fig. 4.6. In the tropics one can distinguish the three regions of major convection activity: Indonesia (around 180), Africa (around 90E) and the Amazon (around 90E). The maximum heating rate is about 1.5 degrees / day. This value seems to be somewhat smaller than the values for latent heat used in similar studies (e.g. Nigam et al., 1988). In the northern hemisphere mid- and high-latitudes the magnitudes are consistent with the GCM values of Nigam et al. (1988). The phase, however, has great discrepancies near the eastern coast of the United States. The magnitude of the thermal forcing is of fundamental importance to the ongoing debate about the relative importance of thermal and orographic forcing on the stationary wave response. We will return to this point in section 6.2.

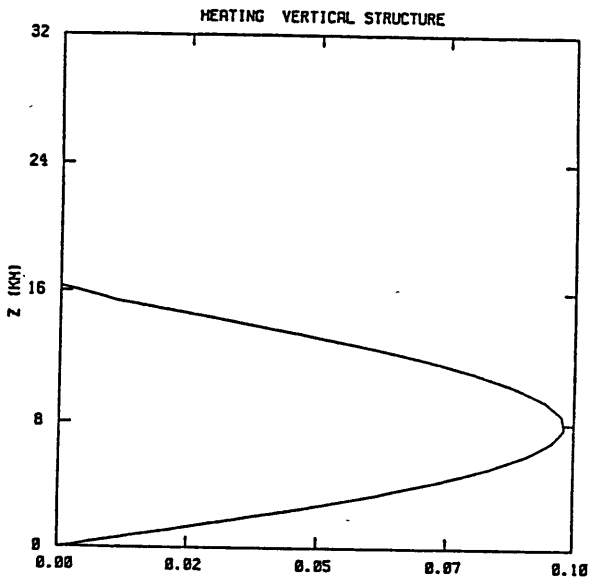

Figure 4.5: Vertical structure of the thermal forcing. It is defined such that its vertical average is equal to 1.

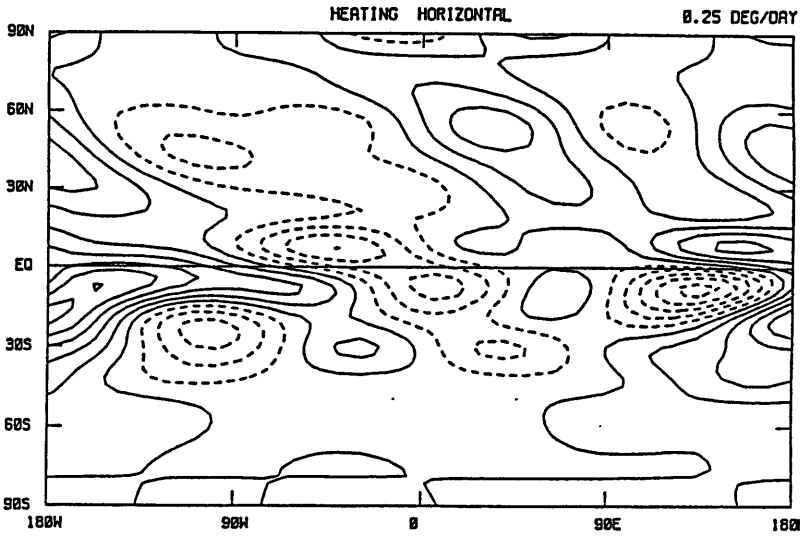

Figure 4.6: Horizontal structure of thermal forcing (contour interval: 0.25 K/day).

Table 4.1: Parameters for *standard, no boundary layer, strong,* and *critical layer* damping.

parameter	standard	no b.l.	strong	no c.l.
$1/a_1$ (days)	10	10	5	10
$1/a_2$ (days)	1.25	0	1.25	1.25
δp (mb)	300	300	300	300
ϕ_w (degrees)	20	20	20	20
$r_{2_{max}}$ (days)	9999	9999	9999	2

Dissipation

Rayleigh friction introduced in the momentum equations is given by

$$r = \cos\phi \max(r_1, r_2) \tag{4.65}$$

where r_1 is specified as in Jacqmin and Lindzen (1985) plus a boundary layer drag

$$r_1 = \left(a_1 + a_2 \exp\left(\frac{p - p_{surf}}{\delta p}\right)\right)\left(1 - \frac{2}{3}\tanh^2\frac{\phi}{\phi_w}\right) \tag{4.66}$$

Notice that a somewhat stronger damping applies to the tropics. The parameters a_1, a_2, etc. are given in table 4.3.3 for the 3 cases to be considered in this thesis: *standard, strong* and *no boundary layer* damping. The term r_2 is either zero or a Simmons-like critical layer damping. It will be used to check the model sensitivity to strong critical layer dissipation. It is given by

$$r_2^{-1} = \max\left[1/r_{2_{max}}(\frac{1}{2}\left(\frac{\cos\phi}{U_o}\right)^2\right] \tag{4.67}$$

In the above equation, U_o should be given in units m/sec. The term $\cos\phi$ in 4.65 was included to handle a numerical singularity of the stationary model near the poles. To avoid reflection from the lid at the upper boundary, a *sponge* layer was introduced in the uppermost levels extending to about 25 km. The final inverse Rayleigh damping (in days) field is shown in fig. 4.7a-d, for the 4 cases to be considered in this thesis. The zonal wind given in 4.3 was used to compute the critical layer shown here. For the *standard* case the average damping time scale is 20 days in mid-latitudes, with a higher damping near the surface to mimic a boundary layer drag. The *strong* damping case is defined such that the dissipative time scale in mid-troposphere is about half the standard case, the boundary layer drag remaining constant. Notice that for this particular basic state, with reduced easterlies in the tropics, the *critical layer* damping field is not very different from the *standard* case.

The Newtonian cooling is given by

$$\gamma^{-1} = \cos\phi \left[\left(c_1 + c_2 \ln \frac{p}{p_{surf}} \right) \left(1 - \exp\left(\frac{p - p_{surf}}{p_w} \right) \right) + c_3 \right] \quad (4.68)$$

The parameters c_1, c_2, etc..., are given below.

$$\begin{aligned} c_1 &= 117 \ days \\ c_2 &= 24 \ days \\ c_3 &= 1 \ day \\ p_w &= 600mb \end{aligned}$$

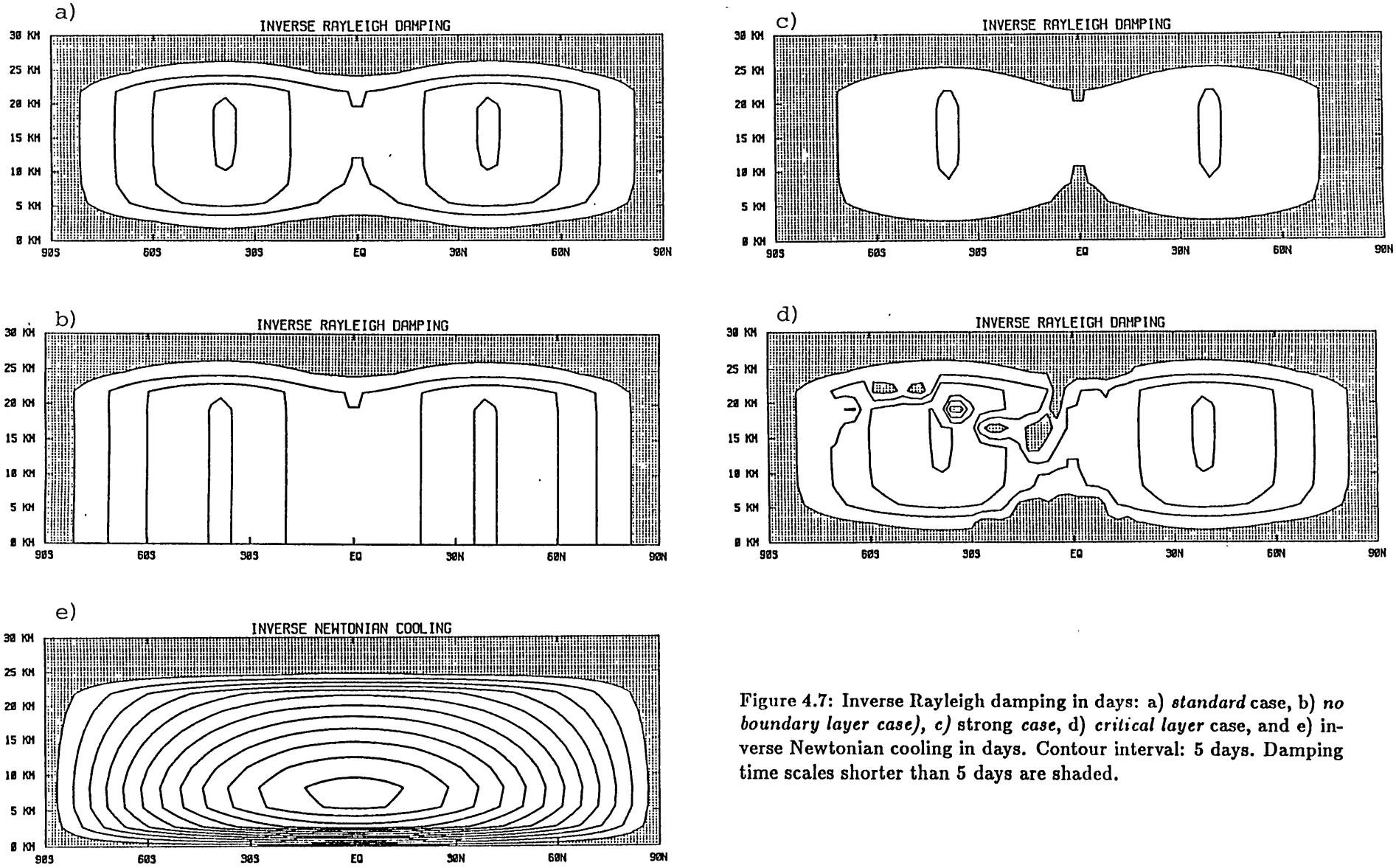

Figure 4.7: Inverse Rayleigh damping in days: a) *standard* case, b) *no boundary layer case), c)* strong *case*, d) *critical layer* case, and e) inverse Newtonian cooling in days. Contour interval: 5 days. Damping time scales shorter than 5 days are shaded.

The inverse Newtonian cooling field (in days) is shown in fig. 4.7e, where a *sponge* layer at the top most levels is also included. In mid latitudes, the inverse Newtonian cooling goes from about 1 day at surface, reaches 60 days at the upper troposphere/lower stratosphere and decreases to below 5 days above 25 km.

4.3.4 Numerics

Time-dependent model

The dimensional linear primitive equations 4.37—4.41 were integrated in time using an explicit Matsuno scheme (Matsuno, 1970). The prognostic and diagnostic steps were implemented in the standard way (Haltiner and Williams, 1980). Since the basic state does not depend on longitude, a semi-spectral method was used, in which the equations are independently integrated for each zonal wavenumber. Finite differences were used for the meridional and vertical directions. A fourth-order implicit Pade derivative formula was used to approximate the spatial derivatives. Boundary conditions at the polar latitudes were specified exactly, using the hemispheric continuation method described with the stationary barotropic model (section 4.2.3). Numerical boundary conditions at the top and bottom of the model were deduced as a 3 point uncentered Pade formula.

A uniform grid was used for the meridional direction. For most of the experiments, the meridional resolution was taken to be 2 degrees. Grid refinement experiments performed with the stationary model (see below) indicated no sizeable changes when the resolution was increased to 1 degree. Since stationary waves have their scales better determined in geometric coordinates, a non-uniform σ coordinate grid was specified. This grid was designed to be approximately uniform in log-p coordinates. Namely, we define the new coordinate

$$z = -H_o \ln \frac{p}{p_o} = -H_o \ln \left[\frac{\Pi_o \sigma + p_{top}}{\Pi_o + p_{top}} \right] \tag{4.69}$$

where H_o is a constant defined such that $z = 30$ Km at 10 mb. In this coordinate system we define a uniform grid:

$$z_k = (k-1)\Delta = \frac{k-1}{K-1} H_o \tag{4.70}$$

for k = 1, ..., K=18. With 18 levels, $\Delta z \approx 1.7$ Km. The σ-grid is obtained by inverting eq. (4.69). All quantities in this thesis are displayed with z as the vertical coordinate. Notice that it is equivalent to a log-σ coordinate system.

An alternate Matsuno / leap-frog scheme with an Asselim (1972) filter was also implemented. Early experiments failed to converge with reasonable time steps (a few minutes or so). With the Matsuno scheme exclusively, the time step used was

$$\Delta t = 2 \text{ minutes.}$$

With this time step no filtering was necessary. Early implementations of the model were tested with an extension of the prescribed solution technique described in Dee and da Silva (1987). The code was further tested with the initial condition being the stationary solution (see section 6.4).

Finally, the top and botton of the model are given by:

$$p_{surf} = 1013mb$$
$$p_{top} = 10mb$$

Stationary model

As the time-dependent model, the stationary model was solved separately for each zonal wave number and spatial discretization was performed with a fourth-order Pade scheme. This was done in order to achieve a maximum degree of compatibility between the two models. As mentioned before, the stationary model was implemented with the equations in nondimensional form.

In order to avoid a lengthy report of the details of implementation, we give here only a schematic description. First, the dependent variables Φ and $\dot{\sigma}$ are eliminated using the hydrostatic and thermodynamic equations (eqs. 4.53 and 4.51). The new system contains only 3 complex bi-dimensional variables (u, v and θ) and 1 one-dimensional

variable (II). After discretization is performed, the coupled system of equations can be put in the form

$$\mathbf{M}\mathbf{x} = \mathbf{f} \tag{4.71}$$

where M is a block tri-diagonal matrix, with each block having the dimension $(3K+1)^2$, K being the number of vertical layers (18). This system is solved using a standard Gaussian elimination procedure. In order to save storage, the subdiagonal blocks were not pre-computed and stored. Instead, the blocks were computed as the Gaussian elimination advanced. As a result, we only needed to store $2*J*(3K+1)^2$ entries of the matrix M.

Grid and resolution were taken as in the time-dependent model. Besides the compatibility test with the time-dependent model (section 6.4), an artificial RHS was specified to force the solution to be simple functions. This procedure was very helpful in isolating bugs early in the implementation.

4.3.5 Model diagnostics

In order to help interpret the results, the quasi-geostrophic index of refraction and the Plumb horizontal wave fluxes were implemented. Their expressions are given below. A short discussion of the method used to analyze Rossby waves is presented in the end of this section.

Quasi-geostrophic index of refraction

The quasi-geostrophic streamfunction on the sphere (multiplied by $\sqrt{p}/N$) can be shown to satisfy the following wave equation (e.g. Nigam and Lindzen, 1989)

$$\frac{1}{a^2 cos\phi}\frac{\partial}{\partial\phi}\left(cos\phi\frac{\partial\eta}{\partial\phi}\right)+\frac{f^2}{N^2}\frac{\partial^2\eta}{\partial z^2}+Q^2\eta=0 \qquad (4.72)$$

where Q^2, the quasi geostrophic index of refraction squared is given by

$$\begin{aligned} Q^2 &= -\frac{s^2}{a^2\cos^2\phi}-\left(\frac{f}{2HN}\right)^2-\frac{1}{U_o a^2}\frac{\partial}{\partial\phi}\frac{1}{\cos\phi}\frac{\partial}{\partial\phi}U_o\cos\phi+ \\ &\quad -\frac{f^2}{pU_o}\frac{\partial}{\partial z}\frac{p}{N^2}\frac{\partial U_o}{\partial z} \end{aligned} \qquad (4.73)$$

The quantity η is related to the quasi-geostrophic stream function by

$$\eta=\frac{\sqrt{p}}{N}\psi \qquad (4.74)$$

As is usually done, the scale height and static stability are assumed constant and the respective values are

$$\begin{aligned} H_o &= 7Km \\ N &= 2\text{x}10^{-2}\,s^{-1} \end{aligned}$$

Plumb's wave activity flux

First introduced by Plumb (1985), this wave activity flux is a useful diagnostic tool for the tri-dimensional propagation of stationary waves.

The meridional and vertical components, when zonally averaged, reduce to the well known EP flux vectors (e.g. Edmon et al., 1980) and have been extensively used to diagnose stationary waves. Here we will only deal with the horizontal component of this flux, which will suffice to illustrate the split of the wave train excited by the Himalayas when the subtropical jet shifts equatorward. Following Plumb (1985), the zonal and meridional components of the wave activity vector is given by

$$\mathbf{F} = (F_\lambda, F_\phi) \tag{4.75}$$

$$F_\lambda = \frac{p}{p_o}\cos\phi\left[v^2 - \frac{1}{2\Omega a \sin 2\phi}\frac{\partial}{\partial\lambda}v\Phi\right] \tag{4.76}$$

$$F_\phi = \frac{p}{p_o}\cos\phi\left[uv + \frac{1}{2\Omega a \sin 2\phi}\frac{\partial}{\partial\lambda}u\Phi\right] \tag{4.77}$$

The above formula was computed with the winds directly taken from the model and also with the geostrophic winds. Since in mid latitudes, where the vectors have their highest magnitudes, geostrophic balance is a very good approximation, it did not matter which formulation to apply. In the calculations presented in chapter 6 we use winds taken directly from the model.

Rossby wave analysis

There are several ways to analyze tri-dimensional data in terms of atmospheric normal modes. Dalley and Williamson (1985) computed the normal modes of the quasi-geostrophic wave equation on the sphere,

for a general flow depending on latitude and height. Using the concept of bi-orthogonality, they project atmospheric data on the numerically derived normal modes. This procedure is lengthy and there is no guarantee that the normal modes obtained this way are more *realistic* than, say, projection on simple external Hough modes. Ahlquist (1982) uses a best- fit technique to *extract* the Lamb external structure and then projects the data onto Hough functions. Lindzen et al. (1984) projects the observed fields at 500mb onto Hough modes.

The method used in this thesis is similar to Ahlquist's (1982). We simply vertically average the fields in the troposphere and lower stratosphere, having the Lamb wave structure $p^{-\kappa}$ as weight. We examined the sensitivity of the results to the highest level considered. No qualitative change was found, even though amplitudes tend to be slightly smaller (10%) when all levels are included in the average. The horizontal structures were expanded in terms of Hough modes, as in the barotropic calculation (section 4.2.3).

Chapter 5

Transients in a barotropic model

5.1 Introduction

This chapter examines the excitation of transients associated with changes in the stationary waves in a barotropic model. We chose the shallow water equations on the sphere, since it is the minimal model resolving ultralong Rossby waves. Stationary waves, on the other hand, are not appropriately treated with this kind of model, as vertical propagation is not taken into account. As we shall see, the shallow water equations have some peculiar behavior associated with the sensitivity of the stationary solution to shifts of the subtropical jet.

The emphasis of this chapter, as was the preliminary emphasis of

the thesis, is on the excitation of ultralong Rossby waves. Even though we find some Rossby wave excitation in this model, the baroclinic calculation of chapter 6 does not support this finding. The results found here are still of some interest, as they illustrate the mechanism of chapter 3 and show the limitations of the shallow water equations as a model of stationary waves in the atmosphere.

The procedure we follow here to examine the excited transients entails two parts. First, we analyze the difference in stationary solution associated with each one of the winds. Second, we investigate the role of dissipation, wave period and transition period on amplitude of transients, as their spatial structure is by and large determined by the difference in stationary solution. The numerical experiments can be schematically described as follows:

i) start with the stationary solution corresponding to the zonal wind $U_o = U_1$;

ii) change the zonal wind from U_1 to U_2, in a characteristic time interval τ;

iii) For $t > \tau$, subtract the stationary solution associated with U_2 and spectrally analyze the transients.

Another problem of interest, which is treated with more detail in the baroclinic calculation of chapter 6, is the establishment of the new

stationary solution. In the next section we briefly consider the evolution and spatial structure of the stationary waves in this model. The excitation of transient Rossby waves is considered in section 5.3.

5.2 Horizontal structure

In this section we analyze the horizontal structure of the difference in stationary solution, its sensitivity to different wind changes, and the establishment of the new stationary wave. A comparison with the theory of chapter 3 is done in the next section, in connection with Rossby waves.

5.2.1 The changes in stationary waves

The results of chapter 3, viz. eqs. (3.48)-(3.49) suggest that the excited transients consist approximately of the difference of the stationary solutions, modified by the factor ξ which depends on the dynamics of propagation of the transient waves. Hence, before we proceed to the integration of the time dependent model, it proves interesting to analyze in some detail the nature of these *differences*. The stationary wave difference field should be interpreted as an upper bound for the transients excited in the time dependent model, as the absolute value of ξ is always less than one. Below we examine the response to heat

and topography, as well as the effect of different wind changes.

Figure 5.1 shows the stereographic projection in the northern hemisphere of the stationary waves for the two different basic states, as well as the difference field. The basic states shown are the *control* case. The left panel shows the response to topography where the response with wind 2 has smaller amplitude but approximately the same phase. This result is consistent with the notion that the waves are absorbed in the critical line present with wind 2. Notice that the difference in stationary solution is concentrated downstream of the Himalayas. The right panel presents the response to thermal forcing. We see that the response with wind 2 is again smaller, but now there is some change in the phase of the disturbances between winds 1 and 2. The difference field in this case is global, consistent with the horizontal distribution of thermal forcing. Notice also that thermally forced stationary wave in this model is about three to four times greater than the topographic response.

In figure 5.2 we show the topographically forced stationary waves and difference fields for two different pairs of zonal winds. In the left panel we consider a equatorward shift of the subtropical jet. The stationary wave response associated with wind 2 (jet displaced equatorward) is reduced, and the wave train emanating from the Tibetan plateau propagates more to the south. This behavior is just the opposite of what we found with the baroclinic model (see chapter 6): there,

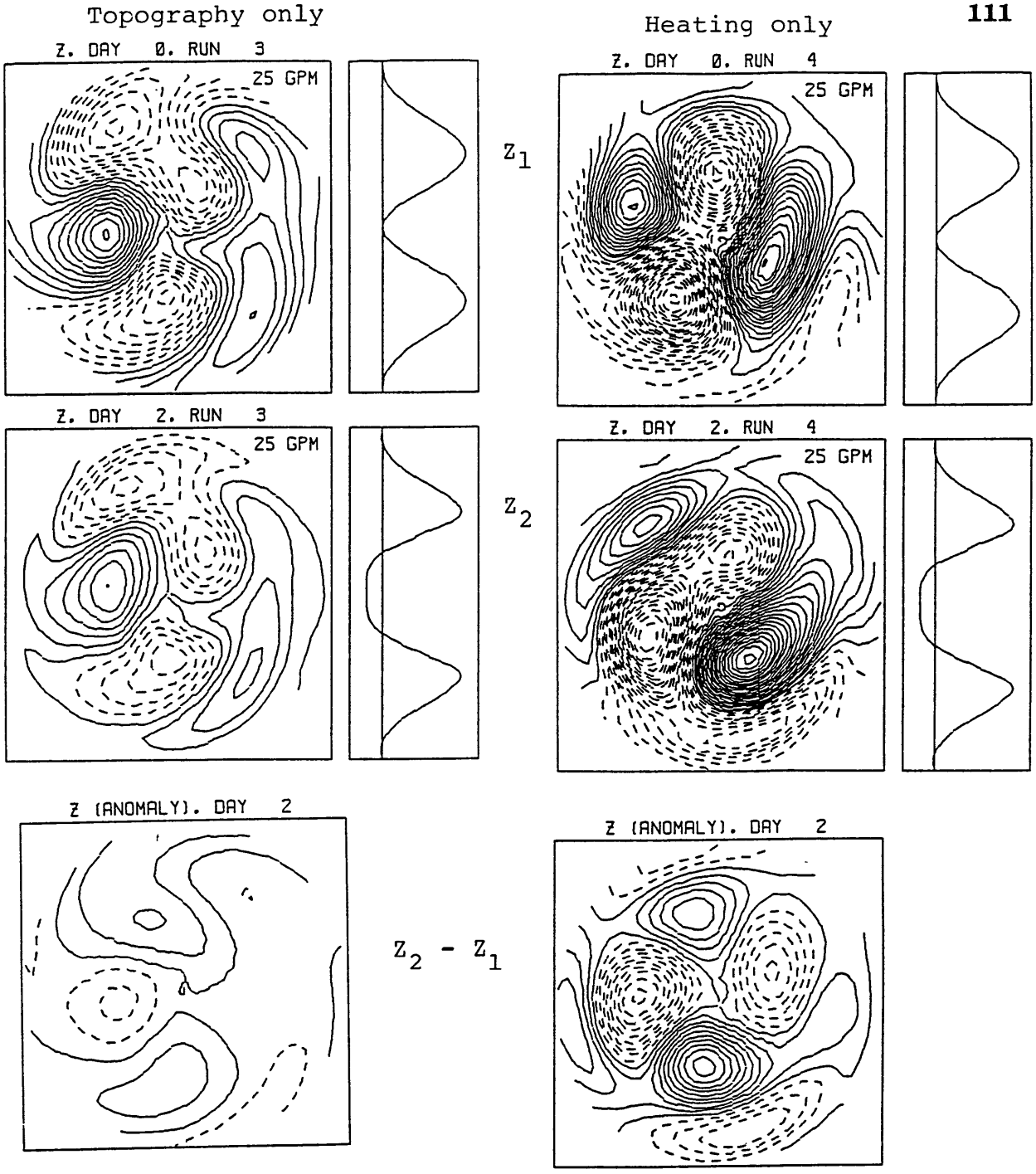

Figure 5.1: Horizontal structure of stationary wave field (geopotential height) and difference field, computed with the control basic states. Topographically forced waves (left panel) and thermally forced waves (right panel). Basic state shown next to the stationary waves. The contour interval is 25 meters for the stationary waves and 50 meters for the difference field. The fields are shown in stereographic projection in the northern hemisphere; the outer latitude is 20 degrees.

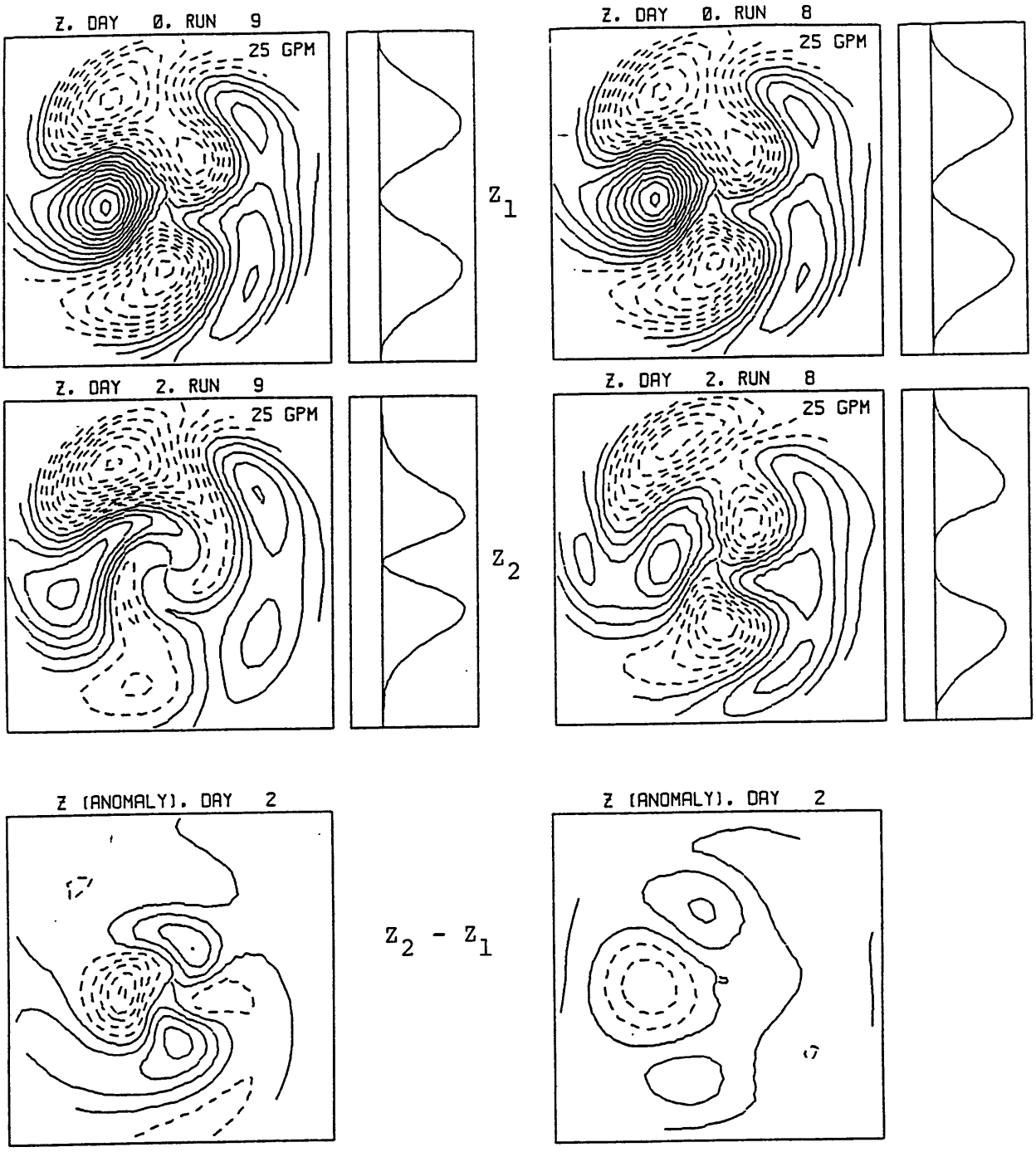

Figure 5.2: As in fig. 5.1 but for topographically forced waves and two different wind changes: jet shift (left panel) and jet weakening (right panel).

an equatorward shift of the jet gives an increased response in mid- and high-latitudes. The difference field shown in the left panel is about twice the difference field obtained with the *control* case and slightly displaced northward. In the right panel we show the response to a change in magnitude of the zonal winds, with wind 1 being as in the control case. The result of a reduction in wind magnitude is not only a decrease in stationary amplitude but also a partial split of the wave train excited by the Himalayas. The difference field in this case is very similar to the control case showed in the left panel of fig. 5.1.

In summary, the difference in stationary solution for various wind changes is very large scale and likely to project onto ultralong Rossby waves. The difference field for the topographically forced waves is concentrated downstream of the Tibetan plateau.

5.2.2 The establishment of the new stationary solution

Next, we consider an example of the time evolution of the geopotential field. We will show that the establishment of the new stationary solution in attained through propagation of *information* with the group velocity of quasi-stationary Rossby waves.

Figure 5.3 depicts the time evolution of the geopotential height, with the control basic states changing in a time interval $\tau = 14$ days.

a)

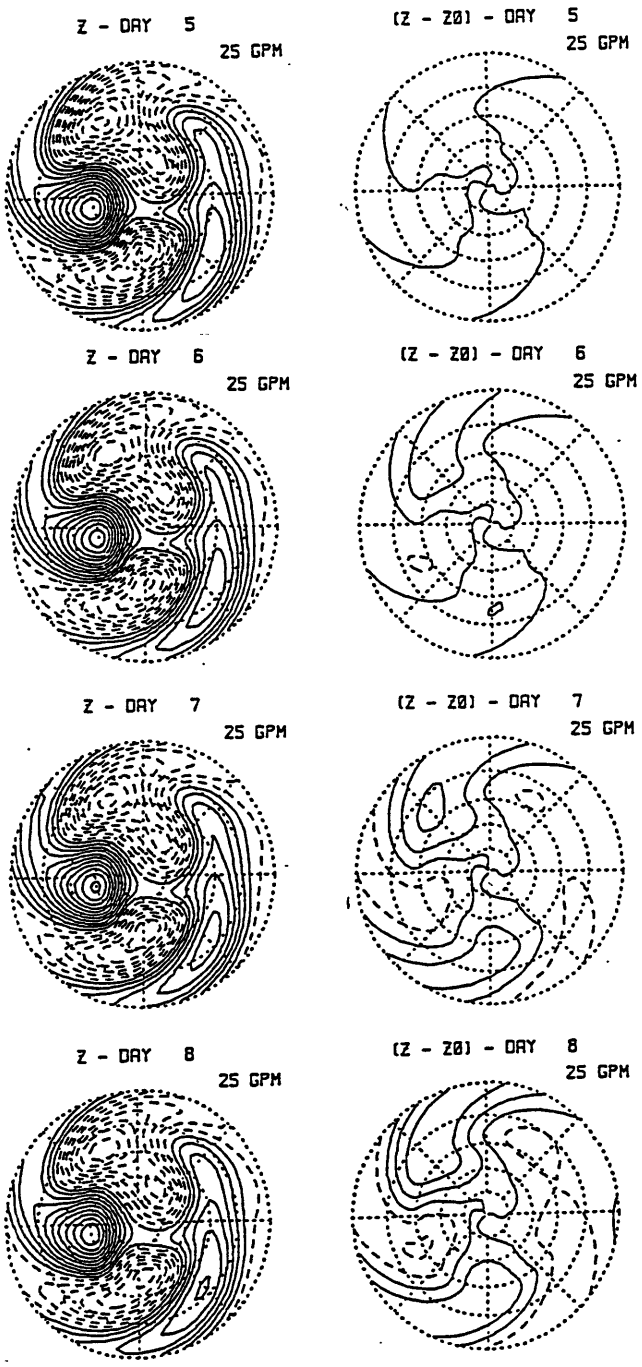

Figure 5.3: Time evolution of the geopotential height (left panel) and anomaly field (right panel): a) from day 5 to day 8, every day (this page); b) from day 10 to day 25, every 5 days (next page). The fields are shown in stereographic projection in the northern hemisphere; the outer latitude is 15 degrees. The contour interval is 25 meters.

b)

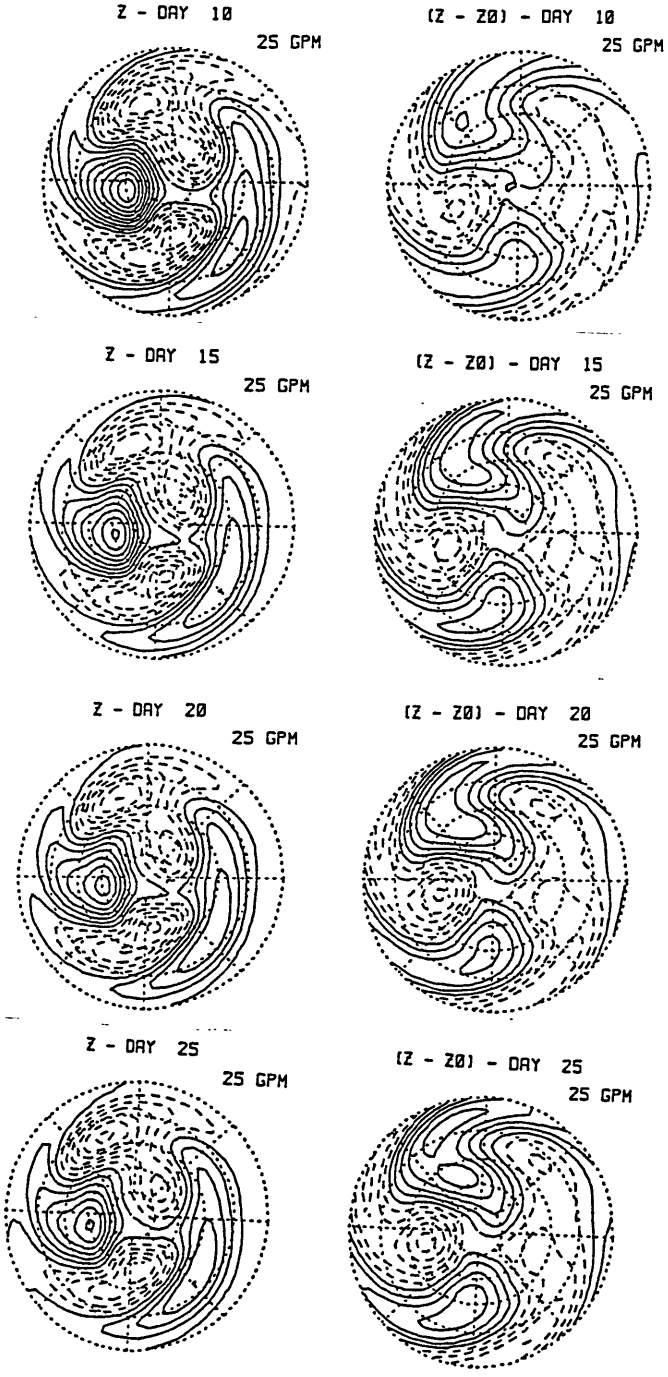

See previous page for caption.

The left panel shows the geopotential height at time t while the right panel shows the difference between the geopotential height at time t minus the initial condition. This field will be loosely called the *anomaly* field. With the 25 meter contour interval there is no visible anomaly field by day 5 (right panel). By day 6 a positive center is apparent right downstream of the Himalayas with 2 small negative and positive centers to the east. Subsequent evolution of the anomaly field is marked by intensification of these centers with virtually no phase propagation. This is the same evolution that one would get if a stationary vorticity source were specified at the Himalayas region (Hoskins and Karoly, 1982). The evolution of the geopotential height field (left panel) is marked by a smooth transition from one stationary situation to another. By day 15, transients are about 20% of the whole geopotential potential and are apparent. Transients will be considered in more detail in the next section.

5.3 Rossby waves

In this section we will establish that Rossby waves can be excited by the adjustment in stationary solution in a barotropic model. We start by analyzing the spectral structure of the difference field, then show that Rossby waves indeed propagate in this model, and finally compare the amplitude of the excited transients with the predictions of chapter 3.

5.3.1 The nature of the stationary wave adjustment

As in the previous section, we start by looking at the difference in stationary solutions. This time, we emphasize the spectral structure of the difference field, as we try to find clues for excitation of ultralong Rossby waves.

Case 1: Topographic forcing only

In this run, the stationary solution (eq.4.16) is computed for the zonal winds shown in figure 3.2 (hereafter referred to as U_1 and U_2) zonal wavenumbers $s = 1, 2, 3$, and linear damping parameter $r = 1/20$ days.

In figure 5.4a we show the amplitude of the difference

$$\Delta \mathbf{W}_S = \mathbf{W}_S[U_2] - \mathbf{W}_S[U_1] \tag{5.1}$$

where the notation $\mathbf{W}_S[U]$ stands for the stationary solution computed with the zonal wind U. Except for zonal wavenumber 1, the differences are dominant in the northern hemisphere. Figure 5.4b shows the spectral analysis of $\Delta \mathbf{W}_S$ in terms of Hough harmonics. Only the first few modes (say $\ell < 5$) are physically relevant since the modes with higher meridional wavenumbers may be part of the continuous spectrum. Observe a relatively small amplitude at $\ell = 1$, with peaks at $\ell = 2$ and/or

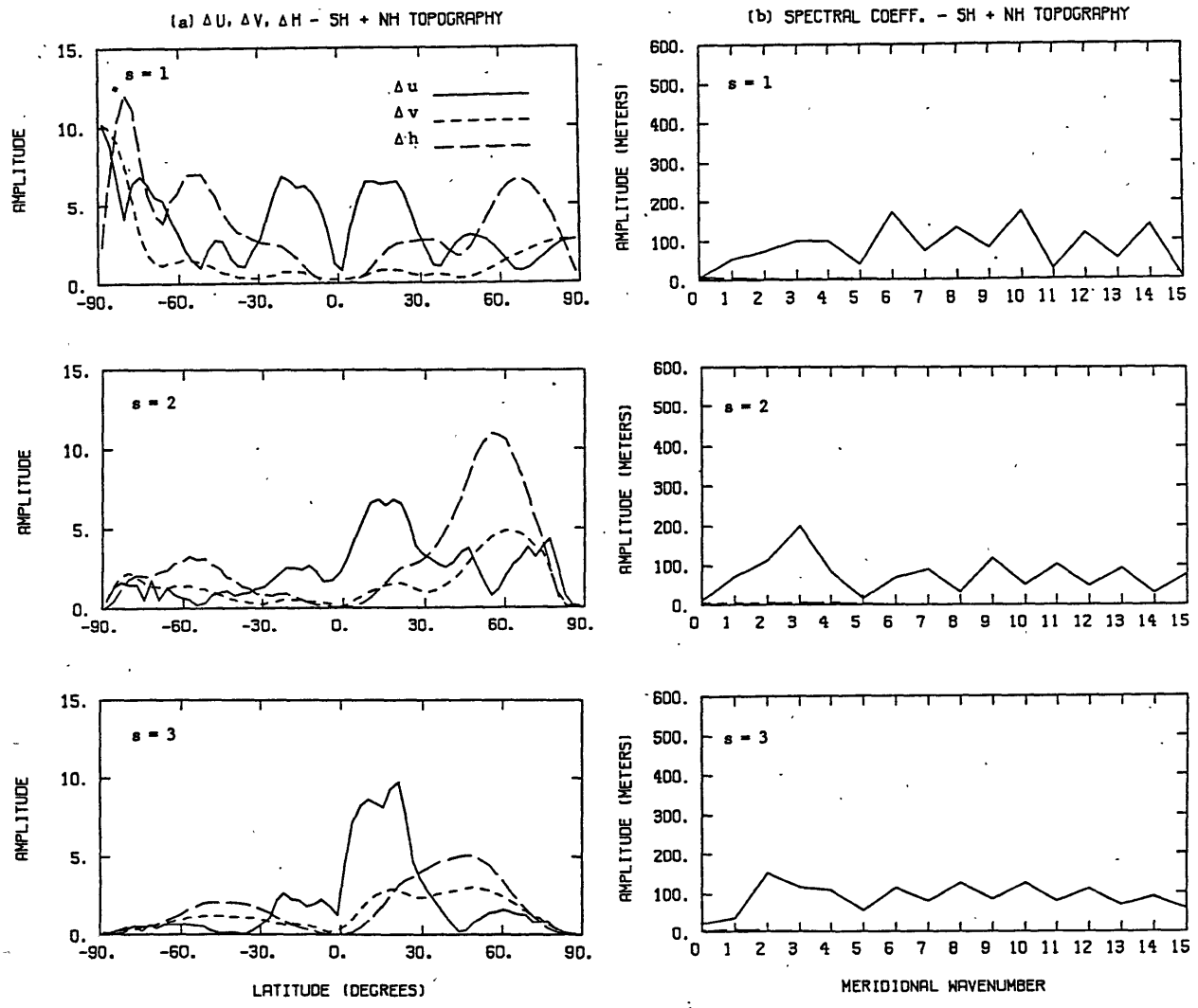

Figure 5.4: Difference between stationary solutions ($\Delta \mathbf{W}_s$,eq. 5.1) with topographic forcing alone, in both northern and southern hemispheres, zonal wavenumbers 1, 2, and 3. Linear damping parameter $r = 1/20$ days throughout the domain. a) Amplitude as a function of latitude, u, v in m/sec and h in dekameters; b) amplitude (in meters) of the spectral coefficients in terms of Hough functions: Rossby modes, full line, and westward and eastward gravity modes (very small amplitudes), short and long dashed lines.

3. Coefficients with zonal wavenumber 1 have amplitudes about 1/3 of the amplitudes of zonal wavenumbers 2 and 3. The spectral coefficients of the stationary solutions themselves (not shown) have the same structure as the differences. Also, the projection onto gravity modes as well as onto mixed gravity-Rossby modes ($\ell = 0$) is negligible.

Case 2: Dependence on southern hemisphere topography

The parameters are the same as in the previous run, with the exception that the topography is now set to zero at the southern hemisphere. The amplitude of the difference $\Delta \mathbf{W}_S$ is shown in figure 4.a. For the three zonal wavenumbers the curves in the northern hemisphere are essentially the same as in the previous case. The results of the spectral analysis are shown in figure 4.b. The spectral coefficients in this case are a smoothed version of those from the previous run, with a slight reduction in the amplitudes.

Case 3: Dependence on $\mathcal{L}$ and F

These runs are performed in order to determine the relative importance of changing the zonal wind that enters the definition of $\mathcal{L}$ (eq. 4.6), while keeping the zonal flow that enters **F** (eq. 4.7) fixed, and vice-versa. The other parameters, including topography being only in the

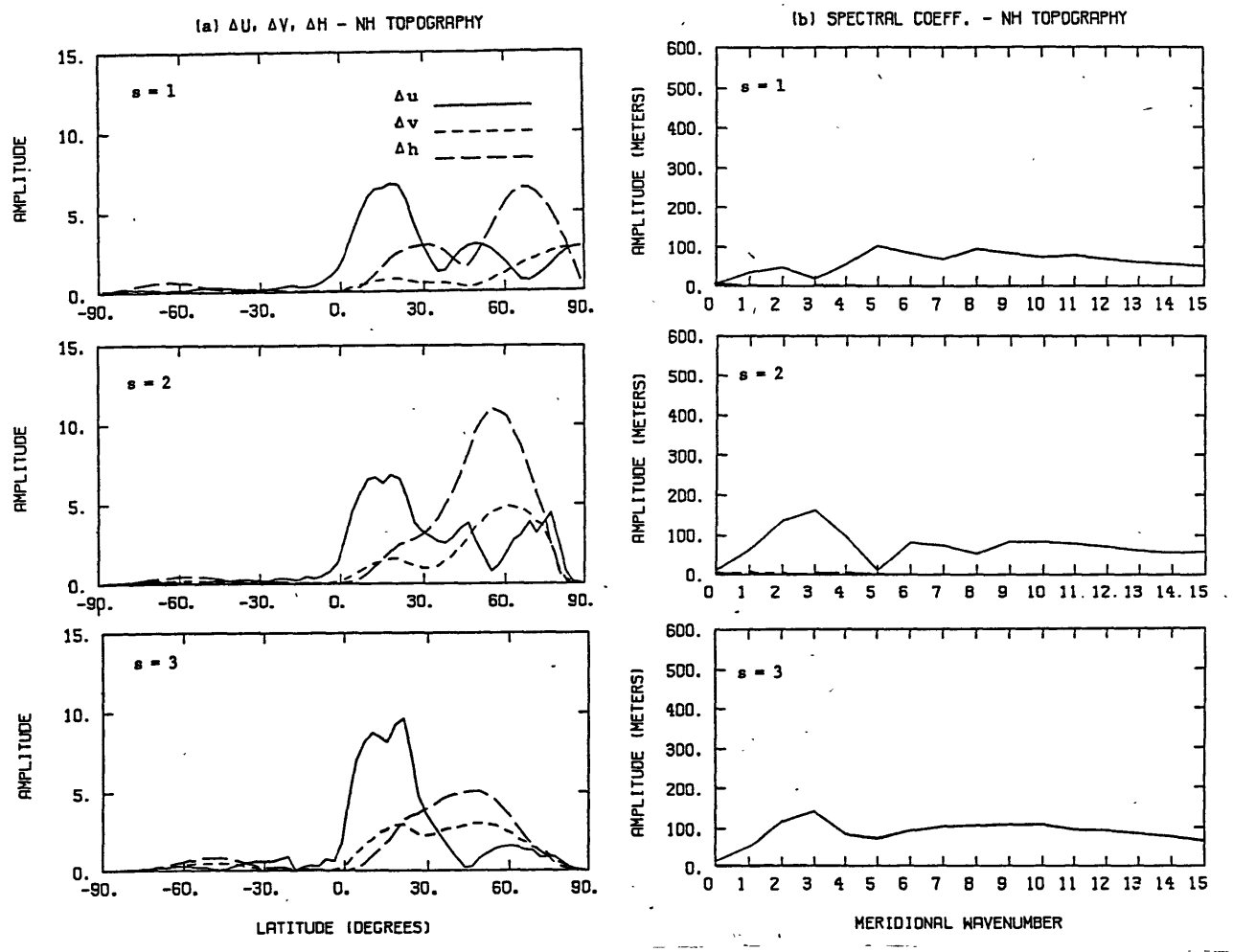

Figure 5.5: Same as fig. 5.3, except for the topography that is set to zero in the southern hemisphere.

northern hemisphere, are as in Case 2.

Figure 5.6 shows the spectral analysis of the difference for the two possibilities mentioned above. One can see that the amplitude of the spectral coefficients associated with changes of U_o only in $\mathcal{L}$ are on average three times bigger than the other case (they are even slightly bigger than the spectral coefficients in Case 2.) The differences themselves (not shown) have the same property.

Case 4: Effect of tropical thermal forcing

In this run we attempt to assess the role of diabatic heating in exciting ultralong waves. In addition to the topographic forcing, which is taken as in Case 2, a mass source is specified in the continuity equation, as described in section 4.2.2. Also a 5-day linear damping is introduced in the tropics within 20S and 20N; a 15-day linear damping is used in mid- and high-latitudes.

Figure 5.7 depicts the spectral coefficients of the function $\Delta \mathbf{W}_S$. The main differences from fig. 5.5b are: 1) with the exception of meridional wavenumber 1, amplitudes are about 2-3 times bigger; 2) the spectral distribution has a somewhat different structure, with peaks in meridional wavenumber 4. In this case, the difference in stationary solution (not shown) has an enhanced amplitude in the southern

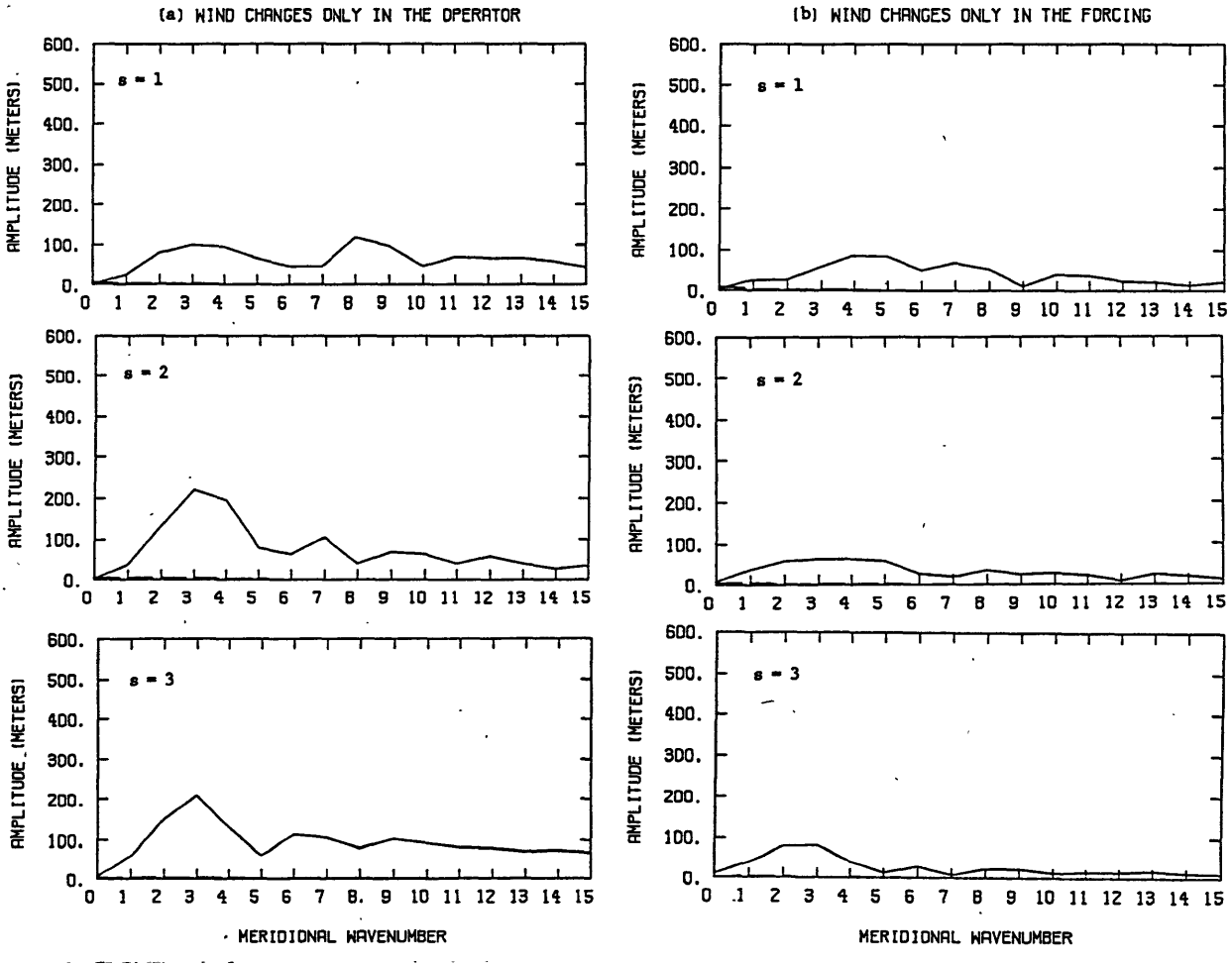

Figure 5.6: Spectral coefficients (in meters) as in fig. 5.4b, except that: a) U_o changes only in $\mathcal{L}$; b) U_o changes only in $\mathbf{F}$.

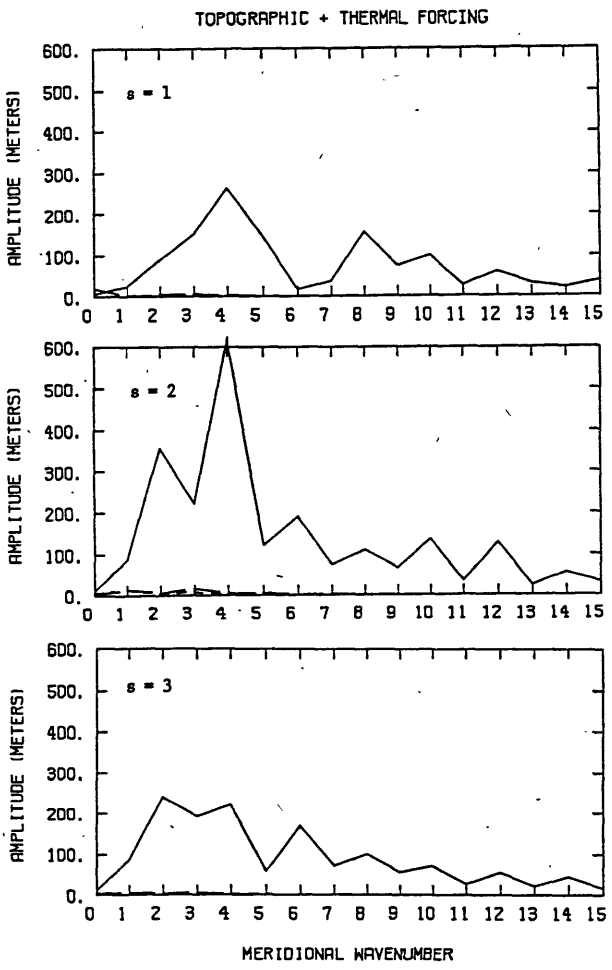

Figure 5.7: As in fig. 5.4b except that the RHS forcing includes the thermal component as well.

hemisphere.

Other Cases

Some runs were performed to assess the dependence of the differences on dissipation and other changes in wind. The effect of linear damping on the stationary solution is simply to reduce the amplitude and smooth out the whole pattern. The spectral distribution remains essentially the same. Wind changes at latitudes higher than 30° are not relevant to the excitation of the ultralong waves; even though they do have an effect on the difference $\Delta \mathbf{W}_S$, the projection on these waves is as in Case 2. Runs with winds having westerlies rather easterlies at the tropics do show cross equatorial propagation; however, spectral coefficients for $\ell \leq 3$ are close to those in figure 4.b; as before southern hemisphere topography is not essential to the picture ($\ell \leq 3$).

Discussion

The cases described above have established the following characteristics of the model: 1) with topographic forcing only, ultralong Rossby waves are available in the differences $\Delta \mathbf{W}_S$, with peaks at meridional wavenumbers 2 and 3; zonal wavenumber 1 has somewhat smaller amplitudes than zonal wavenumbers 2 and 3; 2) the topography in the

southern hemisphere is not essential in determining 1); 3) with thermal forcing the amplitude of the spectral coefficients is increased about 2-3 times; 4) the major contribution for ΔW_S comes from the variations in U_o entering the operator rather than changes in U_o entering the forcing.

Even though the gravest traveling components of the atmosphere, having an equivalent barotropic structure, can be reasonably modeled in a barotropic calculation, the same is not true for the stationary solution, which can have a rather complex vertical structure. Hence, the principal defect of the shallow water equations in modeling the mechanism of chapter 3 is its tendency to overemphasize the projection of the differences onto the external modes (the only modes existent in a barotropic model). In a baroclinic model, the differences having a more complicated vertical structure would project only partially on the external mode. Vertical propagation is also possible, as we will see in chapter 6. There the amplitude of the transient ultralong Rossby are much smaller than what we found here. The results of this section, thus, should be considered only as an illustration of the adjustment mechanism in a *shallow water model.* Application to the atmosphere is not warranted by the findings of chapter 6.

5.3.2 Rossby wave propagation

In this section we ascertain whether ultralong Rossby waves, excited by the adjustment mechanism, propagate with the predicted period (*5 days, 16 days, etc...*).

We show in fig. 5.8 amplitude and phase for the nine modes of interest (zonal wavenumber 1, 2 and 3, and meridional wavenumber 1, 2 and 3.) These coefficients were computed as the projection of the transients onto Hough functions. We see that only modes with meridional wavenumber 3 (16-day wave) have clear regular phase propagation, and the observed frequencies are in good agreement with those computed by Kasahara (1980). The other modes either have a very small amplitude or frequency lower than the predicted. In most of the cases, though, there is westward propagation of the phase.

5.3.3 The excited transients: parametric study

Several runs were performed to study the transients excited in the time dependent model. In this section the dependence on the fundamental parameters is analyzed. As a prototype we consider the case of topographic forcing only, with the mountains set to zero in the southern hemisphere. Modes with zonal wavenumber 3 and modes with meridional wavenumber 3 showed a more regular phase propagation and will

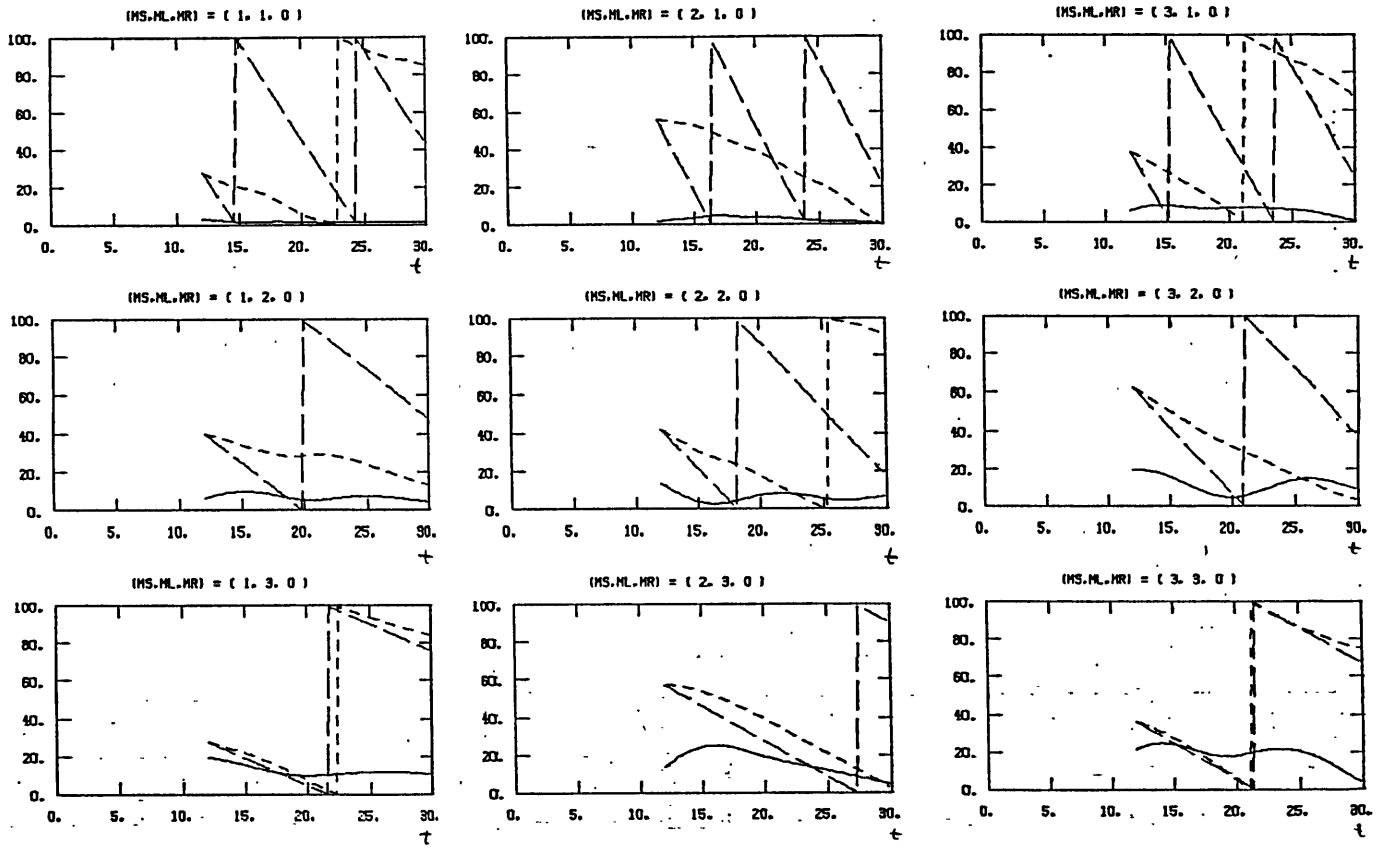

Figure 5.8: Amplitude and phase of Rossby waves in the barotropic model. This run only includes topography in the northern hemisphere, linear damping equal to (1/20 days) and transition period $\tau = 12$ days. Nine modes are shown here: first, second and third columns correspond to zonal wavenumber 1, 2, and 3, respectively; first, second, and third rows correspond to meridional wavenumbers 1, 2, and 3, respectively.

be discussed below.

Case 5: Dependence on τ

In this case the linear damping parameter is taken as 1/20 days and the basic state parameters are as in fig. 4.1. In figure 5.9 we show the amplitude of the excited transients for $t > \tau$, as a function of the transition parameter τ , modes (s, ℓ) = (3,1), (3,2) and (3,3). As expected, the amplitudes decrease with τ , except for mode (3.1) between 15 and 20 days. This can be attributed to the small amplitudes (3 meters) and to the fact that the spectral analysis is performed in terms of Hough functions rather than the adjoint normal modes of the model. In general, amplitudes increase with meridional wavenumber.

Case 6: Dependence on damping

In order to assess the dependence of the results on damping, we present in figure 5.10 the maximum amplitude of the spectral coefficients for $t > \tau = 10$ days. The basic state parameters and the mode indices are as in the previous case. In this range, amplitudes increase with the decrease of the damping parameter and for most cases amplitudes increase with meridional wavenumber, as before.

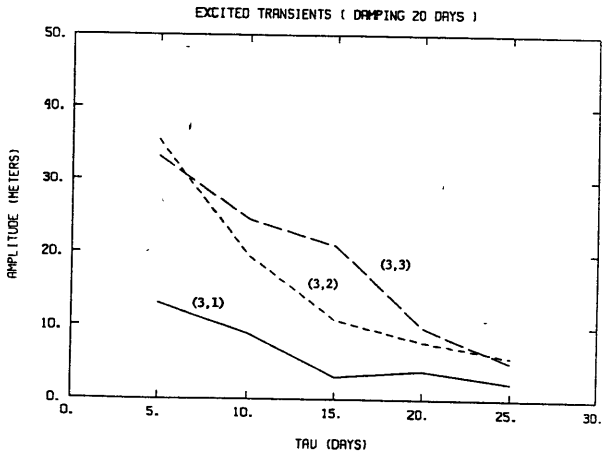

Figure 5.9: Transients excited in the time dependent model. Amplitude (in meters) of the spectral coefficient, modes $(s, \ell) = (3,1)$, $(3,2)$, and $(3,3)$, as a function of the transition period τ (in days). Only topographic forcing in the northern hemisphere and constant linear damping parameter $r = 1/20$ days.

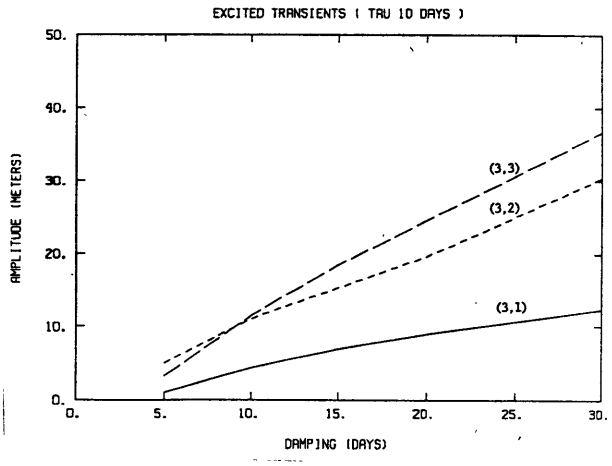

Figure 5.10: Transients excited in the time dependent model. Amplitude (in meters) of the spectral coefficient, modes $(s, \ell) = (3,1)$, (3,2), and (3,3), as a function of the inverse damping parameter $1/r$ (in days). Only topographic forcing in the northern hemisphere and transition period $\tau = 10$ days.

Case 7: Checking the transient efficiency function

In figure 5.11 we show the amplitude of the excited transients (full line) as a function of transition period τ , for mode $(s,\ell) = (1,3)$ with a the damping parameter taken as 1/20 days. A quantity related to ξ, eq. (3.49), is also plotted (dashed line). The qualitative agreement between the two curves is good. Figure 5.12 depicts the amplitude of the excited transients as a function of the inverse of the damping parameter (full line), for mode $(s,\ell) = (1,3)$, in the case $\tau = 10$ days. For comparison, we also show a quantity related to ξ , eq. (3.49), (dashed line.) The two curves depart from each other for small damping time scales. Note that for $1/r$ greater than 15 days the dependence on damping is less pronounced.

Other Cases

Other runs were performed in order to determine the influence of topography and changes in U_o entering only the operator $\mathcal{L}$. The results (not shown) confirm the indications of subsection 5.3.1, namely: 1) southern hemisphere topography has little influence in the excitation of the nine modes considered in Case 1; 2) changes in U_o entering only the operator are more effective in exciting the transients than the variations in U_o entering directly the forcing $\mathbf{F}$.

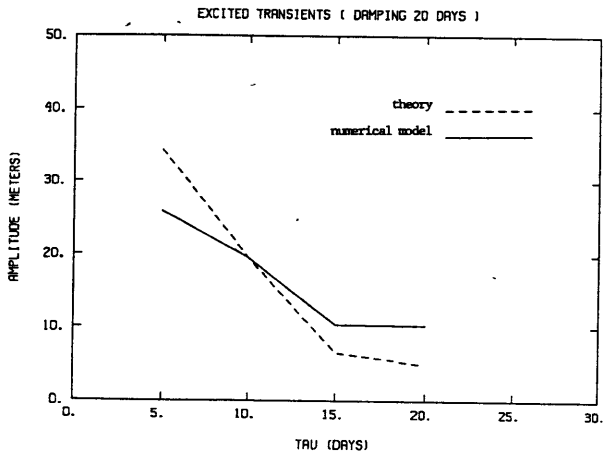

Figure 5.11: Transients excited in the time dependent model, full line, and an estimate of the amplitude based on the approximate formula (3.49), dashed line, as a function of the transition period τ (in days), mode $(s, \ell) = (1,3)$. ξ (eq. 3.49) is adjusted to coincide with the results of the numerical model at $\tau = 10$ days. Only topographic forcing in the northern hemisphere and damping parameter = 1/20 days.

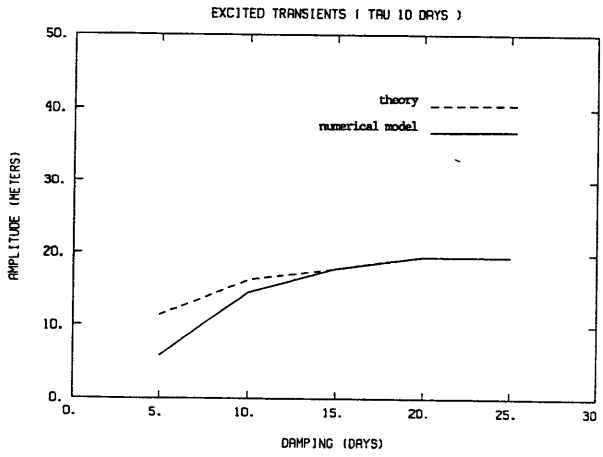

Figure 5.12: Transients excited in the time dependent model, full line, and an estimate of the amplitude based on the approximate formula (3.49), dashed line, as a function of the inverse damping parameter (in days), mode $(s, \ell) = (1,3)$. (eq. 3.49) is adjusted as in Figure 5.11. Only topographic forcing in the northern hemisphere and transition period = 10 days.

Discussion

The parametric study of this section indicates that the estimation of the amplitude modulation based on the heuristic propagation argument (ξ , eq. 3.49), combined with the knowledge of the *differences* (ΔW_S), may be useful in explaining the relative amplitude of the different modes. In particular, the modes with $\ell = 2$, 3 are predominant for two reasons: 1) the difference in the stationary solution peaks at these wavenumbers; 2) those modes having a period longer than the $\ell = 1$ modes are favored by the propagation mechanism (viz. eq. 3.49).

5.3.4 Summary

Despite the limitations of the barotropic model, some aspects of the observations are present in this calculation, especially the peaks in meridional wavenumbers 2 and 3 when only topographic forcing is included. For comparison, in Table 5.1 (from Lindzen et al., 1984) we present the maximum observed amplitudes of these modes and the season in which they occur. The amplitudes are only order of magnitude in agreement with the topographic forcing calculation, which gives amplitudes three times smaller on average. The inclusion of thermal forcing has the effect of producing amplitudes of magnitude comparable with observations; nevertheless, meridional wavenumber 2 tends to have amplitudes greater than meridional wavenumber 3 (see figure 5.6). One should

Table 5.1: Maximum amplitude and season of Rossby modes (from Lindzen et al., 1984.)

Mode (s,ℓ)	*Maximum amplitude* *(m)*
(1,1)	34
(1,2)	65
(1,3)	76
(2,1)	40
(2,2)	65
(2,3)	74
(3,1)	46
(3,2)	60
(3,3)	90

keep in mind that the similarities with observations may be accidental as a similar calculation with the baroclinic model fails to excite Rossby waves (chapter 6).

For reference we show in figure 5.13 the zonal wind at 500mb during July 1979, plotted from the FGGE level III-b gridded data, prepared by the European Center for Medium Range Weather Forecasts (Bengstsson et al., 1982). It seems that the actual changes in the wind are modest compared with the variations in wind assumed in this paper, at least at the tropical latitudes where the changes in the last are restricted. However, at other levels (e.g. 1000mb, not shown) changes are more

5.3. *Rossby waves*

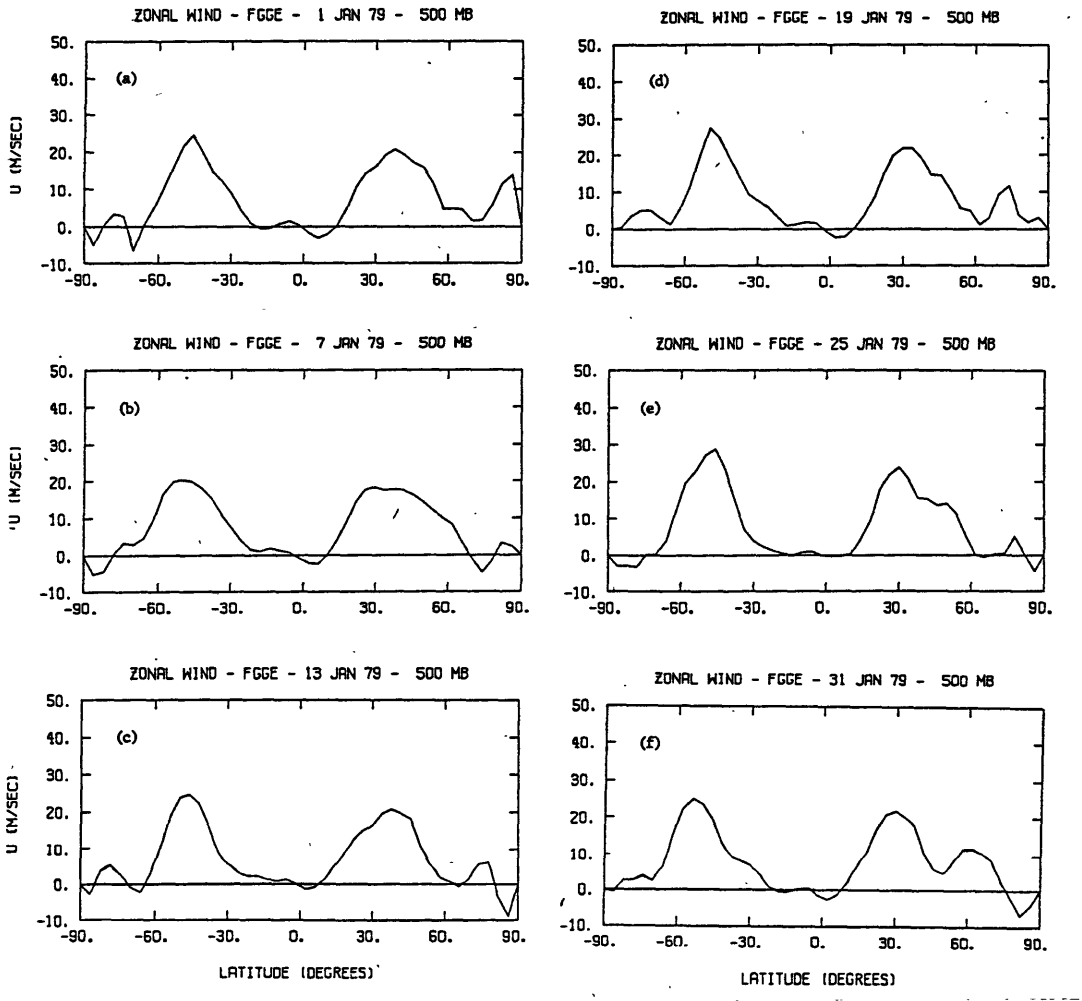

Figure 5.13: Observed zonal winds during January 1979 at 500mb, computed from FGGE data: a) Jan. 1, b) Jan. 7, c) Jan. 13, d) Jan. 19, e) Jan. 25, and f) Jan. 31.

pronounced than at 500b. As we will see in chapter 6, the subtropics is the region of greatest sensitivity for stationary waves in a baroclinic model.

5.4 Discussion

The barotropic calculation of this chapter was carried out in order to illustrate the mechanism of chapter 3 in a minimal model resolving ultralong Rossby waves. Despite the limitations of this model, some aspects of the observed waves did show up in the calculations. In the presence of topographic forcing alone, amplitudes are about half to one-third the observed value and the transient amplitudes increase with meridional wavenumber, suggesting the dominance of the 16-day waves. The reasons for this behavior are threefold: 1) the adjustment of the quasi-stationary component favors higher meridional wavenumbers which have a more tropical structure; 2) transition periods $\tau \approx$ 10-15 days inhibit high meridional wavenumbers less than low meridional wavenumbers (viz. fig. 5.9) ; 3) linear damping, acting equally in all scales, does favor low meridional wavenumbers, but this effect generally is smaller than those in 1) and 2). The introduction of diabatic heating, through a specification of stationary mass source, renders the transient amplitudes 2- 3 times bigger and in some instances comparable with observations, but the dependence on meridional wavenumber is no longer quite in agreement (2 favored over 3.) Given the crudeness

of representing thermal forcing in barotropic models, discrepancies are hardly surprising.

As we will see in chapter 6, the spatial structure of the transients in the baroclinic model has a much shorter meridional scale, and Rossby waves are not excited. Transients in the baroclinic model are quasi-stationary, and there is no sign of westward propagating disturbances.

Chapter 6

Transients in a Baroclinic Model

6.1 Introduction

This chapter deals with the excitation of transients on a global linear baroclinic model. The approach adopted here is similar to the one used to study transients excited on a barotropic model (see chapter 5.) Namely, we specify a given stationary variation due to a change in the zonal flow and analyze the transients excited on the time-dependent model as a function of dissipation and wave period[1]. While the barotropic calculation emphasizes wind changes changes associated with position of the critical line, here we will restrict ourselves to wind changes near

[1] As discussed in chapter 3, the relevant parameters (period and dissipative time scale) should be normalized by τ, the time it takes for the wind to go from one configuration to another.

the northern hemisphere subtropical jet. This choice is based on a recent study by Nigam and Lindzen (1989), which showed that shifts of the subtropical jets of only a few degrees produced substantial changes in the stationary wave pattern. Nigam and Lindzen also conducted an extensive search for other zonal wind sensitive zones in the northern hemisphere troposphere. They concluded that wind changes in the subtropical jet region are by far the most influential region for stationary propagation. The main reason for this sensitivity is the fact that the jet's position determines the *path* for waves excited by the Tibetan plateau.

Another problem of interest, and closely related to the excitation of transients, is the establishment of the new stationary solution. Due to hydrodynamical and numerical instabilities, it is generally very difficult, if not impossible, to attain a stationary solution by integrating a linear time-dependent model. Even when a stable basic state is specified, the numerical scheme generally blows up after a few iterations, at least in our model. An indirect way to access the time scale for establishment of stationary waves is through the kind of experiment considered here. In these experiments we initialize the model with a particular basic state and the stationary solution associated with this flow. Changing the flow from one configuration to another, we monitor the establishment of the *new* stationary solution, by looking at the differences of the solution at time t from the solution at the initial time. By this procedure, we can study among other things the time scale for vertical and meridional

stationary wave propagation. The details will be given in section 6.4.

Unlike the barotropic calculation (chapter 5), in this chapter we concentrate on the horizontal structure and vertical propagation of the transients/stationary waves, rather than their spectral structure. Rossby waves, as we shall see, do not seem to be excited in this calculations, possibly because of the nature of the wind changes considered.

In most cases considered in this thesis, we include only topographic forcing with only three zonal wavenumbers. Thermal forcing is considered only in a few instances as a way to check the adjustment mechanism when the waves are forced through the thermodynamic equation. As we will discuss in section 6.2, there is great uncertainty about the correct thermal forcing, both in amplitude and horizontal structure. Nevertheless, wind changes in the subtropics are not likely to affect the stationary waves forced by heating north of 45N. Furthermore, propagation from the tropics has been shown (e.g. Nigam et al. 1986,1988) to be of secondary importance for stationary waves at mid- and high-latitudes.

This chapter is organized as follows. First we verify the validity of our orographically forced stationary wave simulation, comparing it with results from similar models. Having assessed the validity of the stationary model, we investigate its sensitivity to variations in the subtropical jet, as in Nigam and Lindzen (1989), and the effect of dissipation. In

the following section we use the time dependent model to study the establishment of the new stationary solution, both horizontally and vertically. A parametric study of the excited transients then follows, where its full horizontal structure and slow time evolution is stressed. An assessment of the excitation of ultralong Rossby waves in the model is also performed. It is concluded that there is no clear indication of free Rossby waves propagation, even though the spatial structure of the transients projects on the corresponding Hough modes. We end this chapter with a discussion of the implications of the present study, focussing on its application to persistent anomalies of the northern hemisphere.

6.2 Stationary wave response to orographic forcing

Before we proceed to analyze the sensitivity of the stationary model to variations in the basic state zonal flow, it proves necessary to access the *quality* of our simulations. Since there is no direct way to observe orographically forced waves, we check our results against other linear stationary models.

Horizontal structure

Figure 6.1 compares our model results computed with the monthly mean basic state for January 1979 (see chapter 4, section 4.3.3) with the results of Nigam et al. (1988). Like ours, this is linear primitive equation model with Rayleigh friction and Simmons-like critical layer dissipation; it has 9 vertical levels and the basic state is taken from the GFDL General Circulation Model. Their full model, including thermal forcing, reproduced the main features of the time mean GCM response, which in turn reproduced many of the northern hemisphere winter circulation features. This is one of the few models that display the zonal and meridional wind response in addition to the geopotential response. Figs. 5.1a and 5.1a' compare the eddy zonal wind for the models at 300mb. The phase agreement in the northern hemisphere [2] is good, the major feature being the wave train emerging from the Tibetan plateau and propagating equatorward. The amplitude in our model is about 2.5 times the amplitude in the Nigam et al. model. An explanation for this discrepancy may lie in the difference of basic states. Since in Nigam et al. (1988) the zonal wind has much stronger easterlies in the tropical troposphere, the critical line dissipation is much stronger and waves are effectively absorbed there. The eddy meridional wind fields are shown in figs. 5.1b and 5.1b'. The phase and amplitude of the

[2]In other to avoid deterioration of the stationary wave simulation in the southern hemisphere, Nigam et al. (1988) set the topography in their model to zero south of 65S. Therefore, they show a reduced topographic response in this hemisphere

wave train emanating from the Tibetan plateau are in good agreement. The wave train forced by the Rockies has a more zonal structure in our model, and a slightly reduced amplitude. The eddy geopotential fields are compared in figs. 5.1c and 5.1c'. The major features of the winter northern hemisphere are present in both models. Amplitudes are consistent, but phase only roughly so. For example, with this particular basic state our model fails to produce the Aleutian high in the correct place.

For reference we show in fig. 5.2 the topographically forced stationary wave response for 3 other linear stationary wave models. They are: 1) Lin (1982), a medium resolution ($\Delta z = 2.5$ Km) primitive equation model in log-p coordinates; 2) Jacqmin and Lindzen (1985), a high resolution ($\Delta z = 1$ Km) primitive equation in geometric vertical coordinates; and 3) Chen and Trenberth (1988), a low resolution (11 vertical levels) balance equation model in pressure coordinates, with a coupled lower boundary condition[3]. The observed 500mb climatological stationary waves is also shown in fig. 6.2d (from Jacqmin,1983). Despite different model formulation, resolution, basic state and dissipation, they all reproduce the main observed features, even when thermal forcing is absent. The most obvious discrepancy is the amplitude of the topographic response. Lin's response in the vicinity of the Himalayas are about 2 times the other models' — even bigger than the observed full stationary wave field. Chen and Trenberth and Jacqmin and Lindzen amplitude

[3]Recall that our model has 18 vertical levels ($\Delta z \approx 1.8$ Km)

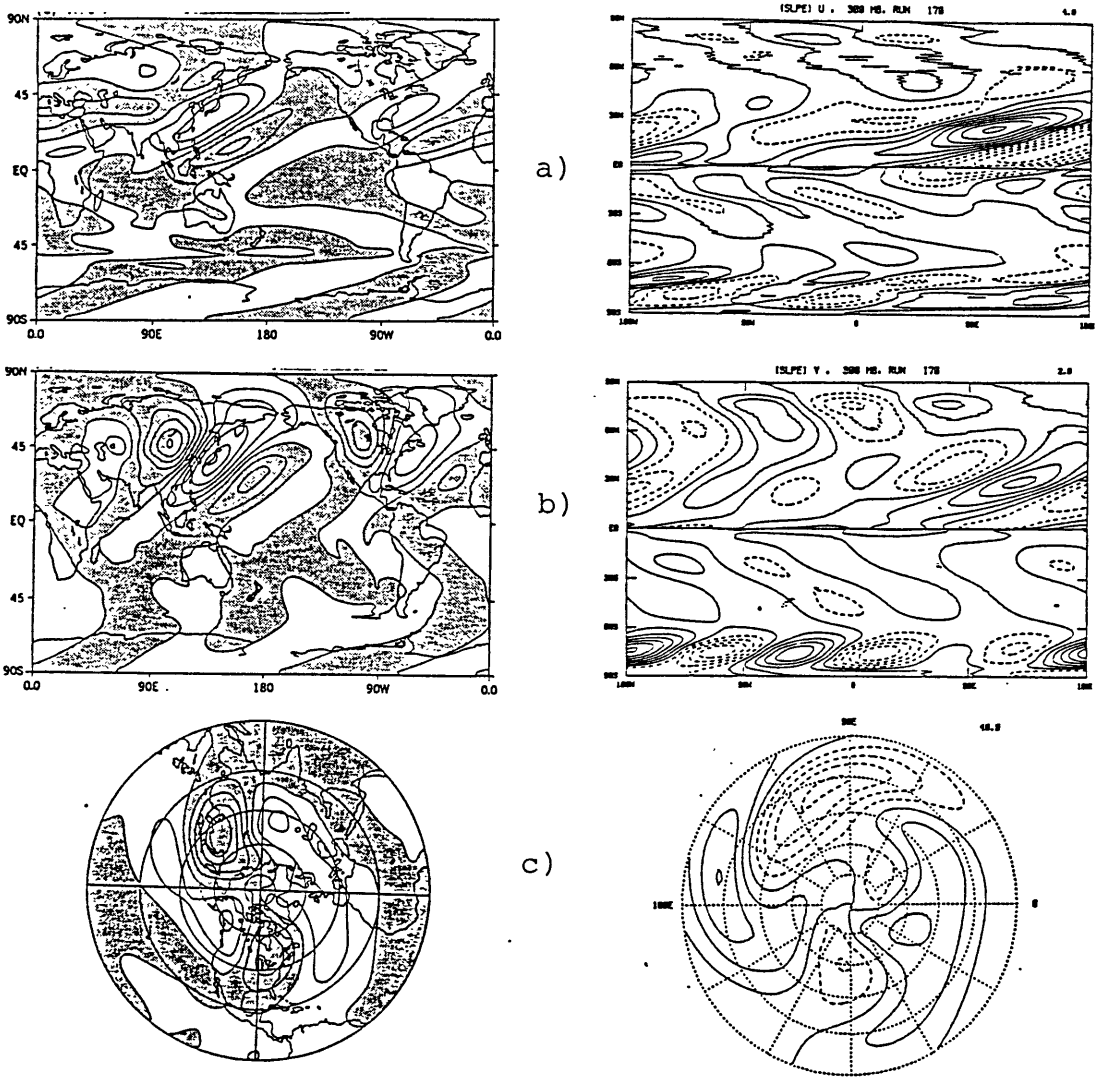

Figure 6.1: Comparison of the stationary wave response obtained with Nigam et al. (1988) model (left panel) and the stationary wave response obtained with our model (right panel): a) zonal wind (contour interval: 4 m/sec), b) meridional wind (contour interval: 2 m/sec), and c) geopotential height (contour interval: 40 meters). All fields shown at 300 mb; a) and b) shows the response at the entire globe and c) only shows the northern hemisphere in stereographic projection.

differ by about 20% and are both slightly smaller than observation[4]. The main features of the observed waves are also captured by our model and the model of Nigam et al. (1988).

Vertical structure

Nigam et al. (1988) did not present plots of their vertical structure. Therefore, we compare our results with Nigam and Lindzen (1989)[5], Lin (1982) and the Chen and Trenberth (1988) simulations. The amplitudes of the stationary waves are shown in fig. 6.3, for zonal wavenumbers 1, 2, and 3, along with the observed stationary wave amplitude as computed by van Loon et al. (1973). For wavenumbers 1 and 2 there is a good general agreement between our results, Nigam and Lindzen (1989) and Lin (1982). For zonal wavenumber 3 and this particular basic state, our model gives amplitude about 40 % smaller than these authors. Chen and Trenberth's (1988) amplitudes for wavenumbers 1 and 2 are roughly in agreement with the other authors in the troposphere, but are about 50 % smaller in the lower stratosphere. On the other hand, Chen and Trenberth's has the biggest amplitude for zonal wavenumber 3 in the troposphere (about 1.5 times Nigam and Lindzen's

[4]It is interesting to note that Chen and Trenberth (1988) showed that their model with a decoupled lower boundary condition produces a much stronger response everywhere (about 80% bigger). Jacqmin and Lindzen (1985), on the other hand, using a decoupled lower boundary condition, obtained amplitudes comparable to Chen and Trenberth coupled boundary condition simulation.

[5]Nigam and Lindzen (1989) uses the same model as Jacqmin and Lindzen, with a different dissipation parameterization.

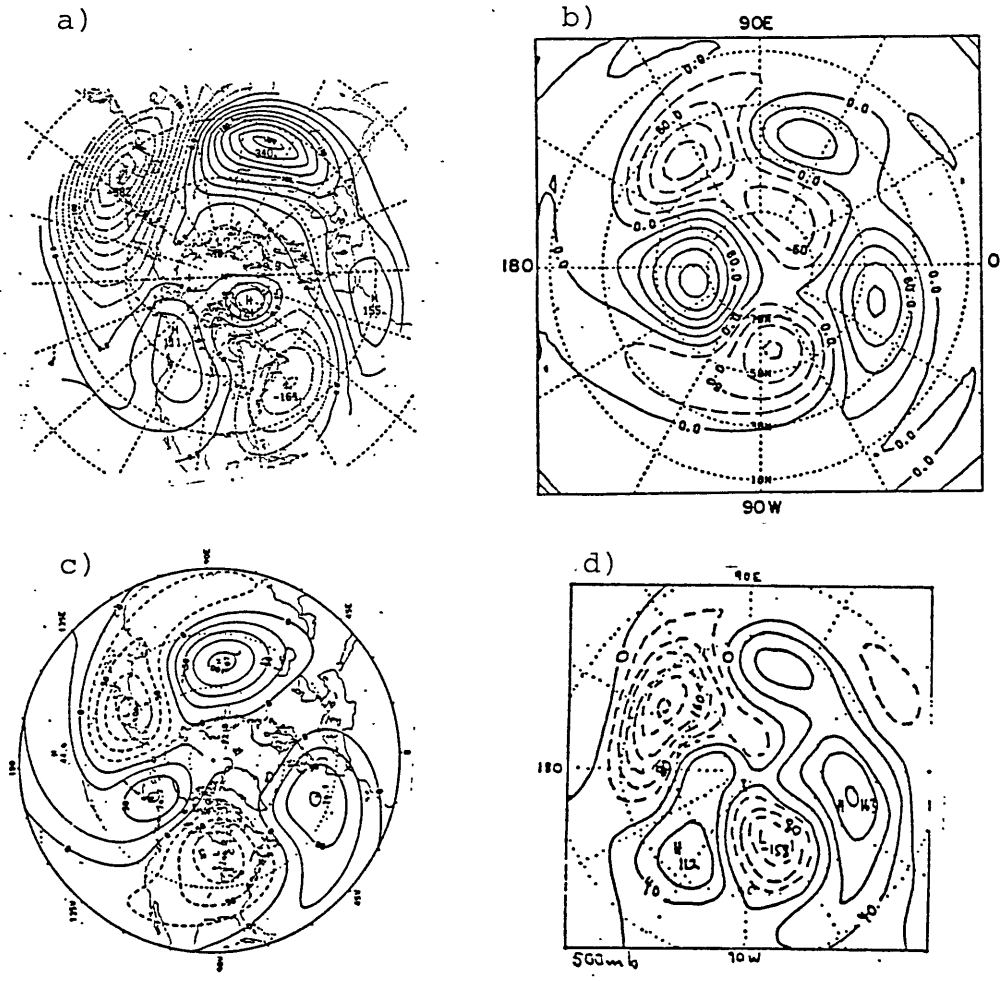

Figure 6.2: Stationary waves at 500mb obtained with 3 different models: a) Lin (1982), b) Jacqmin and Lindzen (1985), c) Chen and Trenberth (1988); and d) the observed stationary waves at 500mb (from Jacqmin, 1982).

amplitude), with substantial propagation into the stratosphere. Except for Lin (1982), all model wavenumber 1 responses are about 3-4 times smaller than the observed stationary waves of van Loon et al. (1973). For zonal wavenumbers 2 and 3, the simulated stationary waves are about the same magnitude as observations. This suggests that heating and/or nonlinearities may be important for zonal wavenumber 1, but perhaps only secondary for zonal wavenumbers 2 and 3.

Discussion

Despite all the differences in formulation, resolution, basic state and dissipation parameterization, all the models have a certain degree of consistency: the wave structures at the troposphere have some resemblance and are reminiscent of the observed stationary waves, even in the absence of thermal forcing. But they also differ by large amounts and the degree of agreement is often a subjective matter. In our view, the simulations obtained with our model are *consistent* with the other studies, and are representative of the kind of topographic response obtained with this kind of linear model.

Discrepancies among stationary models are much greater when thermal forcing is included. Topographic forcing is primarily dependent on the shape of the mountains and on the wind blowing over them[6]. There-

[6]In fact, in sigma coordinates the RHS forcing depends only on the topography. However, the wave response is generally proportional to the wind in the lower levels,

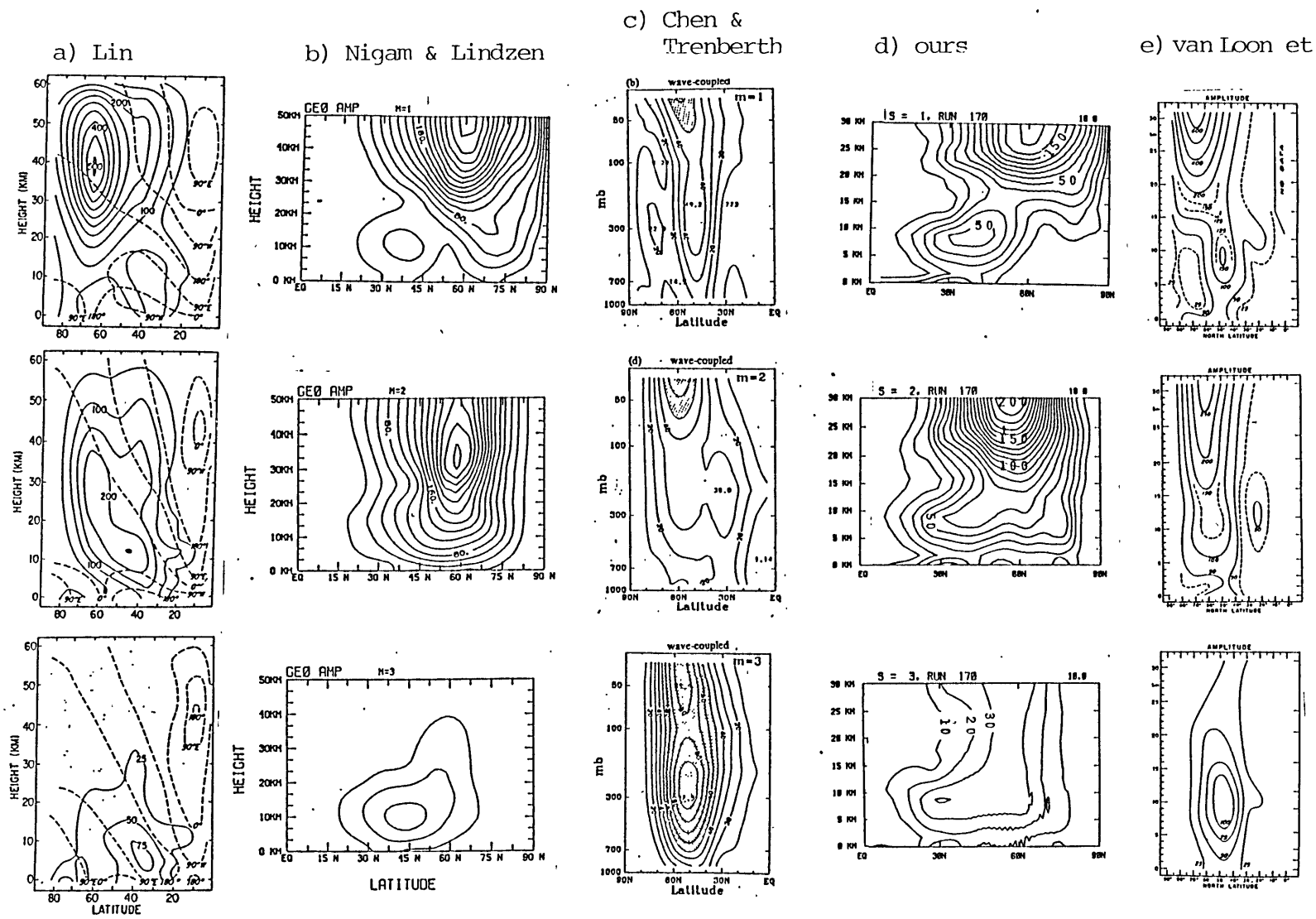

Figure 6.3: Stationary wave amplitudes (in meters) for the following models: a) Lin (1982), b) Nigam and Lindzen (1989), c) Chen and Trenberth (1988), d) our model; and e) observed stationary waves (from van Loon et al., 1973).

fore, topographic forcing depends mainly on the wind magnitude in the lower levels. On the other hand, there are as many thermal forcings as there are models. For example, Nigam et al. (1988) include sensible, radiative, latent heat release and heating due to transients, all taken from the GFDL GCM. Jacqmin and Lindzen (1985) only include latent heat release deduced from rainfall data. Lin (1982) uses the heating field calculated by Lau (1979), which is based on GCM statistics. Chen and Trenberth (1988) use the diabatic heating estimated by Johnson at al. (1985) and Johnson and Wei (1984), computed as residuals of the continuity equation on isentropic surfaces for NMC FGGE IIIa and ECMWF FGGE IIIb datasets. Taking for example the northern Pacific region, Nigam et al. (1988) have a maximum heating rate of 2.8 K/day, while Jacqmin and Lindzen (1985) have a maximum heating rate of 0.5 K/day and the Chen and Trenberth (1988) maximum heating rate is about 1.25 K/day for the NMC dataset and 1.85 K/day for the ECMWF dataset[7]. In view of this, the great diversity of stationary wave response to heat is not surprising: for most of the cases it is translated into the differences in the thermal heating itself. A better understanding of the thermal field is necessary, before questions such as the relative importance of thermal / topographic forcing could be answered. Due to these uncertainties we will not consider thermally

---

so that conceptually we can still think of it in terms of *wind blowing over the mountain.*

[7]Recall that the NMC FGGE IIIa and ECMWF FGGE IIIb are different analysis of the same *raw* data. It is clear that the residual calculation of Johnson at al. (1985) and Johnson and Wei (1984) are very sensitive to the difference in analysis

forced stationary waves in great detail.

The remainder of this thesis will concentrate on the stationary wave response to topography. As a matter of illustration, we will show a few cases where thermal forcing as in Jacqmin and Lindzen (1985) will be included. This will be intended to check whether waves forced through the thermodynamic equation have any effect on our mechanism. Furthermore, the kind of wind changes to be considered here seem to have a reduced effect on the waves forced by heating, at least in the troposphere (see section 6.3).

6.3 Stationary wave sensitivity

Now we proceed to investigate how the topographically forced waves depend on wind changes in the subtropics. Nigam and Lindzen (1989) have conducted an extensive search for other regions of sensitivity. They have shown that *plausible* changes in the polar Night Jet (9^o displacement north and south of its climatological position) has only a modest impact on the waves in the stratosphere. Since the Himalayas is the primary source for stationary waves in the northern hemisphere, it is natural to expect that changes in the vicinity of this forcing will affect the path taken by the waves. By taking different paths, waves change not only their pattern but also their amplitude, since more or less wave activity can now reach the critical layers or travel near the

surface, where strong damping is present. As we will see, wind changes in the subtropics will affect waves not only in the troposphere but also in the stratosphere.

Control changes

We start by showing in fig. 6.4 our two control basic states, along with the corresponding quasi-geostrophic index of refraction. The wind changes are shown in fig. 6.4c, and consist of a dipole centered around 30N, going from 15N to 45N. The result of these changes is a shift in the subtropical jet from 38N to about 27N, with virtually no change in its magnitude (42 m/s). These two basic states were constructed as follows: wind 1 (2) is equal to the January 79 monthly mean zonal wind (see chapter 4, section 4.3.3) minus (plus) half the dipole changes of fig. 6.4c. Notice that since our subtropical jet is stronger than the jet in Nigam and Lindzen (1989), we need a stronger dipole to produce the same jet shift. The most noticeable changes in the index of refraction are associated with a minimum around 45N at 15Km. As shown by Matsuno (1970), Karoly and Hoskins (1982), among others, this minimum in index of refraction acts as a *diverter* for waves excited in the lower troposphere. We will argue in the end of this section that this feature will be main factor responsible for changes in the stationary wave path.

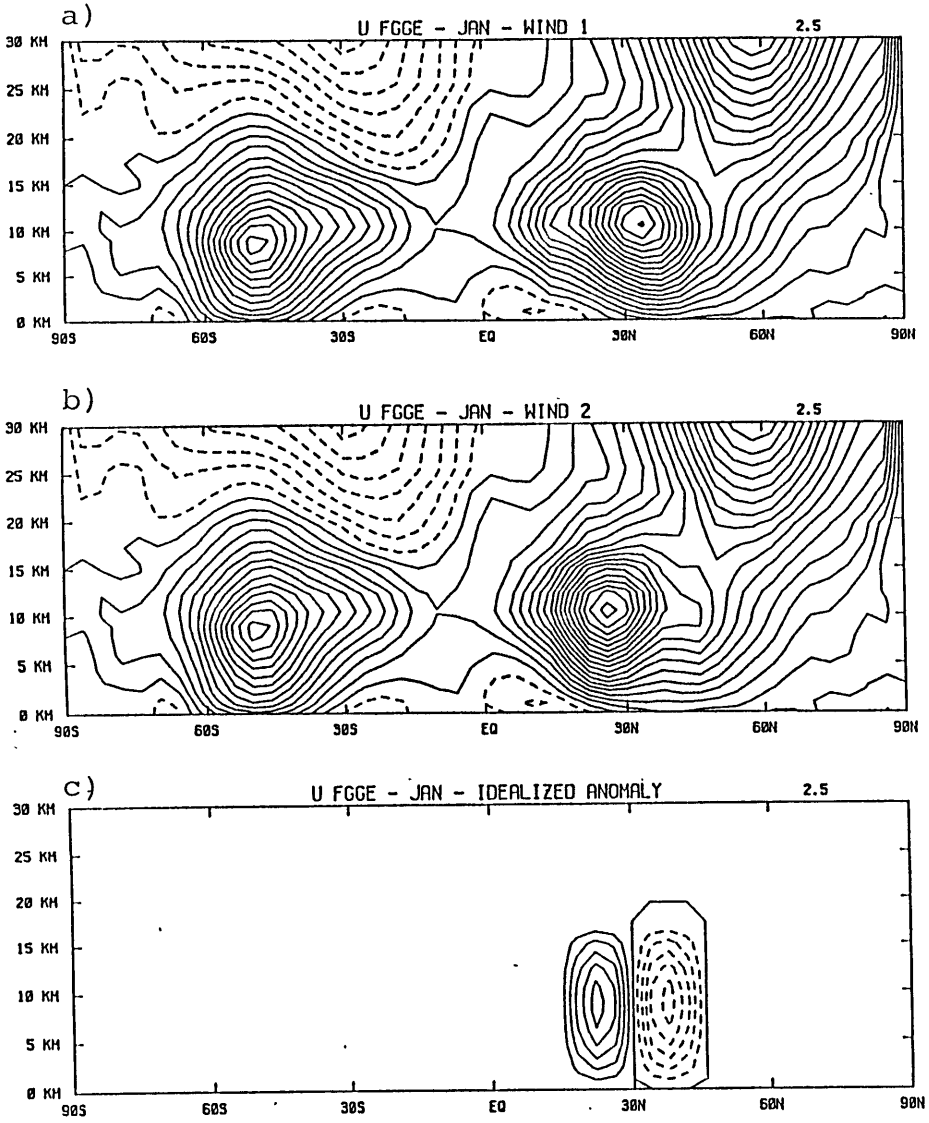

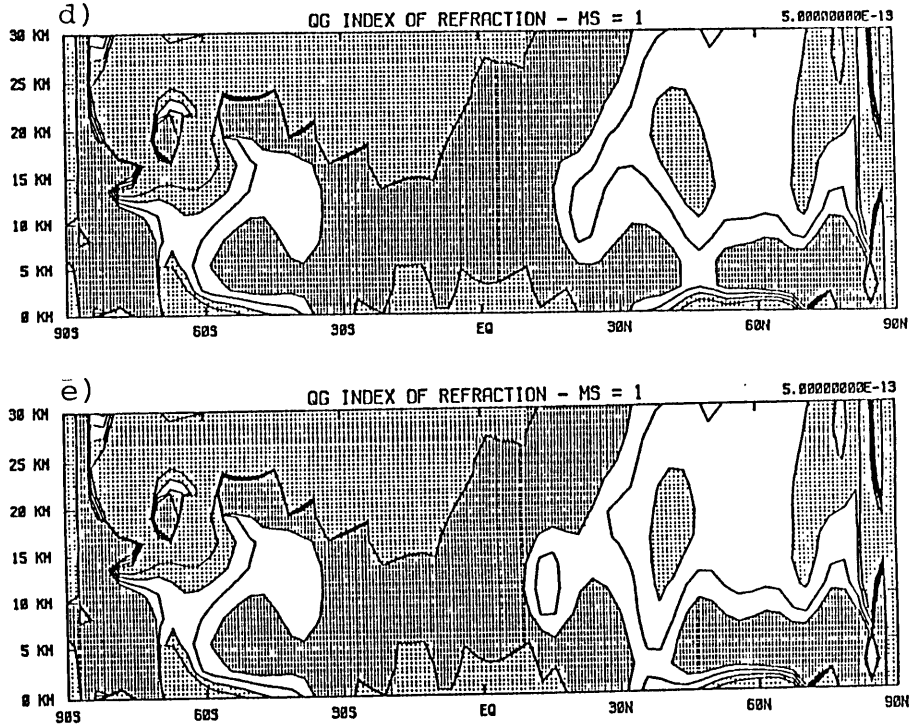

Figure 6.4: Latitude-height distribution of the control basic state zonal wind (contour interval: 2.5 meters.sec): a) zonal wind 1 (U_1), b) zonal wind 2 (U_2), c) zonal wind difference ($U_2 - U_1$); and quasi-geostrophic index of refraction squared (contour interval: 5 x 10^{-13} m^{-2}):d) computed with U_1, and e) computed with U_2. Negative contours of the zonal wind are dashed. Light shading in the index of refraction squared corresponds to values less than 5 x 10^{-13} m^{-2}; dark shading corresponds to values greater than 15 x 10^{-13} m^{-2}.

The stationary wave response for each one of the winds, along with the difference field, is shown is fig. 6.5. The first column depicts the eddy geopotential height at 300mb; the second and the third show the same fields at 150mb and 25mb, respectively. At 300mb and 150mb we see clearly that the wave train excited by the Himalayas has distinct paths for winds 1 and 2. As a consequence, the second stationary solution now has a noticeable Aleutian high, which is practically absent from the stationary wave computed with wind 1. The stationary field as a whole has increased in mid- and high-latitudes, with structural changes concentrated in the vicinity of the Tibetan plateau. The stationary waves in the stratosphere (25mb) have very little change in phase, but amplitude have increased substantially (about 3 times around 180E). Away from the main forcing region (Tibetan plateau) the difference field resembles the stationary wave field computed with wind 2, at all levels. The difference field at the troposphere gives us the impression of a tropically excited wave train, and resembles the PNA teleconnection pattern of Wallace and Gutzler (1981) over the western hemisphere. Also present in the difference field and stationary wave 2 fields are *dipolar* structures which have often been the motivation for nonlinear approaches to blocking and persistent anomalies (e.g., Malguzzi and Malanotte-Rizzoli, 1985a,b,1987)[8]. Notice that the difference field at the troposphere has a shorter meridional scale than the differ-

[8]If these dipolar structures, when added to the basic state geopotential height field, produce a structure with closed streamlines the validity of linear theory should be questioned. Notice that at least at 150mb the dipolar structures have amplitude of about 100 meters are incapable of form closed stream lines.

ence fields obtained with the barotropic model (chapter 5 model.

The vertical structure of the stationary waves and difference field is shown in fig. 6.6 on a zonal-height cross-section for 21N, 47N and 61N[9]. At 21N, we see a wave train emerging from the Himalayan region, propagating upward but not reaching levels above 15 Km. Notice that above 15 km the zonal is quite small which causes dissipation to become increasingly important, leading to wave absorption there. At mid- and high-latitudes every tropospheric feature has a stratospheric continuation. This is consistent with the westward tilts which are indicative of upward propagation. These westward tilts are more pronounced at 21N and 47N and are almost absent in high latitudes. It is interesting to note that for 47N the tilts are pretty much restricted to altitudes above 14 km. This is consistent with the observational results of Wallace (1983) who displayed zonal-height cross-sections below 100mb and found virtually no westward tilt. Because of this lack of tilt and an amplitude maximum around 300mb, Wallace argues that the waves at 40N are probably vertically trapped below the tropopause. This conclusion is not supported by our results. The vertical structure of the difference field is very similar to the vertical structure of the stationary waves themselves, particularly the one associated with zonal wind 2. They peak in the troposphere (around 10 km), and clearly have a

[9]One should be cautious about interpreting the results at the lowest levels. The identification of our vertical coordinate with the geometric z-coordinate is not reliable near the surface, particularly in the vicinity of large mountain ranges like the Himalayas.

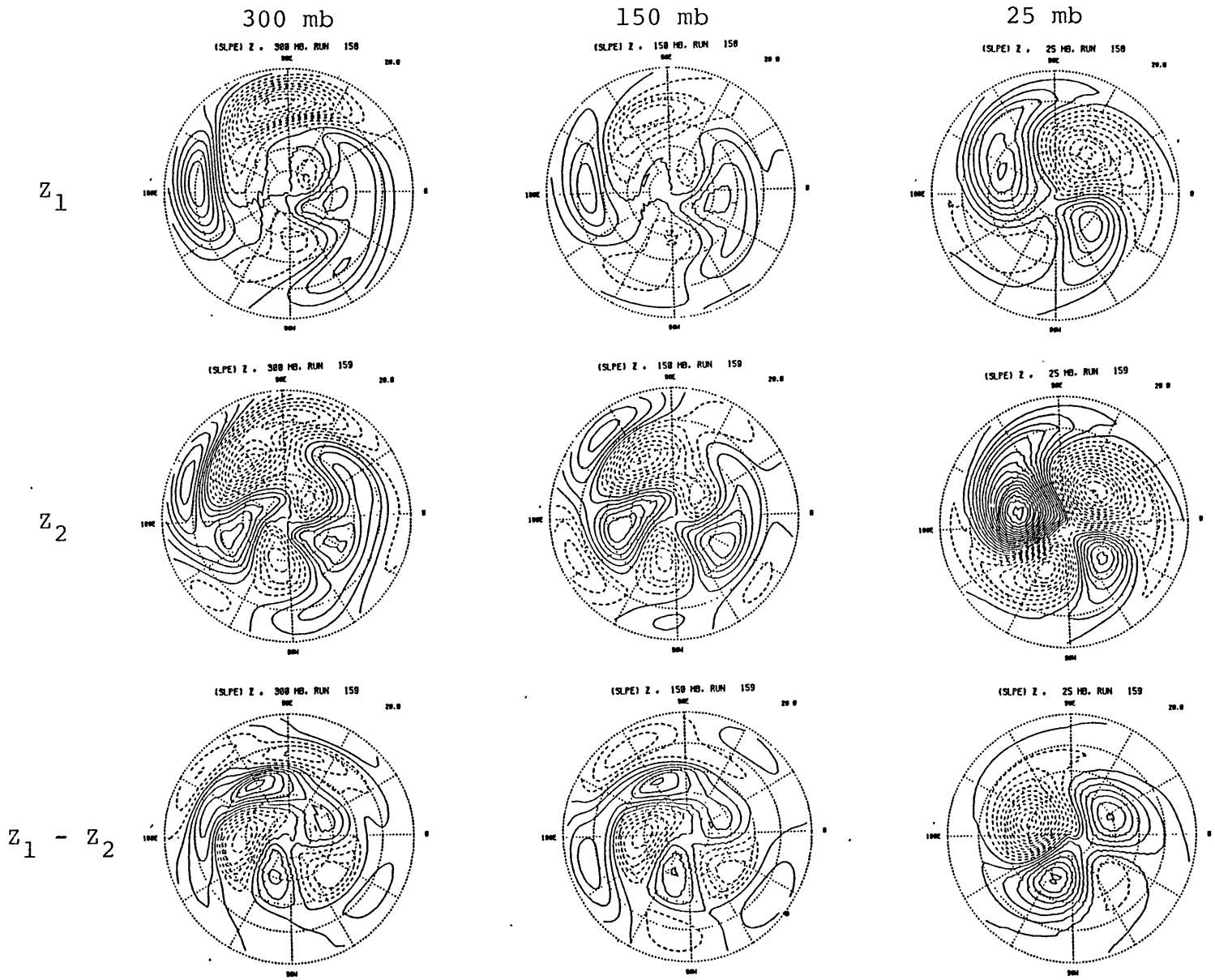

Figure 6.5: Horizontal structure of stationary wave geopotential height and difference field (control case). First, second, and third columns correspond to 300mb, 150mb, and 25mb. First and second rows correspond to the stationary waves computed with U_1 and U_2. The third row shows the stationary waves computed with U_1 (first row) minus the stationary waves computed with U_2 (second row). Contour interval is 20 meters, negative contours are dashed. The fields are shown in stereographic projection in the northern hemisphere; the outer latitude is 15N.

stratospheric continuation.

The horizontal wave flux activity first introduced by Plumb (1985) is depicted in fig. 6.7[10]. This figure confirms what we already have seen in the previous plots: the Tibetan plateau is the main source of wave activity in the northern hemisphere. For zonal wind 1, the wave activity originating at the Himalayas almost completely propagates equatorward. For zonal wind 2, part of the wave activity propagates northward to mid- and high-latitudes. The wave activity flux associated with the difference field is suggestive of waves excited at the tropical latitudes. Of course, there is no tropical source in our model.

Before we discuss the above results, we examine the effect of thermal forcing, damping and different wind changes in the subtropical jet.

Changes associated with thermal forcing

Next we set topography to zero and include thermal forcing similar to Jacqmin and Lindzen (1985) (see fig. 4.5, chapter 4). Jacqmin and Lindzen's forcing includes only latent heat release and are for the most part concentrated in the tropics.

Figure 6.8 shows polar plots at 300mb, 500mb and 25mb of the

[10]Since this flux was derived under the assumption of quasi-geostrophy its meaning at the tropics is questionable.

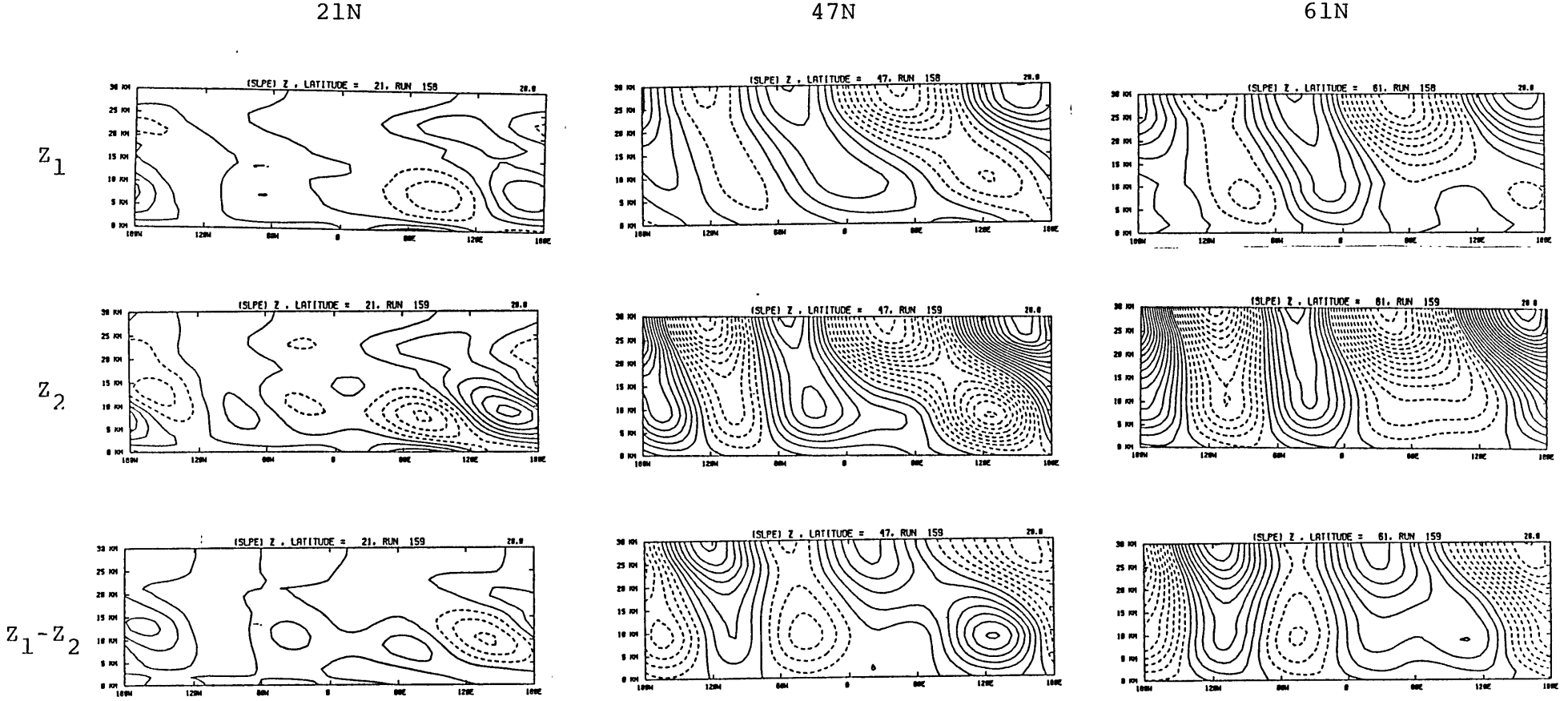

Figure 6.6: Zonal height cross section of the stationary wave geopotential heights and difference field (control case). First, second, and third columns correspond to latitudes 21N, 47N and 61N, respectively. First and second rows correspond to the stationary waves computed with U_1 and U_2. The third row shows the stationary waves computed with U_1 (first row) minus the stationary waves computed with U_2 (second row). Contour interval is 20 meters, negative contours are dashed.

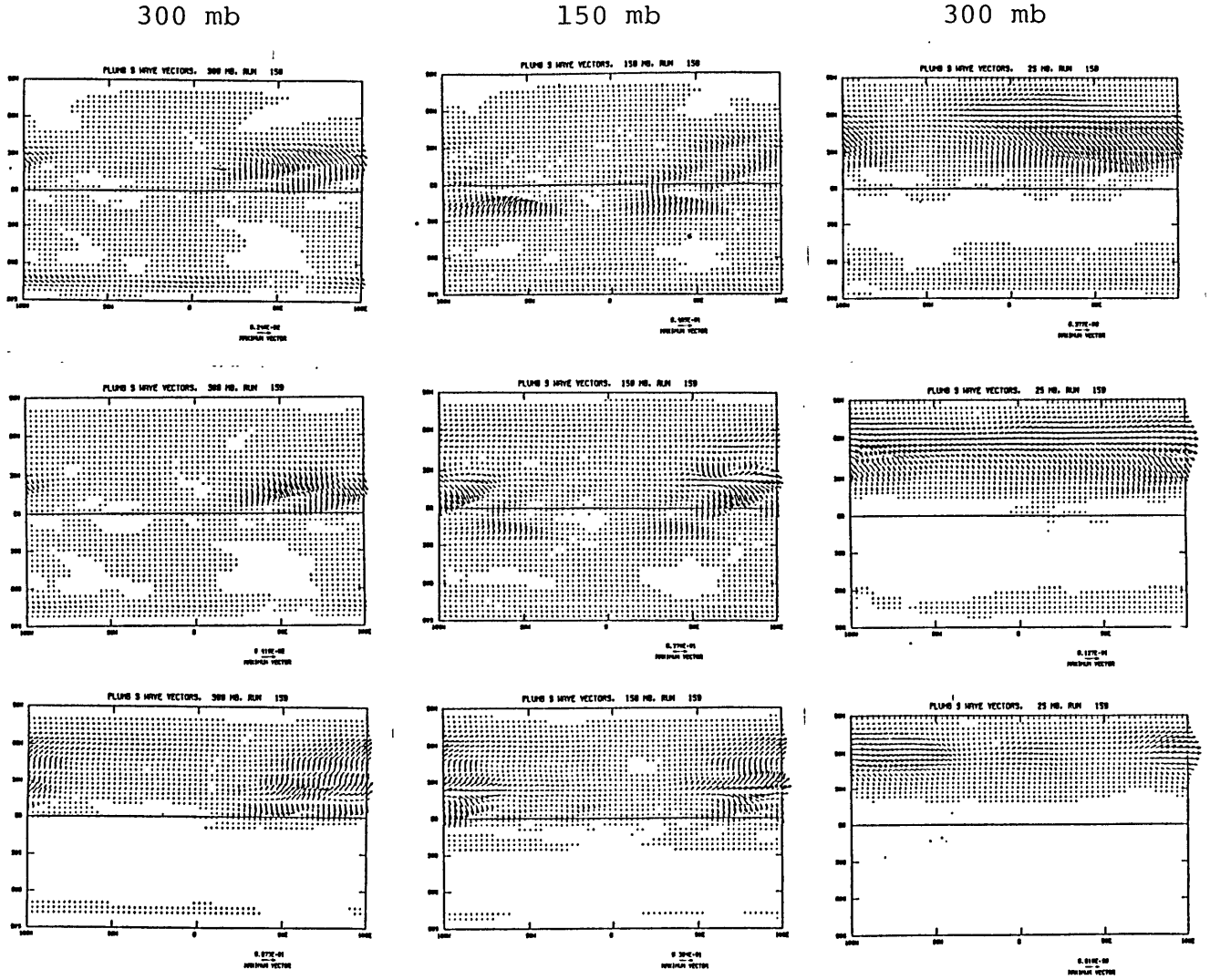

Figure 6.7: Plumb's horizontal wave flux (control case). First, second, and third columns correspond to 300mb, 150mb, and 25mb. First and second rows show the wave flux for the stationary waves computed with U_1 and U_2. The third row shows the wave flux for stationary waves computed with U_1 (first row) minus the wave flux for stationary waves computed with U_2 (second row). The magnitude of the maximum vector length is shown below each plot. Units:m/sec^2.

stationary waves and the difference field. As pointed out by Jacqmin and Lindzen, this thermal forcing produces stationary waves that are about 40% of the topographically forced waves in the troposphere. At the stratosphere (25mb), the thermally forced waves can be comparable in amplitude to the waves forced by topography in some places. At 300mb and 150mb the difference field is generally small and has a very short meridional scale. This is hardly surprising since the waves are apparently forced by latent heat release in the Pacific storm track and are not very much affected by wind changes in the subtropics. The difference field in the stratosphere is about the same order as the the difference field for the topographic waves. The high around 60W is in phase with its topographic counterpart while the low at 30E is out of phase.

In summary, thermally forced waves are more likely to play a role in the adjustment mechanism only in the stratosphere.

Effect of dissipation

Since dissipation is generally a very *ad hoc* factor entering linear models, it is always worthwhile to check the dependence of the results on damping. The linear damping fields are showed in fig. 4.7a of chapter 4. Fig. 6.10 shows the horizontal structure of the stationary waves and the difference field in the absence of boundary layer drag. The phase of

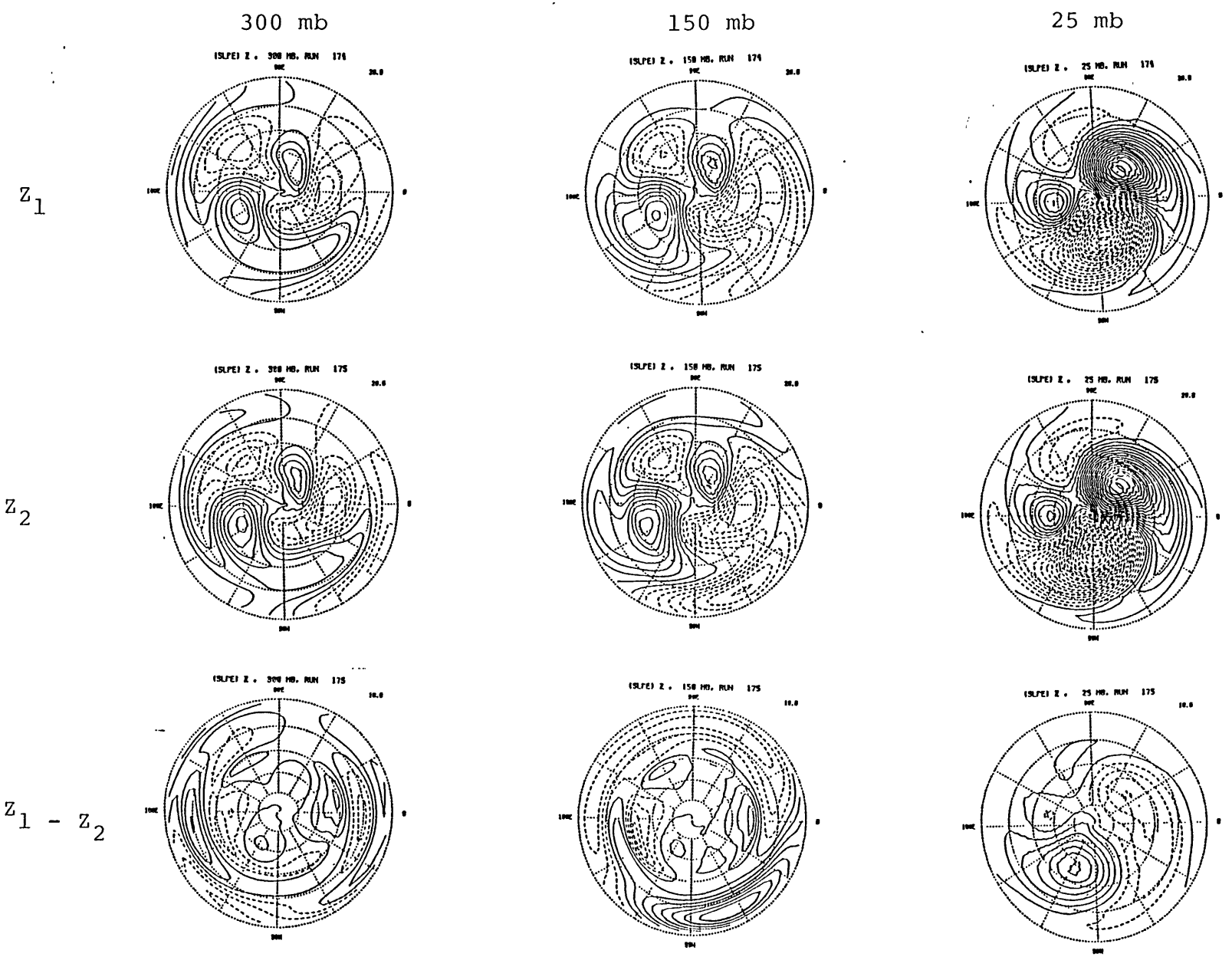

Figure 6.8: As fig. 6.5, but for the horizontal structure of stationary wave geopotential height and difference field with thermal forcing alone.

stationary waves and the difference field is very similar to the control case (fig. 6.5). However, amplitudes are about 50% higher on average away from the forcing region. This is characteristic of waves propagating horizontally near the ground, rather than the effect of damping on the local response. The stationary waves and difference field for the strong damping case (twice the control case) are presented in fig. 6.10. As before, the phases are very similar to the control case, but now, due to the increased dissipation, the amplitudes are reduced. On average, amplitudes are about 80% of the amplitudes shown in fig. 6.5. The inclusion of critical-line damping (see section 4.3.3) did not introduce any noticeable modification of the control case results and therefore will not be presented.

In summary, damping appears to have a small effect on the phase of the disturbances, and influences amplitudes according to its strength. Amplitudes are more sensitive to boundary drag than they are to the doubling of linear damping in the interior. Critical line dissipation is of secondary importance, at least for these basic states. Nigam and Lindzen (1989) also found the same dependency on boundary layer drag.

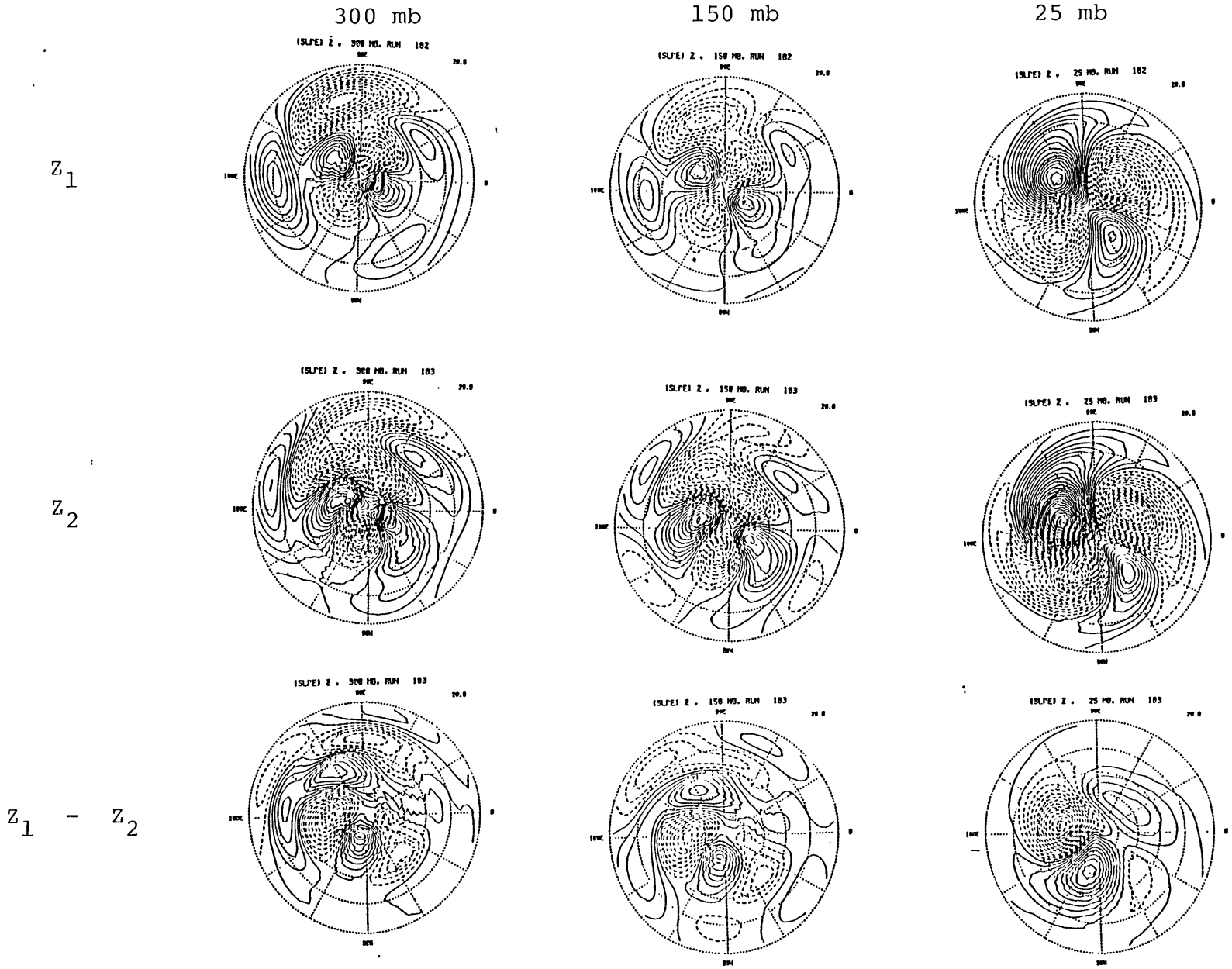

Figure 6.9: As in fig. 6.5, but without boundary layer drag.

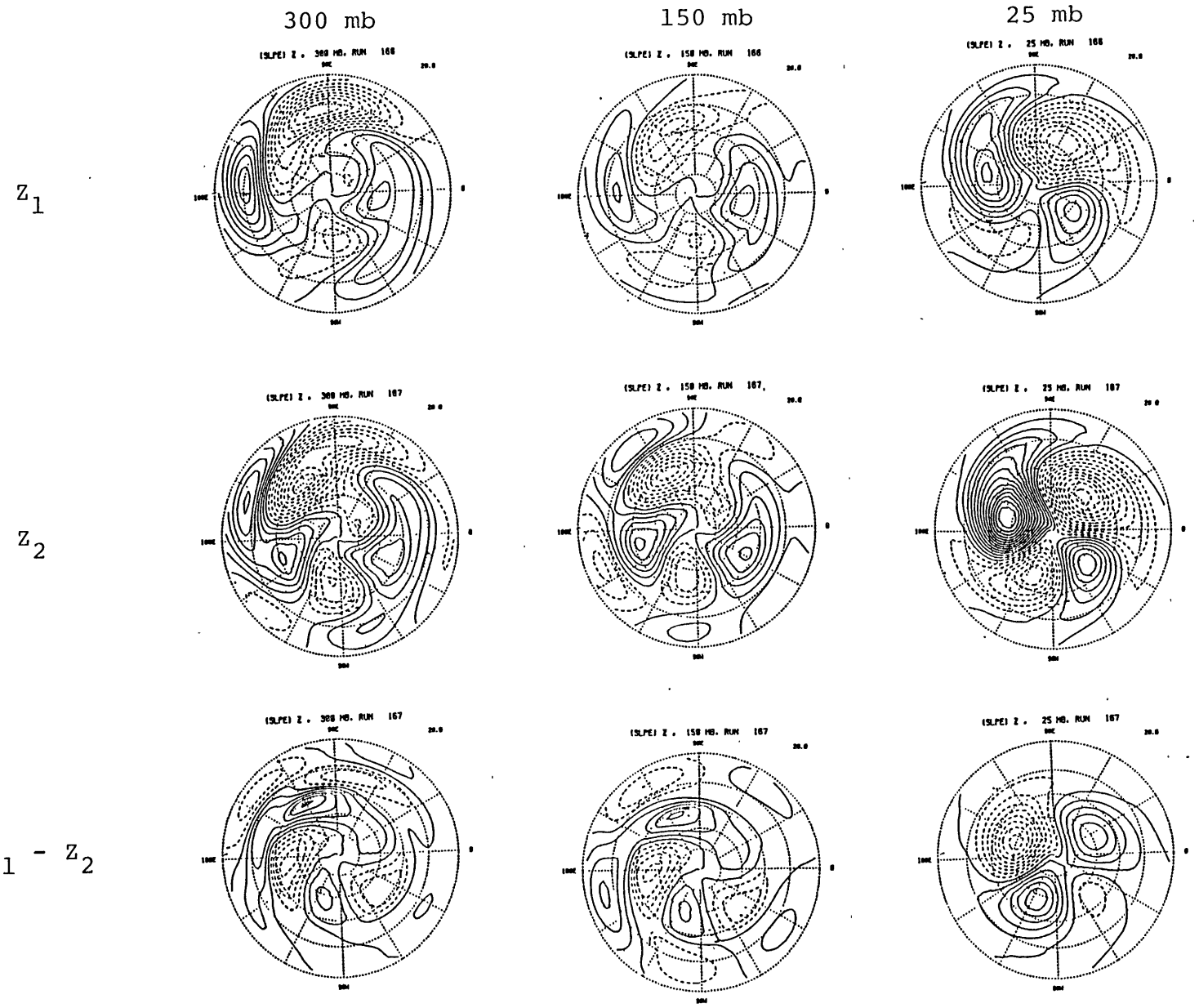

Figure 6.10: As in fig. 6.5, but with strong damping in the interior.

Other wind changes

The dipolar wind change of the control case (see fig. 6.4) is based on Nigam and Lindzen's (1989) idealized wind change. It is designed to roughly mimic wind changes associated with angular momentum redistribution. We now examine the effect of other ways to shift the subtropical jet. In fig. 6.11 we show wind changes as well as difference fields at 300mb. For ease of comparison, we also show the control case plots. The monopole case of fig. 6.11a is simply one half of the dipole used in the control case. The difference field associated with this jet shift is very close to the control one, with amplitudes only slightly smaller, in agreement with the findings of Nigam and Lindzen (1989). The dipole wind change shown in fig. 6.11 has half the amplitude of the control dipole. The associated difference field has approximately the same phase, but now amplitudes are about half the amplitudes of the control case. Conversely, the stronger dipole depicted in fig. 6.11 has twice the amplitude of the control case and the associated difference field has amplitudes about 1.6 the control case. The last wind shift shown is a *broad* dipole with the same amplitude as the control case. The difference field has phase of about 15 degrees eastward of the control case and amplitudes ranging from 1 to 1/3 of the amplitudes of the control run. An inspection of the stationary wave fields (not shown) indicates that the wave train excited by the Himalayas does not completely split when the wind 2 associated with this broad dipole

is taken as basic state.

Nigam and Lindzen (1989) considered a basic state in which the subtropical jet was about 30 m/sec. Despite the fact that their stationary wave fields differs somewhat from ours, their difference fields have about the same magnitude as our control case (about 120 meters in the troposphere).

Spectral structure

As in chapter 5, we now present the spectral structure of the difference field. This is done in order to determine whether Rossby waves are *available* in the stationary wave differences, which is a necessary condition for excitation of these modes in the time dependent model (see chapter 3 and 5.)

Comparison of fig. 6.5c with fig. 5.5 of chapter 5 shows that the difference field amplitude for the barotropic model is just about 30% higher than the baroclinic case, with phases roughly in agreement in the north Pacific region. However, the difference field in the baroclinic model has a shorter meridional scale. This is apparent in the Hough coefficient distribution depicted in fig. 6.12. Projection onto models with meridional wavenumber less or equal to 2 is virtually zero. Modes with meridional wavenumber equal to 3, the so-called 16-day waves, have on average less than 1/3 the amplitude found in the barotropic

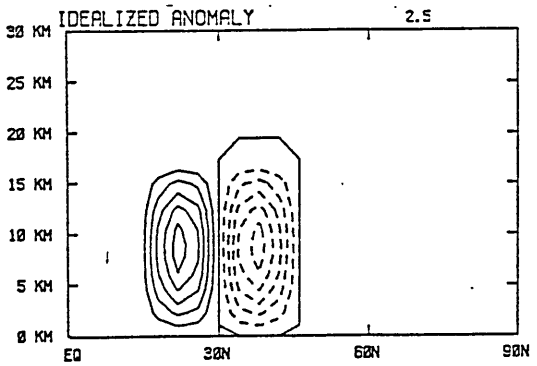

a)

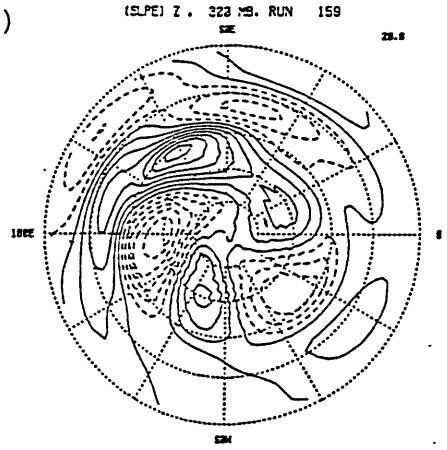

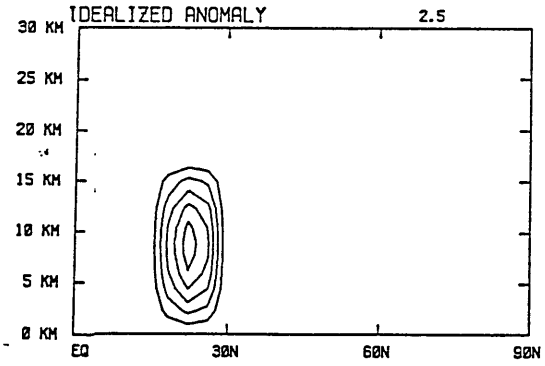

b)

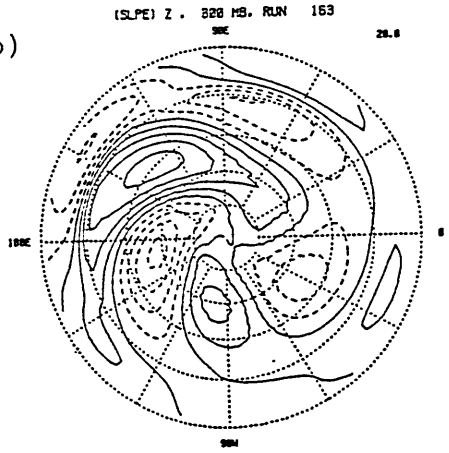

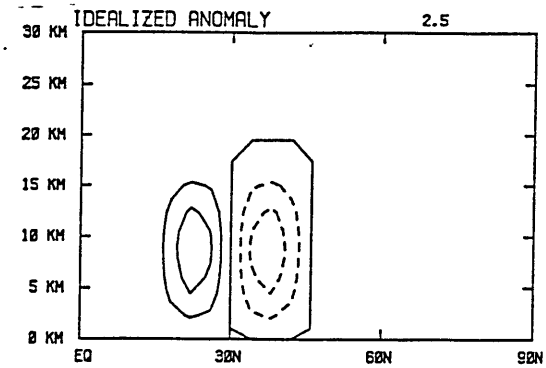

c)

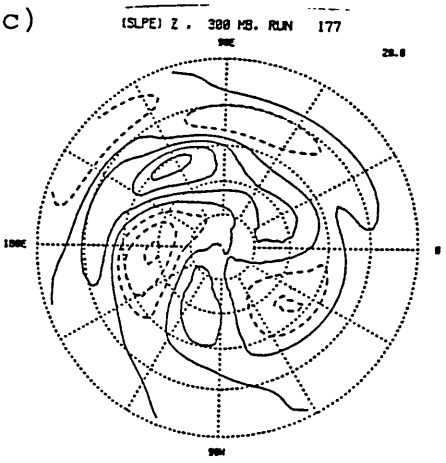

(See caption on next page)

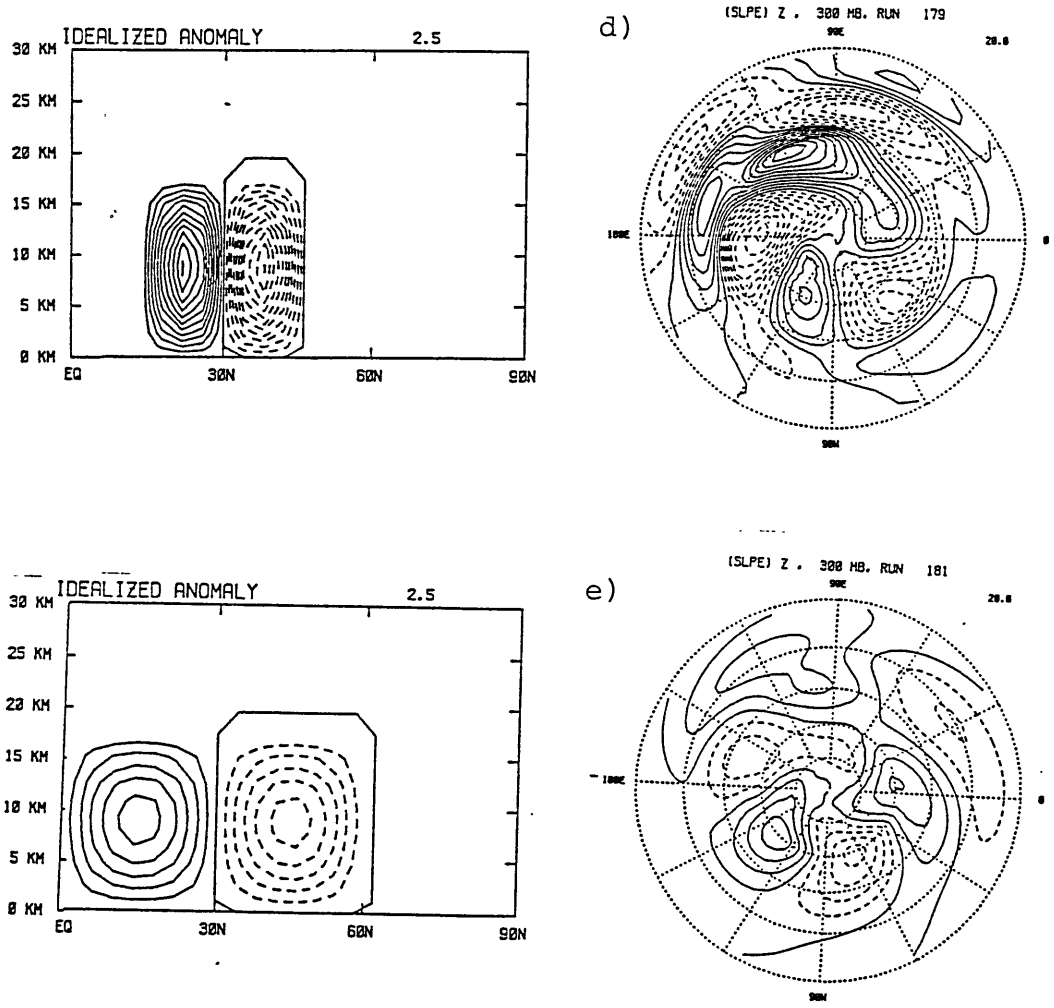

Figure 6.11: 300 mb stationary wave difference field for various changes in zonal wind. The left panel shows the difference in zonal winds (contour interval: 2.5 m/sec) and right panel shows the stereographic projection in the northern hemisphere of the difference field (contour interval: 20 meters): a) control case, b) monopole, c) weaker dipole (previous page), d) stronger dipole, and e) broader dipole (this page).

calculation. The highest amplitude for these waves is about 75 meters, found for zonal wavenumber 3, which is just half of what was found for the barotropic case. As we will see in section 6.5, Rossby waves are not excited in the baroclinic time dependent model.

Discussion

Since Charney and Drazin (1961), the upward propagation of stationary waves has been accepted as an inherent property of Rossby waves. This problem was further studied by Dickinson (1968) who, like Charney and Drazin, emphasized wind magnitudes as the main factor determining planetary wave propagation. Matsuno (1970) was the first to demonstrate that the full meridional gradient of the basic state potential vorticity, involving wind shear and curvature, should be included in order to achieve an accurate description of the quasi-geostrophic index of refraction. Lin (1982) and Karoly and Hoskins (1982), among others, confirmed Matsuno's results that the minimum in index of refraction right above the tropopause around 40N acts as a *diverter* for waves excited from below[11]. Waves diverted poleward will find their way by propagating upward in the wave guide formed by this minimum and the turning point in high latitudes; at the stratosphere the wave *rays* follow the maximum in refractive index associated with the Polar Night

[11]More precisely, this minimum in Q^2 acts as lid, preventing propagation to the stratosphere at these latitudes. The net result is an alteration of the wave path, which vears northward causing propgation to the stratosphere to occur northward.

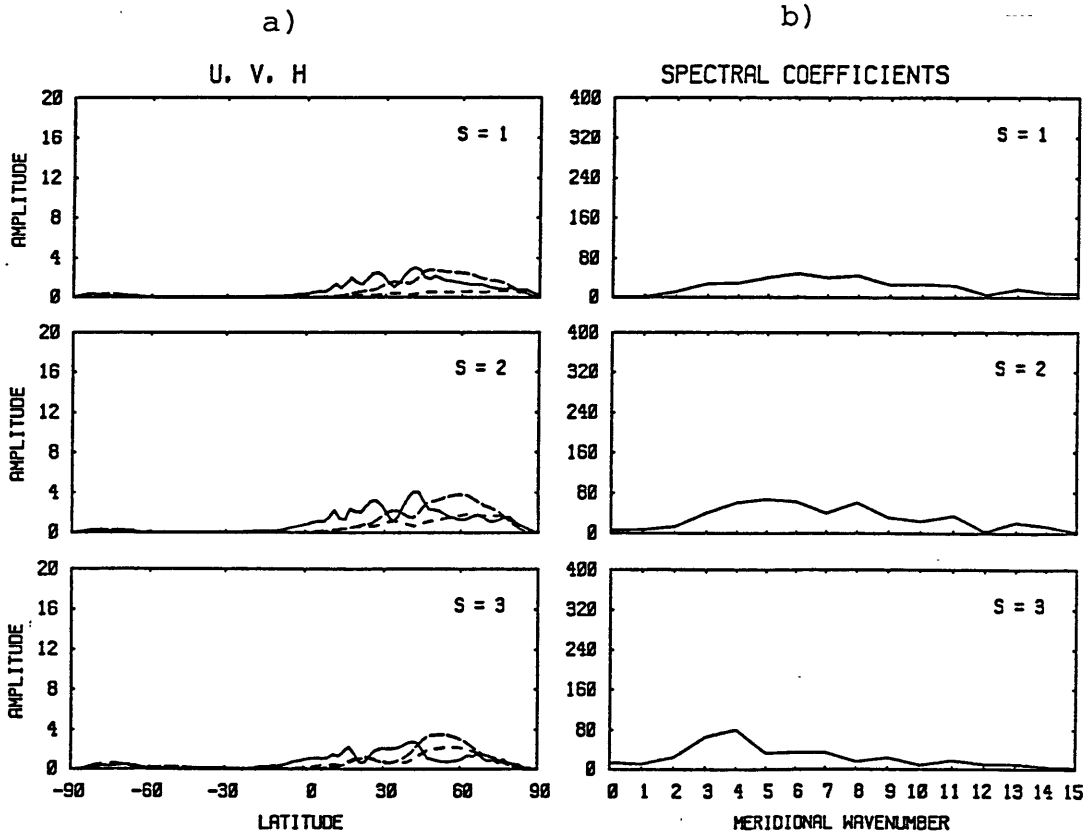

Figure 6.12: Hough function spectral coefficients (control case): a) amplitude of the difference in stationary waves used in the spectral decomposition (u, v in meters, Z in dekameters) for each zonal wavenumber; b) amplitude of spectral coefficients in terms of Hough functions (meters), for each zonal wavenumber.

Jet (PNJ). The other portion of the waves diverted equatorward will eventually be absorbed in the tropical critical latitudes, provided there is enough dissipation there.

The above dependence on zonal winds can be understood in light of quasi-geostrophic wave theory and the concepts in the last paragraph. A schematic illustration is given in fig. 6.13. in terms of an idealized index of refraction squared (Q^2), where only the relevant features are shown. The minimum around (45N,16Km) is somewhat in between the subtropical and the polar night jets and corresponds to a minimum in the meridional gradient of potential vorticity (see Matsuno, 1970). The turning points at high latitudes, where Q^2 changes sign, are associated with the term $s/cos\phi$; the increase of Q^2 toward the surface and equatorward is related to the vanishing of the zonal wind at these places. According to ray tracing theory (e.g. Karoly and Hoskins, 1982), wave rays are refracted toward regions of increasing Q^2. Thus, waves excited by the Himalayas would propagate northward *near* the surface up to a certain latitude (45N) where they would then *bounce* in the lower boundary and start propagating upward. This latitude corresponds to the apparent lower level wave source region reported by the Eliassen-Palm flux calculations in stationary wave models (Lin, 1982; Jacqmin and Lindzen, 1985). The relative position of the Q^2 minimum relative to this latitude determines the path to be taken by the waves. When the subtropical jet is shifted equatorward this minimum also shifts equatorward and more rays are diverted northward/upward.

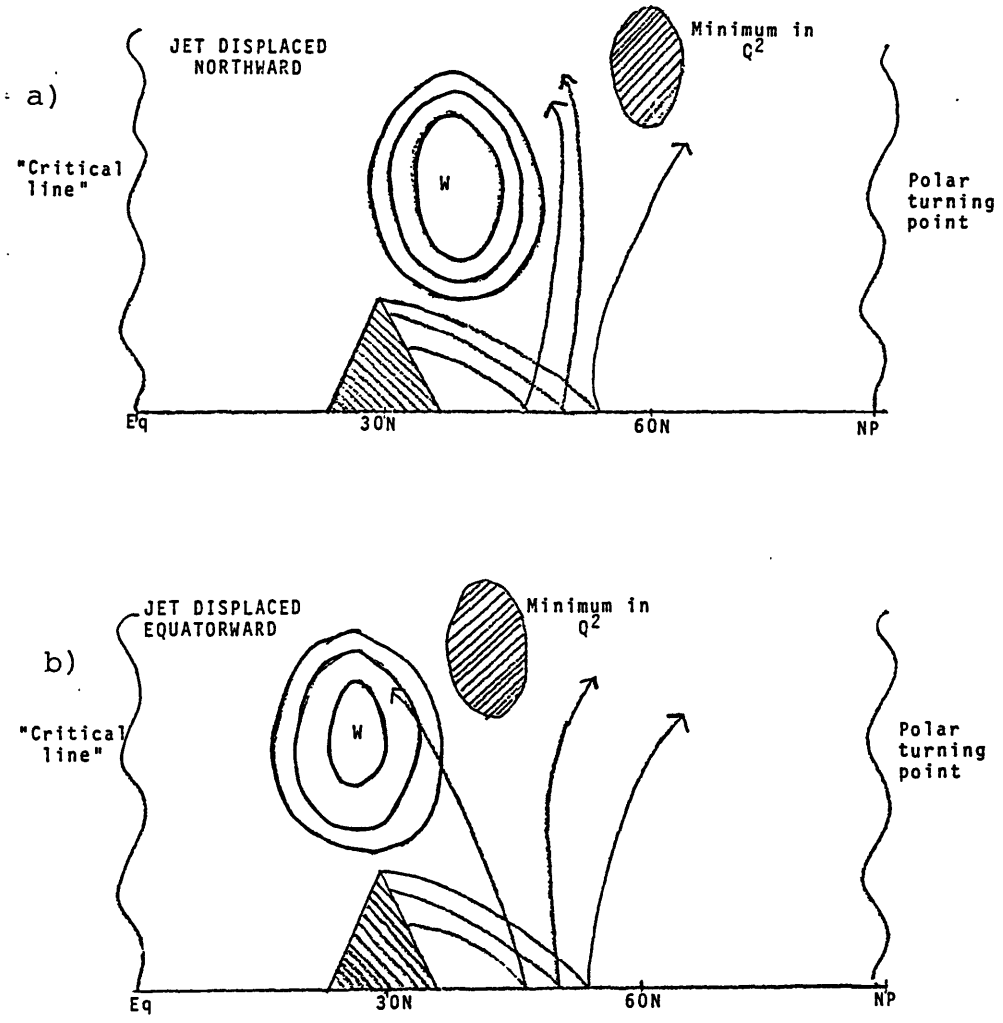

Figure 6.13: Schematic index of refraction associated with the subtropical jet shifted: a) northward, and b) equatorward.

This mechanism explains why the wave train excited by the Tibetan plateau (see fig. 6.5) splits for a jet displaced equatorward. Notice that the *barrier* causing this split is at the same latitude as the minimum in index of refraction reported in fig. 6.4. This mechanism is the heart of the schematic picture given by Nigam and Lindzen (1989).

6.4 The establishment of the new stationary wave

The establishment of stationary waves is an interesting problem in its own right. The time scale for meridional and vertical propagation of stationary wave energy is easily estimated using the group velocity computed from the Rossby wave dispersion relation, $\sigma = U_o - \beta/(k^2 + \ell^2 + m^2)$ (see for example Karoly and Hoskins, 1982). Even though energy propagation speeds can be estimated in a steady model with dissipation, to the best of our knowledge this calculation in a baroclinic time dependent model has not been done yet. One reason for this is the fact that numerical and hydrodynamic instabilities make it virtually impossible to integrate the equations from a zero initial condition to the full establishment of the forced solution. An alternative to this procedure is to start with a zonal wind and its *steady* solution, shift the wind from one configuration to another and monitor the establishment of the new stationary solution. Since the solution at time t has a stationary wave kind of balance, it poses no burden on the numerical

scheme. For large zonal and meridional scales baroclinic stability is not likely to play a major role.

The key quantity to be used in this section is the geopotential at time t minus the initial condition. We will call this quantity the *anomaly* field. If the initial condition were some sort of climatology, the solution at time t would be an excursion from the climatology, i.e. an *anomaly*. Unless otherwise noted, the term anomaly will be used in this sense.

Checking the steadiness of the stationary solution

The stationary and time dependent models (see chapter 4) were designed to have a high degree of compatibility. Unfortunately, it is not always possible to do so exactly, but only to the order of accuracy of the numerical schemes. In order to check the *steadiness* of the stationary solution in the time dependent model, as well as the possible effect of instabilities, we consider an initial value problem with no wind changes. We show in fig. 6.14 the time evolution from day 1 to day 7 of the anomaly field. The model was initialized with the stationary solution associated with the wind 1 of the control case. In the zonal-height cross section of fig. 6.14 the contour interval has been lowered to 5 meters in order to monitor the small changes in the initial days. Although the stationary solution is not exactly steady, the departures

from steadiness are fairly small compared with the changes that occur when the wind is allowed to vary (see below). By day 7, the amplitudes at the troposphere are at most 12 meters and about 5-6 meters in the stratosphere.

The control case

The control case for the time dependent model consists of the same wind changes as for the control stationary case (see previous section), and a transition period $\tau = 7$ days, in which the wind shifts from one configuration to another. Damping and resolution are also as in the stationary model ($\Delta\phi = 2$ degrees and $\Delta z \approx 1.8Km.$) The value of the parameter τ was chosen so that in the end of the transition period the *new* stationary solution is a little more than half established. The dependence on τ will be discussed later in this section.

Fig. 6.15 presents the time evolution of horizontal structure of the anomaly field at 300mb, 150mb and 25mb, for 7 consecutive days. The initial condition is chosen to be the stationary solution associated with the wind 1. At day 1, we have amplitudes in excess of 10 meters only at 300mb and 150mb, right downstream of the Tibetan plateau. One day later (day 2), the amplitude at this center has increased to about 25 meters at 300mb and to about 20 meters at 150mb. Also, other centers have *popped out* downstream, slightly northward. At day 2, there is

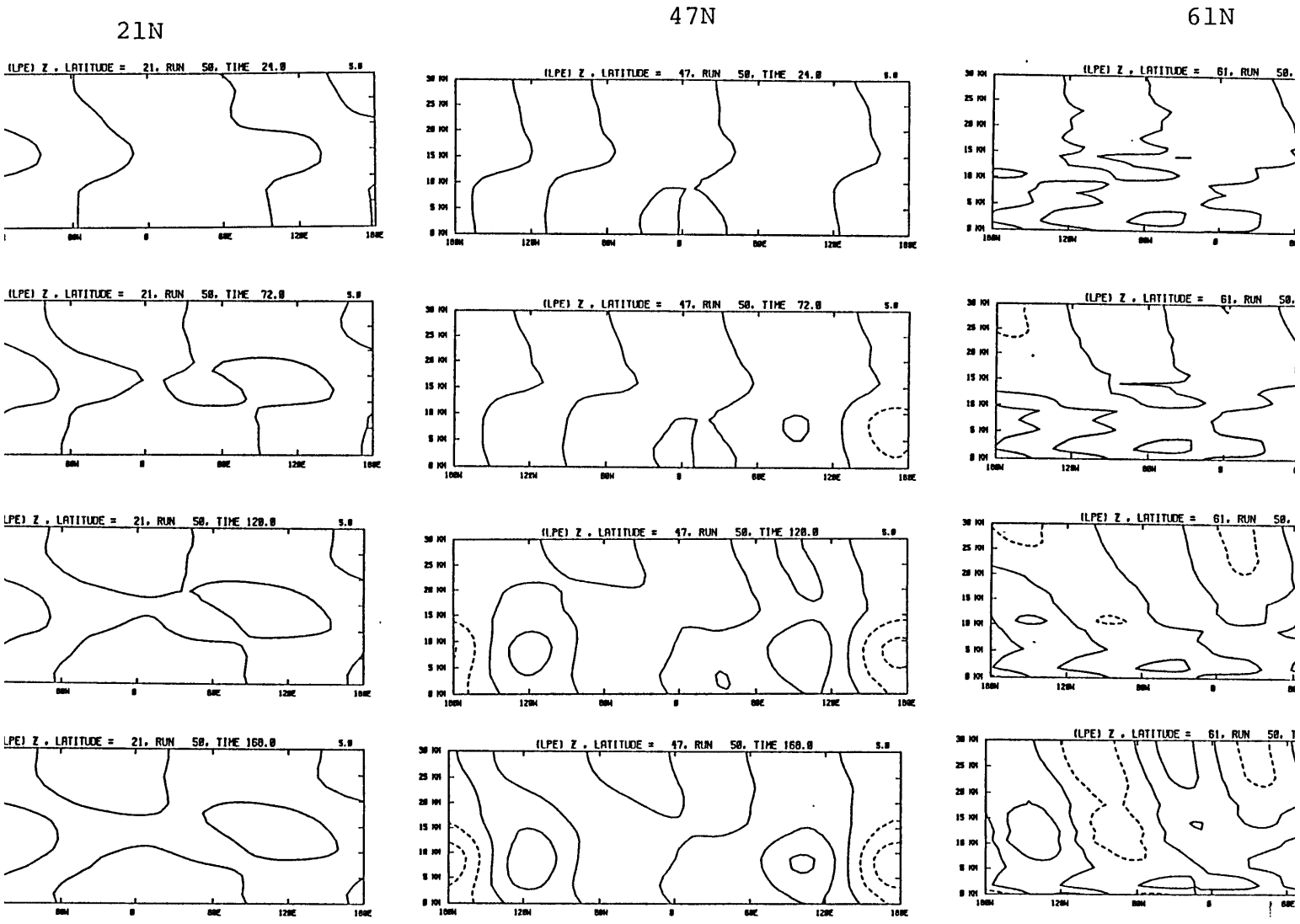

Figure 6.14: Zonal-height cross section of the anomaly field for a basic state independent of time. First, second and third columns correspond to latitudes 21N, 47N, and 61N respectively. Rows one through 4 correspond to days one through seven. The field shown is the geopotential height and the contour interval is 5 meters. Negative contours are dashed.

no noticeable disturbance at the stratosphere (25mb). By day 3, the centers at 300 and 150mb continue to develop and by now there are disturbances in the stratosphere (25mb) of about 10 meters. From day 4 to day 7 the disturbances at all levels appear to grow in place, with only a slight eastward-northward propagation. Comparing fig. 6.15g with fig. 6.5c[12], we see that at day 7 most of the centers have already developed in the right place, but amplitudes are only about 60-70% of their final value. There is also a tendency for centers to be slightly to east of their final position. Notice that meridional energy propagation is almost always accompanied by zonal propagation. This development is similar to what we would get if a vorticity source were specified at the Himalayan region with the wind kept constant (e.g. Hoskins and Karoly, 1982). Except for the shorter meridional scale present here, the development is similar to the barotropic development (section 5.2.2.)

Fig. 6.16 depicts the zonal-height cross-section of the same quantities presented in fig. 6.15, at latitudes 21N, 47N and 61N. At day 1, there is no noticeable disturbance at these latitudes, which is consistent with the initial development seen in fig. 6.15a. By day 2, there is indication of a wave train emanating from the Himalayan region (80E-120E) and propagating eastward at 47N, in the troposphere. Amplitudes are only slightly in excess of 15 meters. At 21N and 61N amplitudes are on average less than 5 meters at this time, with a minor negative center at 61N, right downstream of the Himalayas. One day later (day 3),

[12]Beware of different contour intervals.

300 mb 150 mb 25 mb

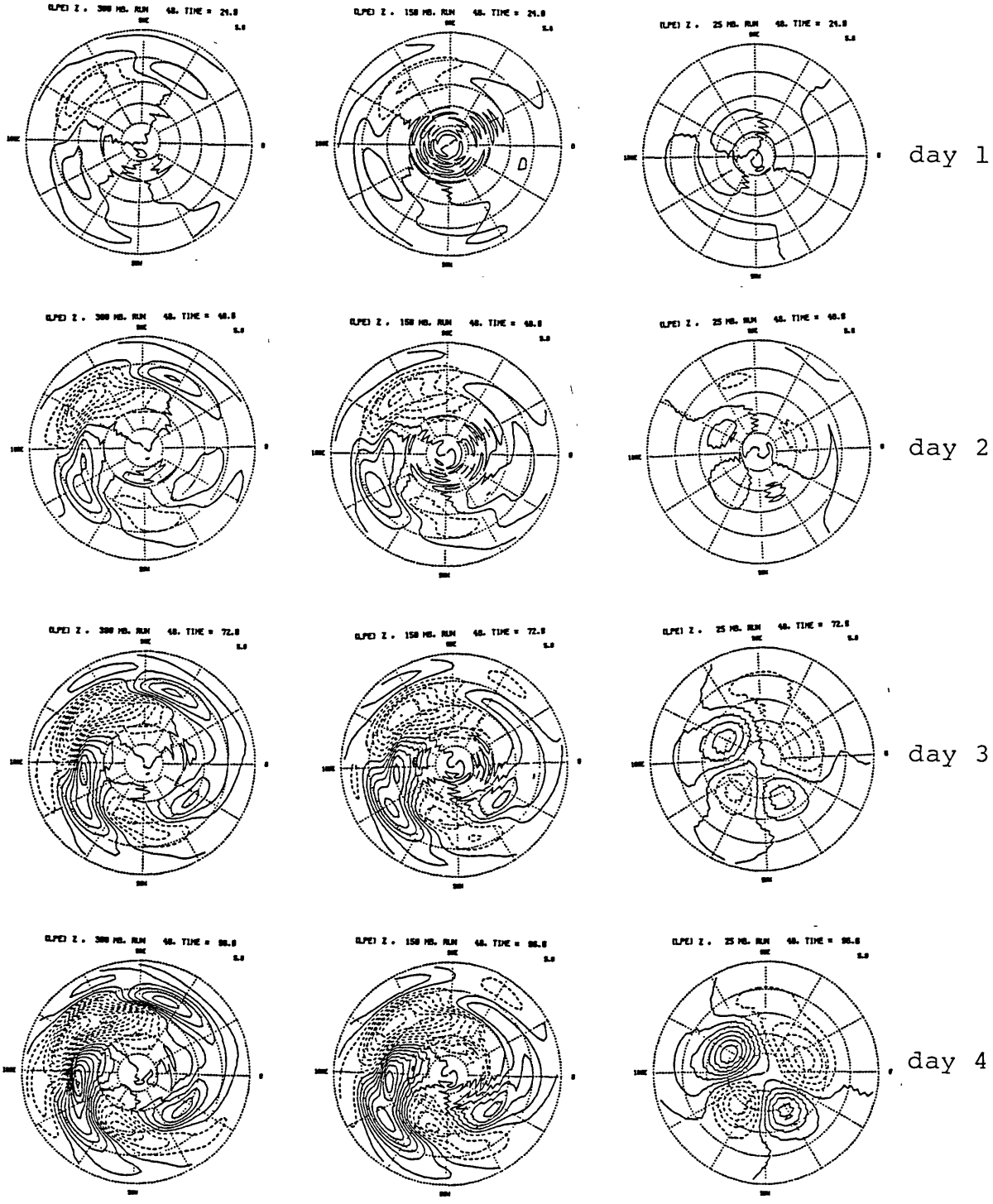

day 1

day 2

day 3

day 4

(See caption on next page)

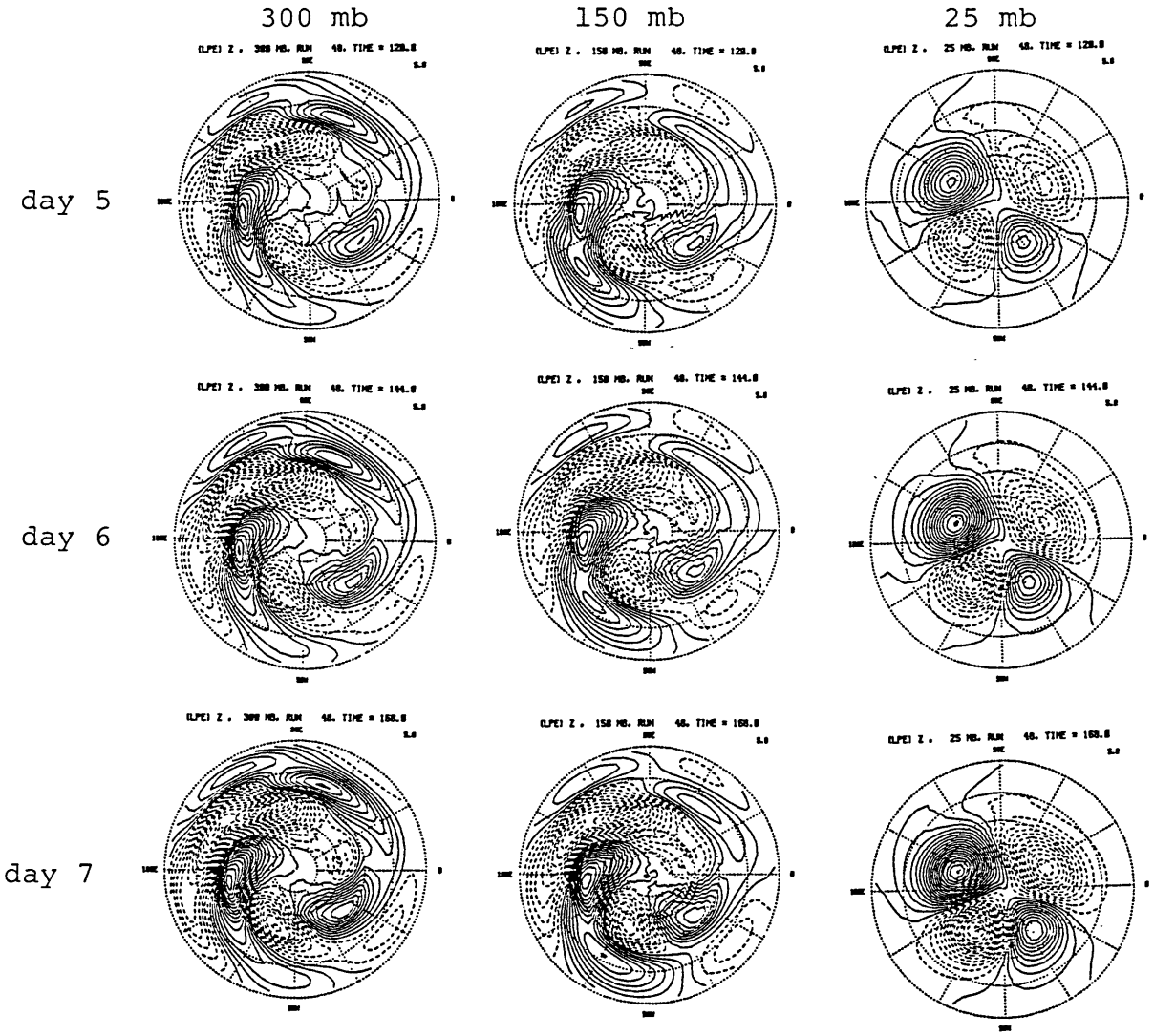

Figure 6.15: Time evolution of the horizontal structure of the anomaly field (control case). First, second and third columns correspond to 300mb, 150mb and 25mb. Rows one through four (previous page) correspond to days one through four, and rows three to seven (this page) correspond to days three through seven. The anomaly field is shown in stereographic projection in the northern hemisphere; the outer latitude is 15N. The contour interval is 5 meters and negative contours are dashed.

the wave train at 47N starts propagating upward and its amplitude is now about 25 meters. Sign of upward propagation is also seen at 61N, while the disturbances at 21N are beginning to develop. Subsequent development is marked by amplification of the tropospheric centers accompanied by upward propagation, except in the subtropics (21N). By comparing figs. 6.16g and 6.6c we see that the stationary solution is more rapidly established in mid and high latitudes. As seen in the horizontal structure, by day 7 the centers are slightly to east of their final position.

Reversing the wind shift

Now we investigate how the development of the new stationary solution is affected when we force a transition from the state 2 to state 1 of the control case. Namely, we swap wind 1 with wind 2 in the control run, and initialize the model with the stationary solution of the old wind 2. The stationary wave difference field, of course, is just the negative of the fields shown in figs. 6.5 and 6.6.

In fig. 6.17 we show the zonal-height cross-section of the anomaly field, at 2 day intervals. The same qualitative development noted in fig. 6.16 takes place. However, there is a substantial reduction of propagation to the stratosphere. Until day 3 the two developments are very similar, both showing more of a tropospheric structure. After

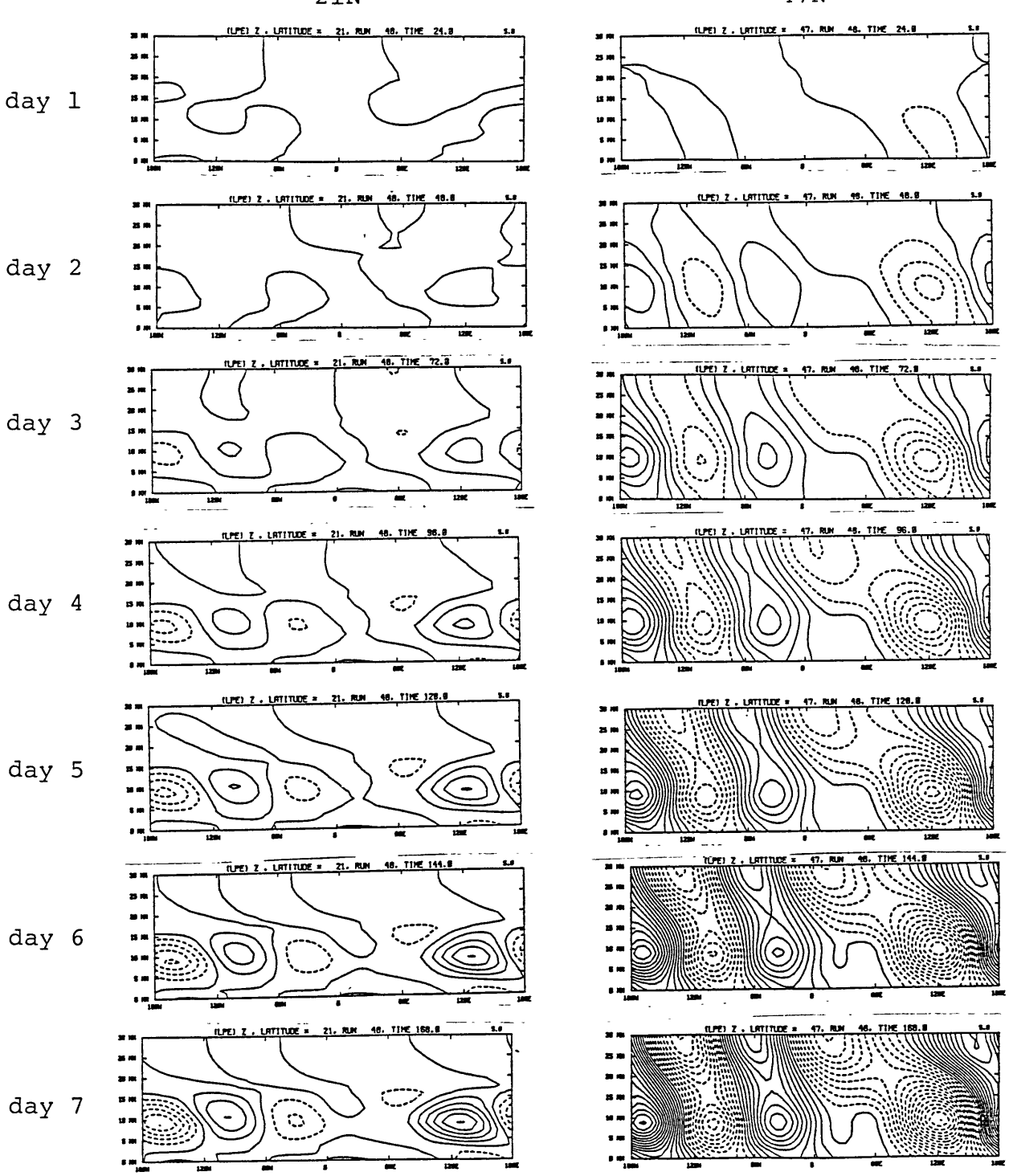

(See caption on next page)

day 1

day 2

day 3

day 4

day 5

day 6

day 7

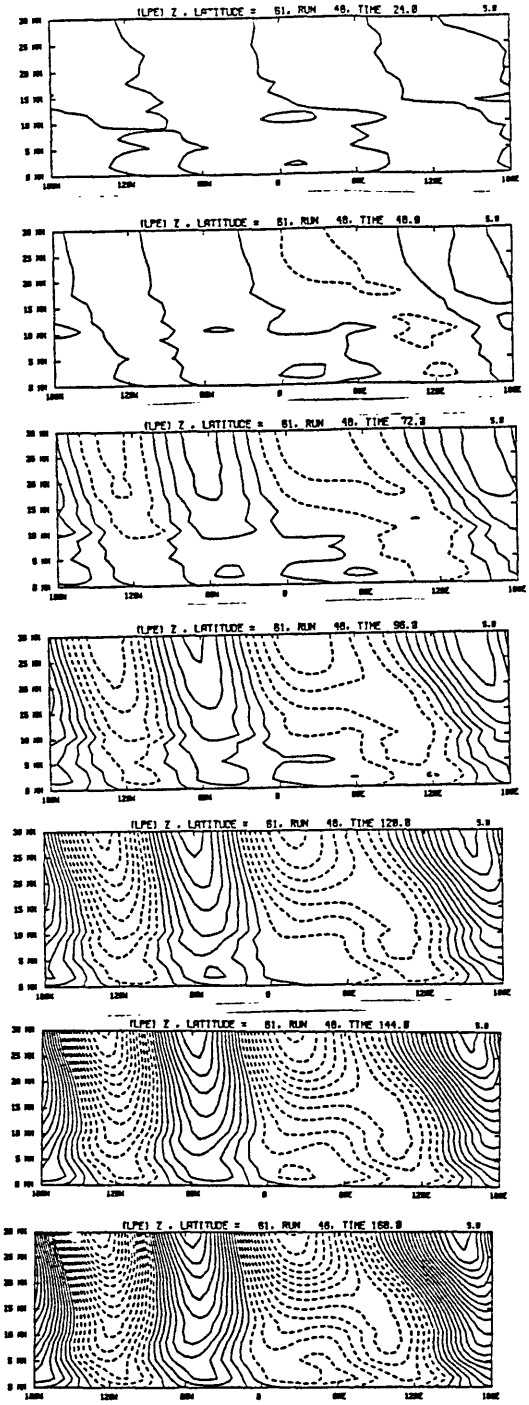

Figure 6.16: Time evolution of the longitude-height cross-section of the anomaly field (control case), from day 1 to day 7: a) at 21N, b) at 47N (previous page), and c) at 61N (this page). Contour interval is 5 meters and negative contours are dashed.

day 3, the control case starts showing increasingly upward propagation to the stratosphere, which does not happen for this case. Even in the troposphere the amplitudes are about 60-80% smaller than in the control case.

This seemly contradictory behavior can be understood we recall that the stationary waves initially in the stratosphere are associated with propagation from below. When we switch from wind U_2 to wind U_1, we introduce a cut-off in the propagation from the troposphere to the stratosphere. We can think of it as isolating the troposphere from the stratosphere. So, the waves in the stratosphere shifts toward the second steady solution primarily through the local dissipation, which has a longer time scale than the usual Rossby wave dispersion. Therefore, in this case the establishment of stationary waves is chiefly determined by dissipation, rather than by the dispersive properties of stationary Rossby waves, at least in the stratosphere.

Dependence on τ

Now we investigate whether the establishment picture emerging from the control case is particular to the value of τ chosen. We will consider two cases: 1) a faster wind change (τ=3); and 2) a slower wind change (τ=14 days). We show in fig. 6.18 the anomaly field at 300mb for the case τ =3 days (left panel) and for the case τ =14 days. As in

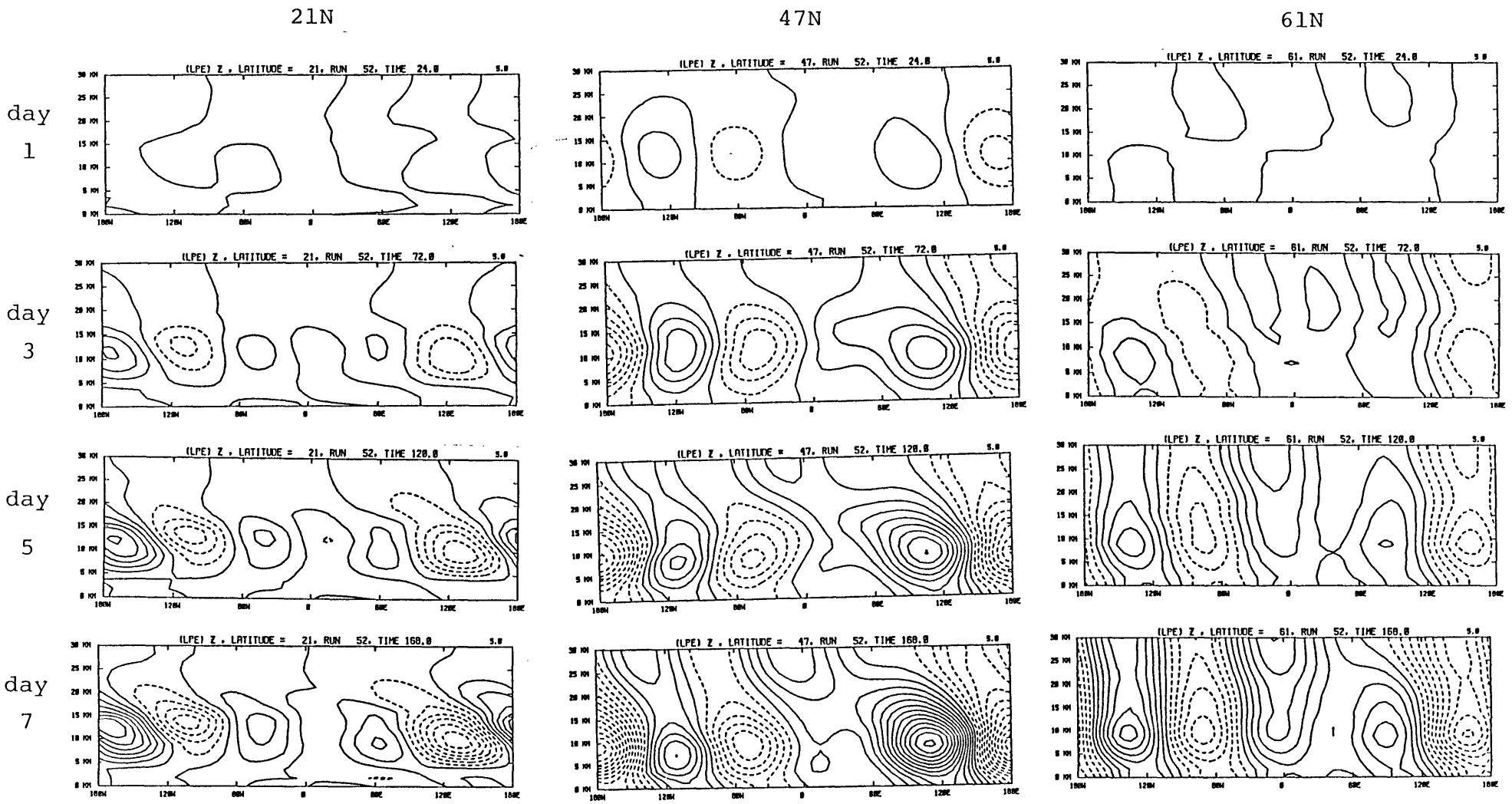

Figure 6.17: As in fig. 6.14 but for the reversed wind shift case. Also, the anomaly field is shown here every 2 days (instead of daily).

the control case the anomaly field shows the same sign of Rossby wave energy propagation from the Tibetan plateau. The main difference here is the rate at which energy propagates downstream of the Himalayas. For example, by day 3 the negative center around 150E has amplitude of about 55 meters for $\tau = 3$ days, about 40 meters for $\tau = 7$ days and about 30 meters for $\tau = 14$ days. The phase of the anomaly field is fairly independent of τ, with the centers slightly displaced eastward for longer τ.

Discussion

In this section we have established that there is no qualitative difference between changing locally the forcing or changing locally the medium. In both cases, information propagates with the group velocity of stationary Rossby waves.

We have thus far concentrated on the establishment of the new stationary solution during the transition period, i.e., the period it takes the wind to go from one configuration to another. Since in the control case most of the features are already established by this time, we proceed to present the evolution of the transients after this time.

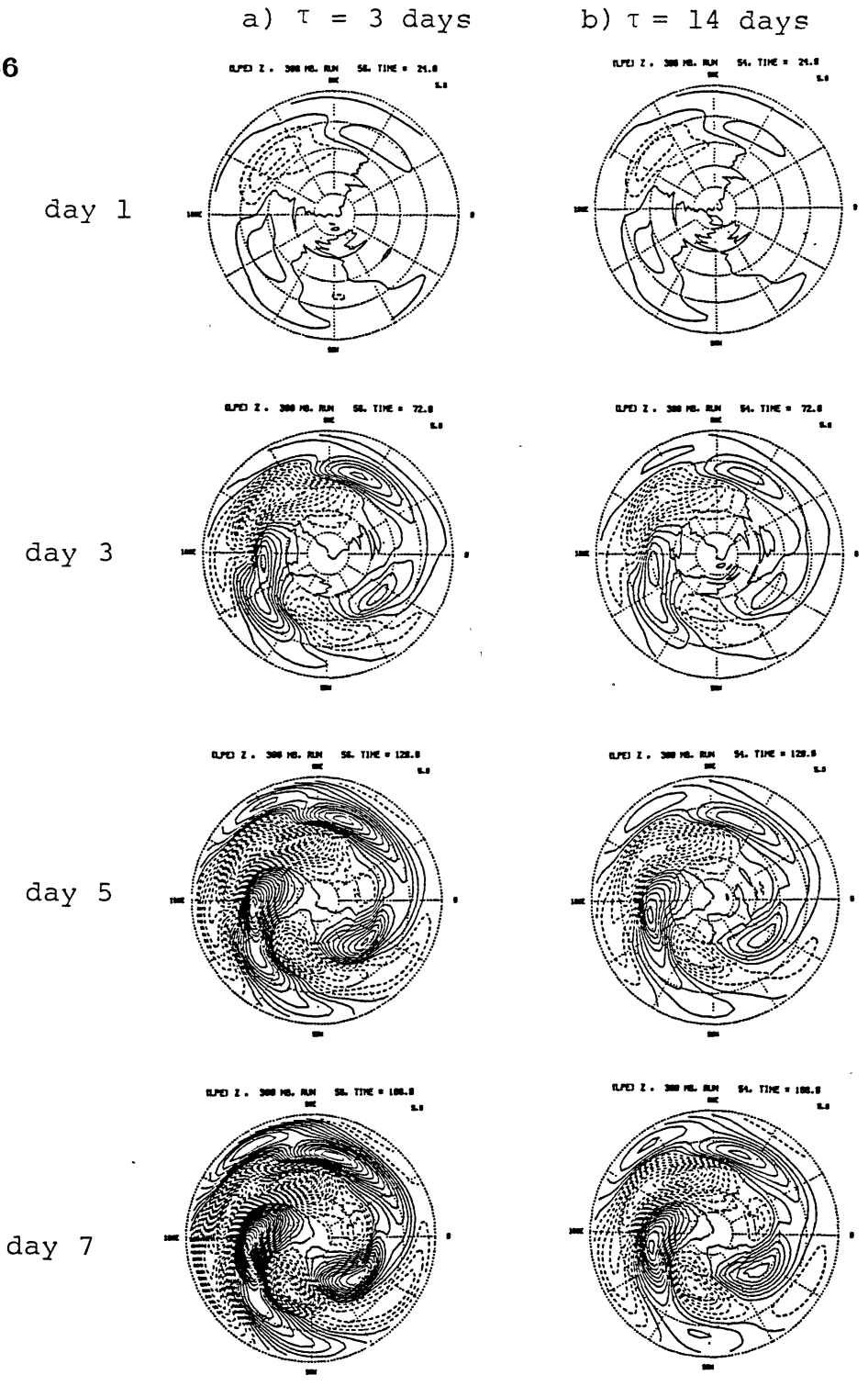

Figure 6.18: Time evolution of the anomaly field at 300mb for a) τ = 3 days and b) τ = 14days. Fields are shown from day 1 to day 7, every 2 days. Contour interval is 5 meters; plotting convention is as in fig. 6.14.

6.5 Transients excited as adjustment of the stationary waves

In a traditional forced problem with dissipation, the term *transient* is used to designate those disturbances which preceded the establishment of the forced steady solution. An unambiguous definition is only possible when the basic state does not vary in time. The experiments designed in this thesis are intended to circumvent this problem. Wind changes are allowed to occur in an interval τ, followed by a period of steady winds, where *transients* are analyzed. In the last section we clearly see the propagation of information from one point to another, consistent with the notion of group velocity in a dissipative medium. The difficulty of defining the transients in this case is purely technical. During the wind transition period we concentrated on the departures from the initial condition, and through comparison with the difference in stationary solutions, we implicitly analyzed the transients.

In this section we turn to consider the transients explicitly as in chapter 5. For $t > \tau$, transients are defined as the solution at time t minus the stationary solution computed with zonal wind 2. Notice that in the limit $t \to \infty$ the transients approach zero, provided no instabilities are present. In this limit, the second stationary solution would be fully established. The problem of practical interest is to determine how big t must be for this.

The control case

In fig. 6.19 we show the horizontal structure of the transients at 300mb, 150mb and 25mb, from day 7 to day 13. Notice that the contour interval used in this figure is 20 meters, and not 5 meters as in the previous section. By day 7, the transients are reminiscent of the difference in stationary solution (fig. 6.5). Notice that the transient centers are located slightly eastward of the same centers in the difference in stationary solutions. This signature was also seen in the previous section in the anomaly field. The amplitudes are about 60% of the difference in stationary solution, but are centers are slightly displaced northward. The time evolution of the transients is marked by a slow eastward/northward displacement, with amplitudes decaying in time. A simple inspection indicates that this very low phase speed is consistent with the scale of the disturbances, through the classical Rossby wave formula $c = U_o - \beta/(k^2+l^2)$. The amplitude decay follows a simply e^{-at} law, where a is an averaged Rayleigh damping coefficient. Notice that there is no sign of disturbances propagating westward, which is consistent with the absence of Rossby waves to be reported below.

The zonal-height cross section of the transients is shown in fig. 6.20. Comparison with fig. 6.6 again shows a similarity with the difference in stationary solutions with individual features slightly shifted eastward. The decay of the transients in all levels is as inferred from the horizontal structure.

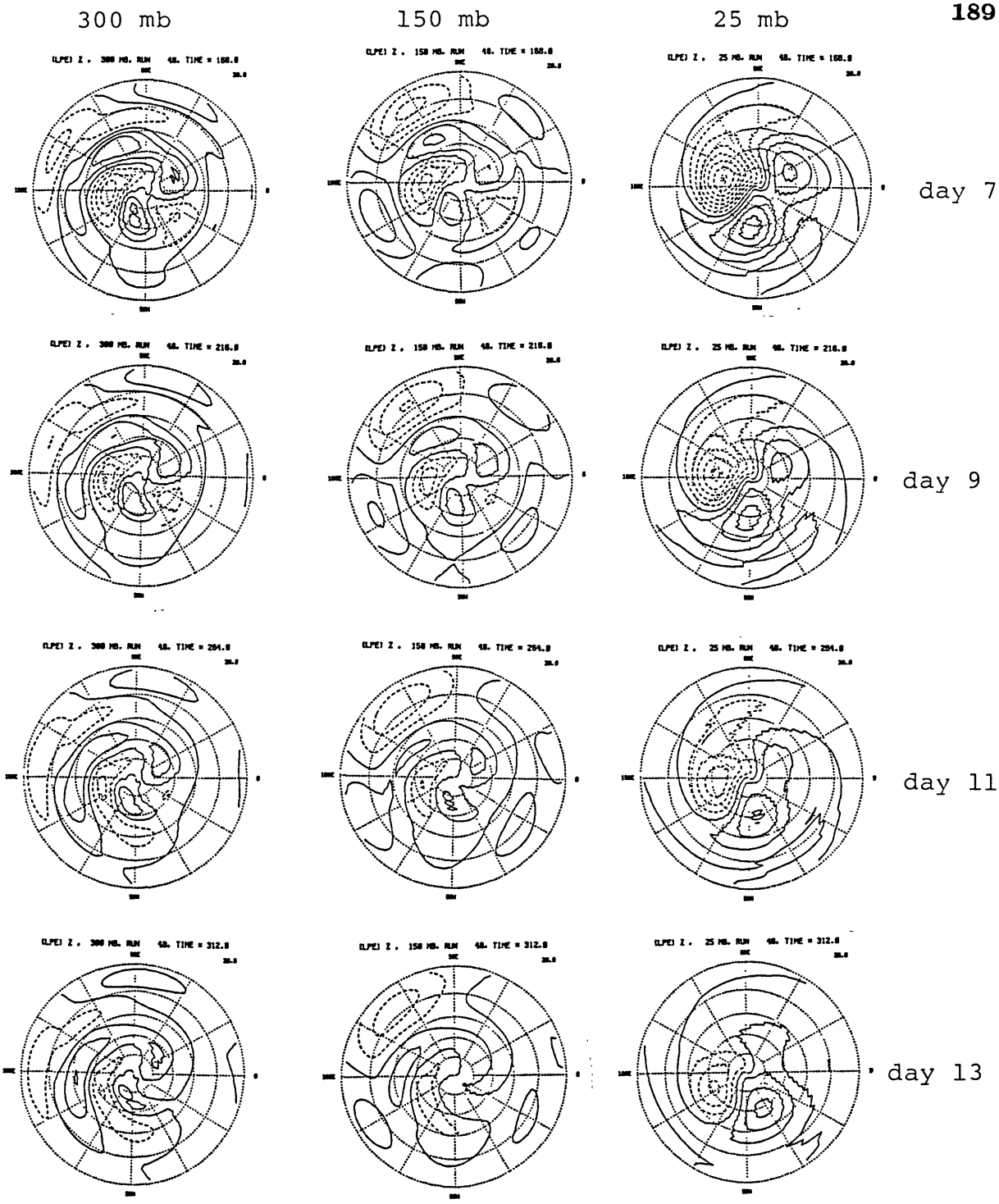

Figure 6.19: As in fig. 6.14 but for the horizontal structure of transients from day 7 to day 13, every 2 days. The contour interval is 20 meters.

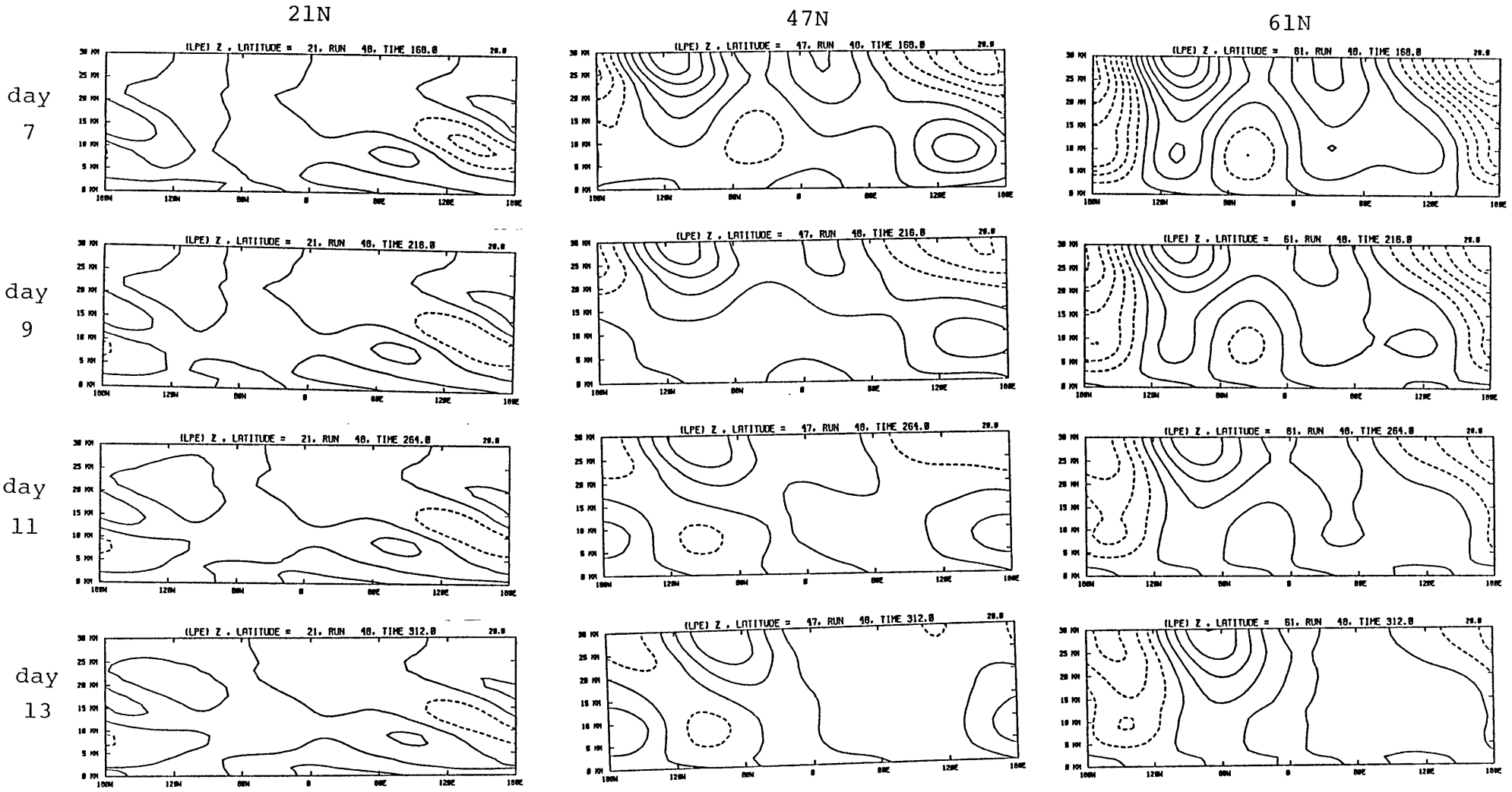

Figure 6.20: As in fig. 6.14 but for the vertical structure of transients from day 7 to day 13, every 2 days. The contour interval is 20 meters.

Dependence on transition period and dissipation

As suggested by the simple theory of chapter 3, there are 2 parameters determining the nature of the transients[13]. They are the disturbance period and the damping time scale, both normalized by the transition period. The disturbance *phase speed* accounts for the effects of propagation during the adjustment process. For example, chances are that for transition periods matching half the wave period destructive interference will likely occur; however, this effect depends strongly on the particular way the wind shift occurs. The effect of dissipation is straightforward: transients are dissipated as they are produced. For the cases considered here, the observed wave periods are in the range [80,200] days, which normalized by τ fall in [5,65]. Accordingly to the theory of chapter 3 (see fig. 3.2), dissipation will be the major player in determining the amplitude of transients right after the wind shift takes place.

In order to illustrate this dependence on the ratio dissipation / transition period we show in fig. 6.21 a scatter diagram of the observed *transient efficiency*, along with the dissipative limit of the transient efficient function (ξ, eq. 3.49) deduced in chapter 3. The observed transient efficiency is determined as follows. For each of the runs, we visually inspect the 300mb/150mb contour plots of the transients at

[13]Recall that in chapter 3 we implicitly neglect instabilities, which fortunately are not relevant here.

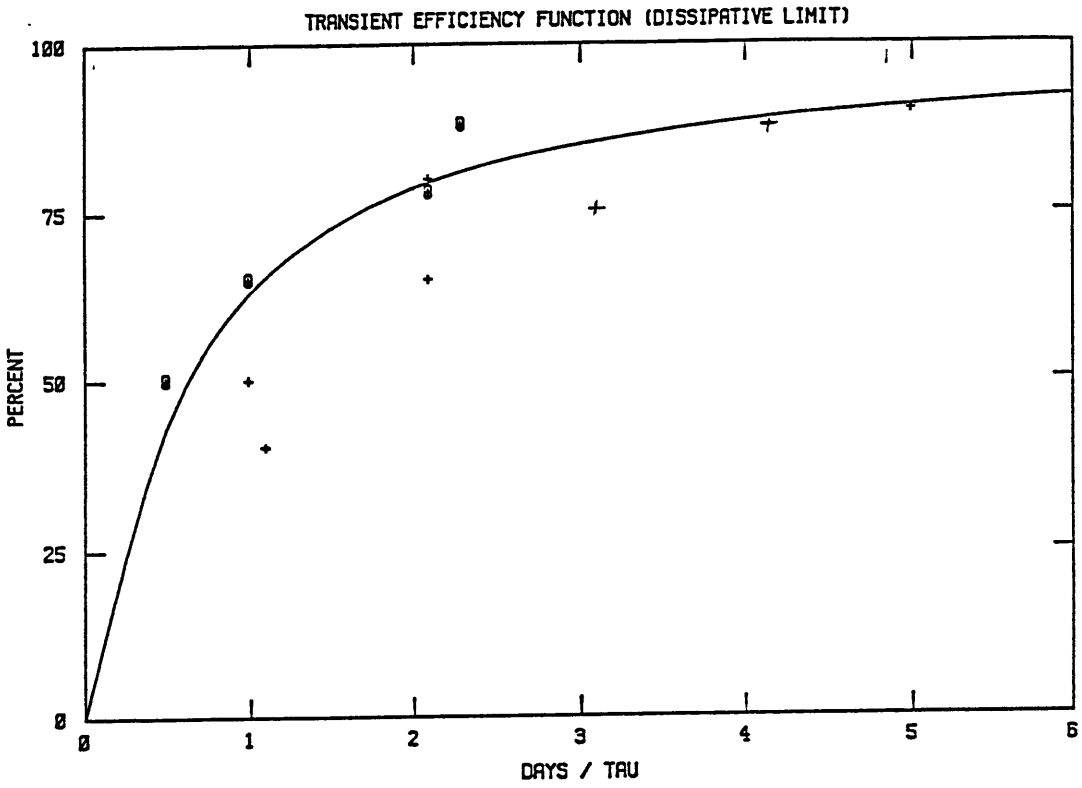

Figure 6.21:: Transient efficiency function: comparison of the theory with the results of the baroclinic model. The solid curve is the theoretically predicted transient efficiency function (eq. ??). The "+" correspond to the transient efficiency taken from the model for different combination of parameters. See text for more detail.

$t = \tau$ and by comparing with the corresponding difference in stationary solution, determine the ratio 100 * (transient amplitude) / (difference in stationary wave amplitude). Since linear damping is not constant all over the domain, the determination of the normalized damping parameter is not a trivial task. For all the cases shown we used the damping parameter at the location of the feature analyzed. This is expected underestimate the effective dissipation that acted on the transients. There are two groups of runs in fig. 6.21: the ones marked with crosses have boundary layer dissipation as in the standard case; the ones marked with circles have a reduced or absent boundary layer drag. The agreement with the theoretical curve is rather good, especially if one takes into account the fact that cases with boundary drag should have its abscissa decreased by 1 or 2 units.

On the excitation of Ultralong Rossby waves

We end this section with a few words about the excitation of transient ultralong Rossby waves, which was the focus of the barotropic calculation (chapter 5). As is apparent from the time evolution of transients, there is no signature of westward propagating disturbances. This is confirmed by the plots of the Rossby wave amplitude and phase shown in fig. 6.22 for the control case. The (u,v,z) fields used for the Hough function expansion are obtained as a tropospheric average, weighted by the external structure $p^{-\kappa}$ (see chapter 4 for details). As mentioned in

section 6.3 the stationary wave difference field projection onto Rossby modes are much smaller than in the barotropic case. The only mode with significant projection is the 16-day wave with zonal wavenumber 3, and even then amplitudes are about 1/3 of those in the barotropic model. All 9 modes showed virtually no sign of westward propagation[14]. After day 7 (end of the transition period) amplitudes are smaller than 20 meters. This suggests that the transient field is mostly composed of the continuum modes; the projection onto ultralong Rossby modes is due to the loss of orthogonality associated with shear in the zonal flow (Held, 1985; Farrell, 1988).

The absence of Rossby wave propagation is not particular to the control case. In a wide range of transition parameters, dissipation and subtropical wind changes the same behavior was observed. The main differences from the barotropic model is the structure of the stationary wave difference field, which is mainly determined by the wind changes and the possibility of vertical propagation. As we have seen, during the transition period (control case) transients are associated with the establishment of the new stationary wave. This is characterized by zonal, meridional as well as vertical propagation. These features are very distinct from the global westward propagating Rossby waves. After this establishment period, the transients are generally small and no regular westward propagation is observed.

[14]Recall that only after day 7 transients have a precise definition.

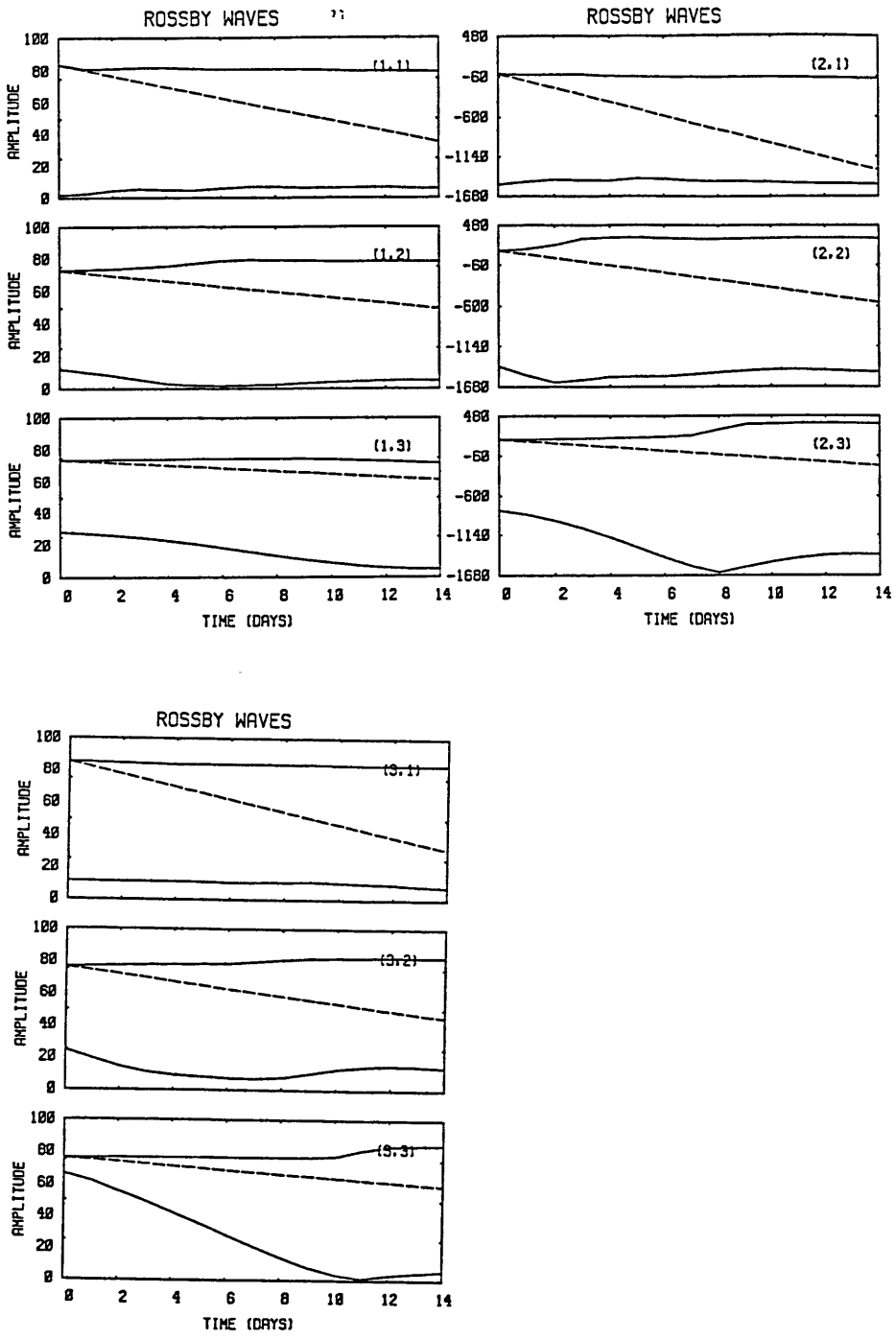

Figure 6.22: Amplitude and phase of ultralong Rossby waves as a function of time (control case).

The possibility of Rossby wave excitation with different wind changes has not been thoroughly investigated in this thesis. The wind changes in the subtropics, as considered in this chapter, is very efficient generating changes in stationary waves in mid- and high-latitudes, but not the ultralong waves. As hinted by the barotropic calculation, zonal wind changes in the tropics may generate large scale stationary wave changes in these latitudes which indeed can excite the ultralong waves. This hypothesis can be tested by trial and error or, more generally, one can ask the question: *What are wind changes that optimally excite Ultralong Rossby waves?* Prescribing a change in stationary wave, one can solve the inverse problem for the best basic state. We will not attempt to do this here. It will constitute future research by the author.

6.6 Observed wind changes and dissipation

Having determined the model dependence on its basic parameters, a natural question is: *What is range of parameters relevant to the real atmosphere?* Wind changes as the one assumed here can happen in the interannual, interseasonal as well as in the synoptic time scale. We consider each one of these possibilities below.

Nigam and Lindzen (1989) showed plots of the departure of the monthly mean zonally averaged zonal wind during December 1980, 81,

82, 83, 84 and 85 from the December climatology for these 6 years. They concluded that the wind changes are as large as the perturbations they assumed in their model, which are enough to produce jet shifts as the ones considered here. Unfortunately, they did not show the corresponding stationary wave departure from the climatology for these 5 years. If the mechanism proposed is correct, this interannual wind anomaly should be accompanied by changes in stationary waves of the order described here.

Fig. 6.23a (from Randel, 1989) shows the zonally averaged zonal wind at 300mb as a function of latitude and time of the year. We see that the from September to December the subtropical jet shifts almost 10 degrees equatorward. For reference, in fig. 6.23b,c we show the observed stationary waves[15] for zonal wavenumber 1 and 2, at 300mb. It is apparent that an increase in wave amplitude follows the jet shift, which also coincides with the advance of Winter. The zonal wavenumber 1 amplitude shifts equatorward as Winter approaches while zonal wavenumber 2 shows little sign of meridional propagation. Since significant wind changes associated with the Polar Night jet are also occurring in this time scale, a direct comparison with our results is not particularly meaningful.

As an example of wind changes in the synoptic time scale, we present

[15]Randel (1989) computes the observed stationary wave as a 30 day running mean.

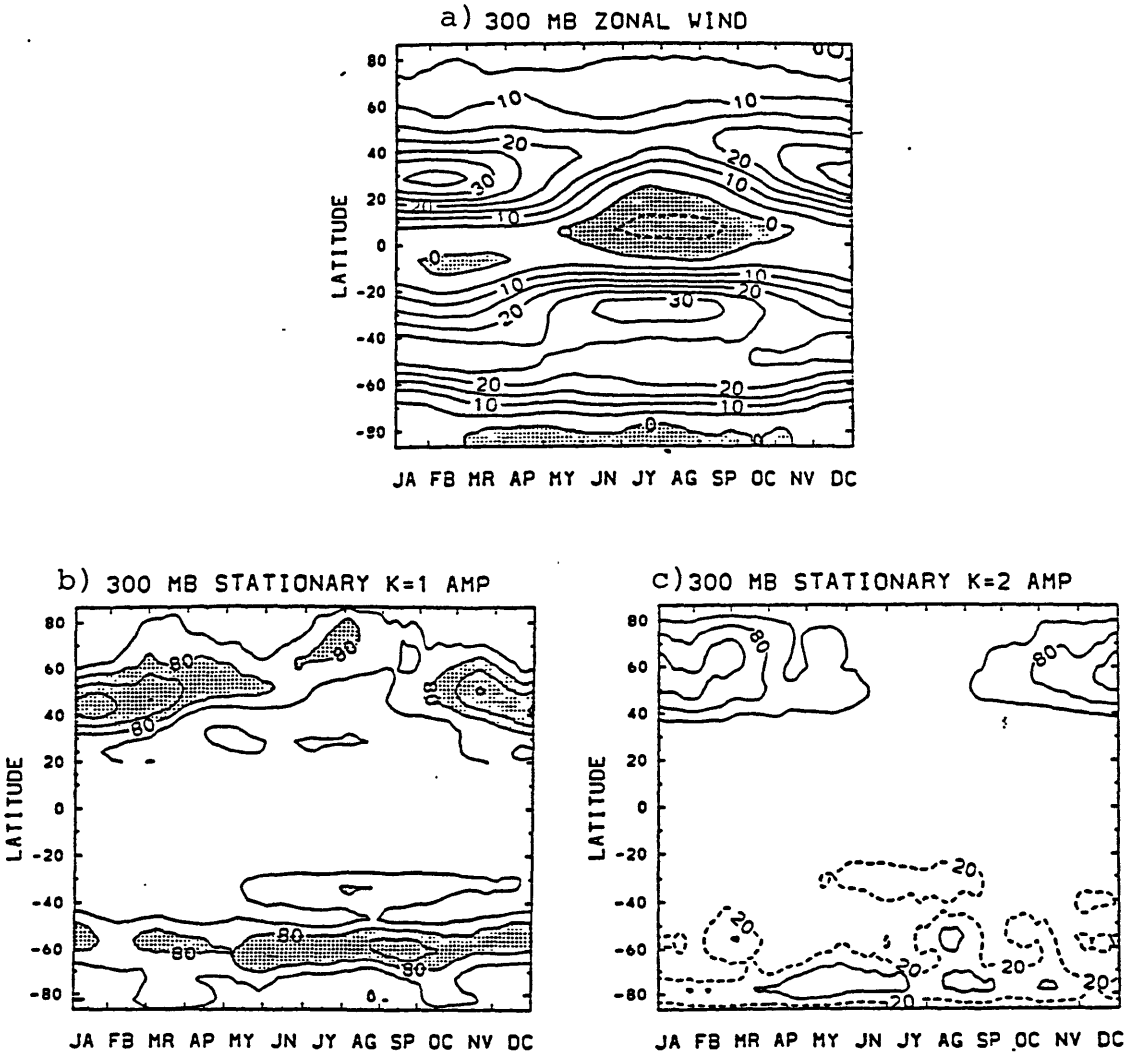

Figure 6.23: a) annual variation of the zonal wind at 300mb; amplitude of stationary waves at 300mb as a function of the month of the year: b) zonal wavenumber 1, and c) zonal wavenumber . From Randel, 1989.

in fig. 6.24 the zonally averaged zonal wind, from January 9 to January 13, 1979, computed from the FGGE IIIb level data set prepared by the ECMWF (Bengstsson et al., 1982). In this period of 5 days the zonal wind shifts about 7 degrees northward, contrary to the trend in the northern hemisphere Winter. In this particular month, from January 1 to 31, the subtropical jet shifts about 3 degrees equatorward. It should be noted that zonal wind measurements at the jet stream level are more susceptible to errors, and daily values such as the ones showed here should be considered with some caution.

The determination of the causes for wind changes is often a difficult task. In some events the alteration of the zonally averaged zonal wind may not be independent of the changes in wave activity. For example, it has been suggested (e.g. Weickmann et al., 1985; Lau et al., 1987) that fluctuations in convection in the tropics, most notably over the maritime continent, are accompanied by changes in zonal wind in the subtropics, near the eastern coast of Asia. Such wind changes conceivably would affect the stationary waves excited by the Tibetan plateau by a mechanism similar to the one presented here. However, in this situation the partition zonal mean and waves (departures from zonal mean) is inappropriate: the local flow alteration induced by convection has a zonal mean and a wave component as well, which are not independent. In fact, from the results of this section, one should expect changes in stationary waves only downstream of this local wind

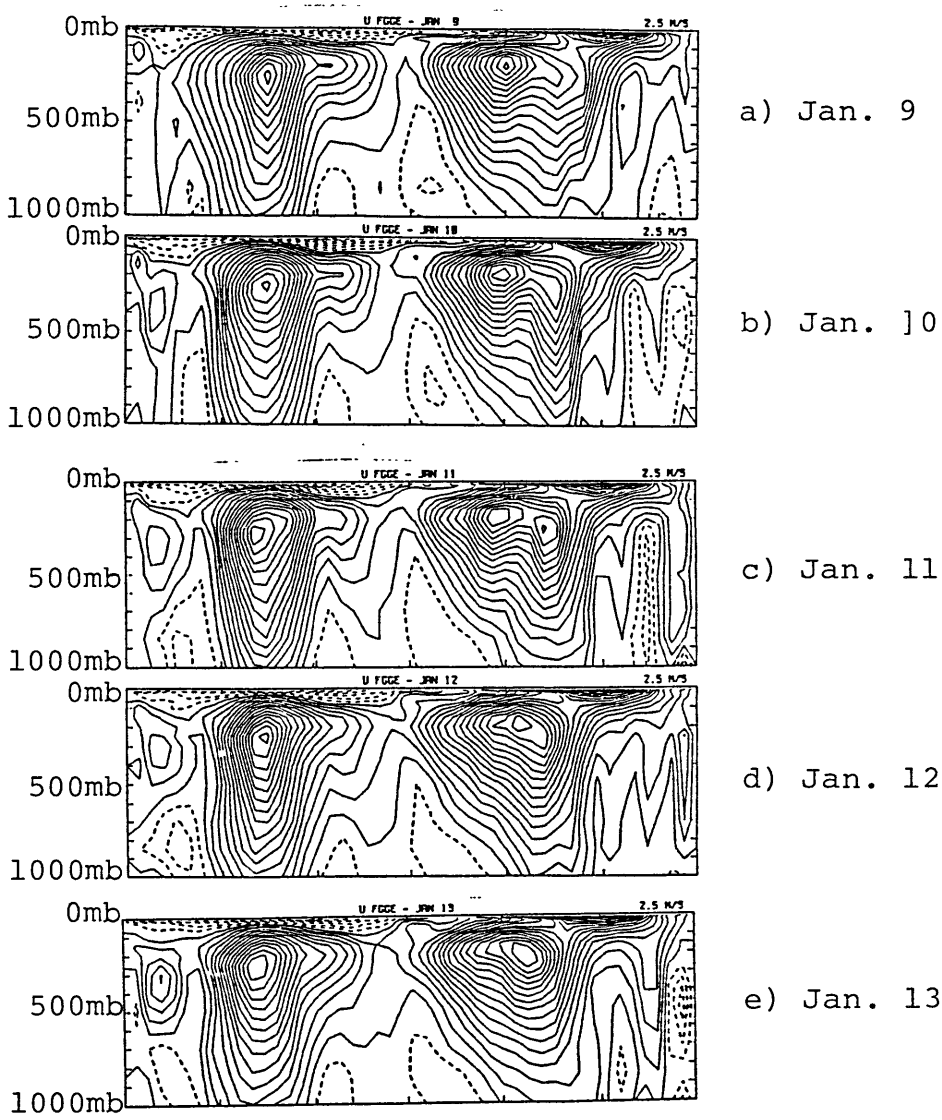

Figure 6.24: Observed meridional height cross-section of the zonally average zonal wind from January 9 to January 13, 1979. Computed from the FGGE IIIb dataset.

change[16]. We return to this problem when we compare our results to Dole's persistent anomalies.

While, even though crudely, we can make an assessment of the transition periods relevant to the atmosphere, the problem is not so simple for the dissipation parameters. To be sure, damping must be included in stationary models in order to make the problem mathematically well defined. The common rational for the introduction of this dissipation is as a crude parameterization of the transient eddies effects as well as the wind drag at the surface, necessary to the global angular momentum balance. Values of Rayleigh friction at the interior is generally taken from 5 days (in the tropics) to 30 days (in mid- and high-latitudes). The boundary layer drag is generally taken to be about 1 or 2 days. The plausibility of these parameters is assessed through comparison of the model simulation with the observed waves. Due to all the other uncertainties involved, this assessment is a very delicate, if not impossible, task.

From the above discussion, it seems that the best we can do is to estimate a broad range of the parameters relevant to the atmosphere. Crudely, we estimate that values of the normalized damping time scale above 1 are not unlikely. The corresponding transient efficiency is 50% and up (see fig. 6.21).

[16]Recall that information propagates with the group velocity which is mostly eastward for stationary Rossby waves.

6.7 Application to persistent anomalies

In this section we explore the potential of changes in the subtropical jet to explain some of the features of Dole's (1982) persistent anomalies in the northern hemisphere Winter. When the jet is displaced from its climatological position, and establishment of a new stationary solution occurs, a subsequent departure from the wave climatology should follow. This will be the perspective adopted here: we will regard the *anomaly field* discussed above as a departure from *climatology* and compare the results with Dole's (1982) PAC persistent anomaly cases. The fact that wind 1 is not exactly the climatological wind is of minor importance, as we only concentrate on qualitative features. Also, the observed anomalies include the zonal component as well as other wave numbers. Nevertheless, for the PAC cases to be considered here the dominant zonal wavenumbers are 1, 2, 3, 4 and 5. Because stationary waves with zonal wavenumber greater than 3 are very small, the control case includes only the 3 first wavenumbers.

Dole's definition of persistent anomaly (PA) is very simple and intuitive. An anomaly is considered persistent at a particular point when it exceeds a threshold value for a sufficiently long time. Upon identifying key points for PA's, composites are made with respect to the first day an anomaly exceeds the threshold. There are three major regions of persistent anomaly activity: 1) the Pacific region (PAC), 50N,165W, 2)

the Atlantic region (ATL), 50N,20W and 3) the Northern Soviet Union (NSU), 60N,60E. For each region, there are positive and negative PA's, with a high degree of symmetry. In this section we will restrict ourselves to the positive PAC anomalies, since this region is downstream of the Himalayas and positive anomalies have sign consistent with a equatorward jet shift. The pictures shown below uses a threshold of 100 meters for at least 10 days.

In fig. 6.25 we show time composites of low-pass filtered anomalies at 500 mb for 15 PAC positive cases from day -4 to day +6. Comparing with fig. 6.5 of this chapter we notice the following:

- Observed amplitudes are greater than what could be expected from changes in stationary solution (about a factor of 2).

- By day +6, when the anomaly is fully established, the horizontal pattern at 500mb bears some resemblance with the difference in stationary solutions at 300mb (see fig. 6.5 with signs reversed). The most striking difference is the almost total absence of disturbances upstream of the main center (50N, 165W). The observed anomalies have their maxima slightly to the south. This may be associated with the fact that the field shown in Dole's is the geopotential height normalized by the factor sin 45° / sin ϕ. For this case, there are more similarities between the PA's in 500mb and the difference in stationary solution at 150mb, in particular

the dipolar structures.

- The time evolution of the observed anomalies has much in common with the time evolution of the model anomalies. Developments subsequent to day zero are marked by downstream amplification of the centers, with virtually no phase propagation. As noted before, this behavior is characteristic of stationary Rossby wave energy dispersion on the sphere as in Hoskins and Karoly (1982).

The zonal-cross section for the unfiltered positive PAC anomalies is shown in fig. 6.26, from day -3 to day 0, at 45N and 20N. The main points to be noted are:

- Comparing the observed anomalies at day 0 with the difference in stationary solution (fig. 6.6 with signs changed) we first notice that the observed anomaly at 20N has a much more localized structure. The upstream positive feature present in the model anomalies does not have an equivalent in this observation, and the negative feature is placed more to the west. However they peak approximately at the same height (250-300mb). At 45N the same relationship between model and observation is also present. The lack of confinment of the model anomalies is hardly surprising with this zonal trucation (3 zonal wavenumbers). Also, due to the Dole's technique there is a tendency for the composite anomalies

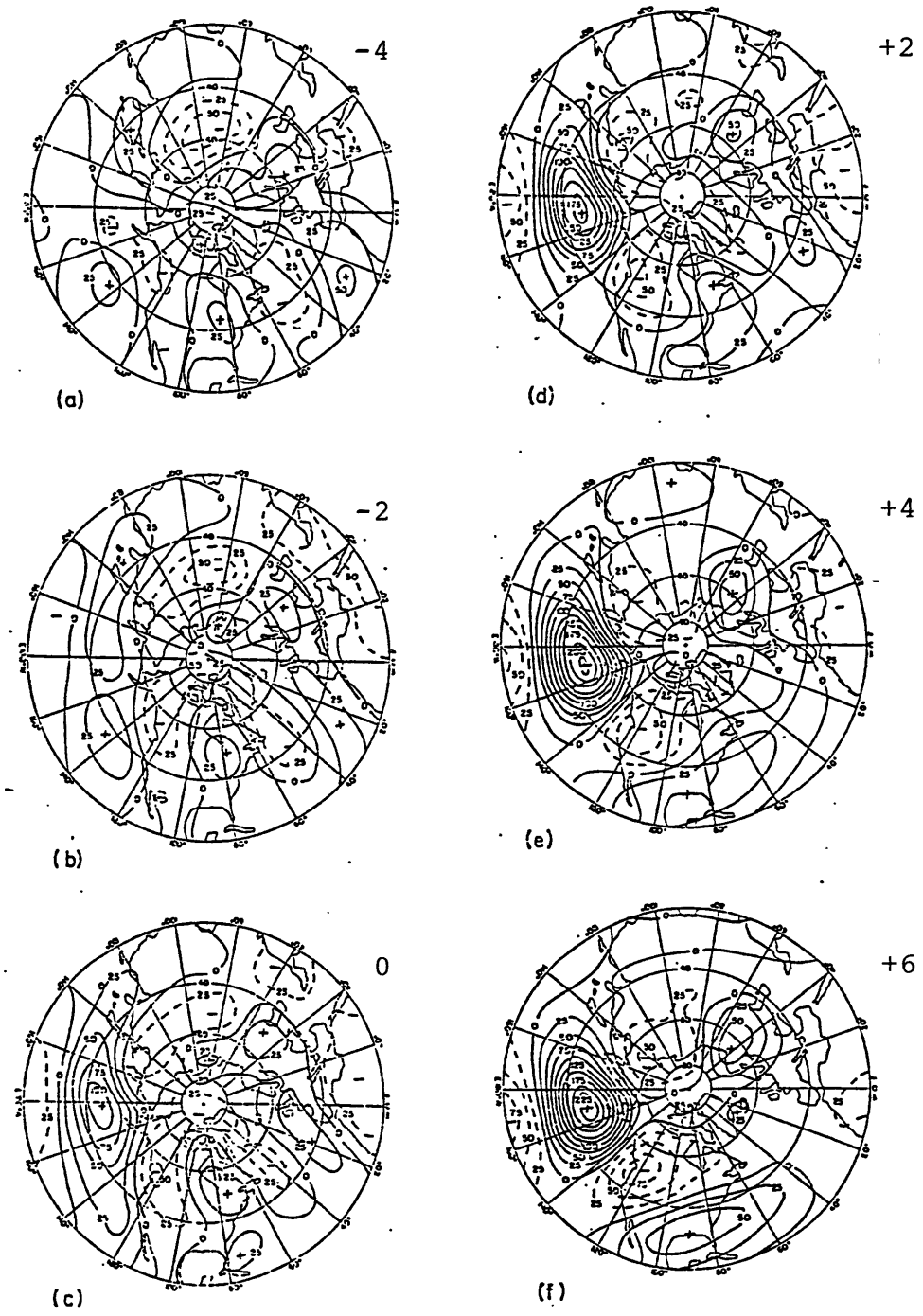

Figure 6.25: Composite persistent anomaly evolution for the PAC positive case at 500 mb: a) day -4, b) day -2, c) day 0, d) day +2, e) day +4, and f) day +6 (from Dole, 1982).

to be more confined than the individual cases (Dole, personal communication).

- Prior to onset, at 45N the observed anomalies have indication of a less localized feature. Westward tilts are apparent by day -3 and slowly decrease as day 0 approaches. The evolution of the model anomaly (fig. 6.16) also shows a slight tilt reduction as establishment takes place.

- Since Dole (1982) shows only anomalies below 100mb it is hard to determine whether or not propagation to the stratosphere is occurring. As hinted by the model calculations, vertical propagation can happen even when the tropospheric structure of the disturbance has an almost equivalent barotropic structure. Propagation is possible right above the tropopause where westward tilts do occur.

From the above discussion it is clear that, at least for the 100 meter threshold, the adjustment of the stationary solution cannot account for the whole persistent anomaly field. However, there are some similarities between the evolution of model and observed anomalies that suggests that perhaps there are some common mechanisms.

Perhaps the most serious limitation of our model when compared with the persistent anomalies of Dole is the fact that our basic state is the zonally averaged zonal wind. With this kind of basic state, the

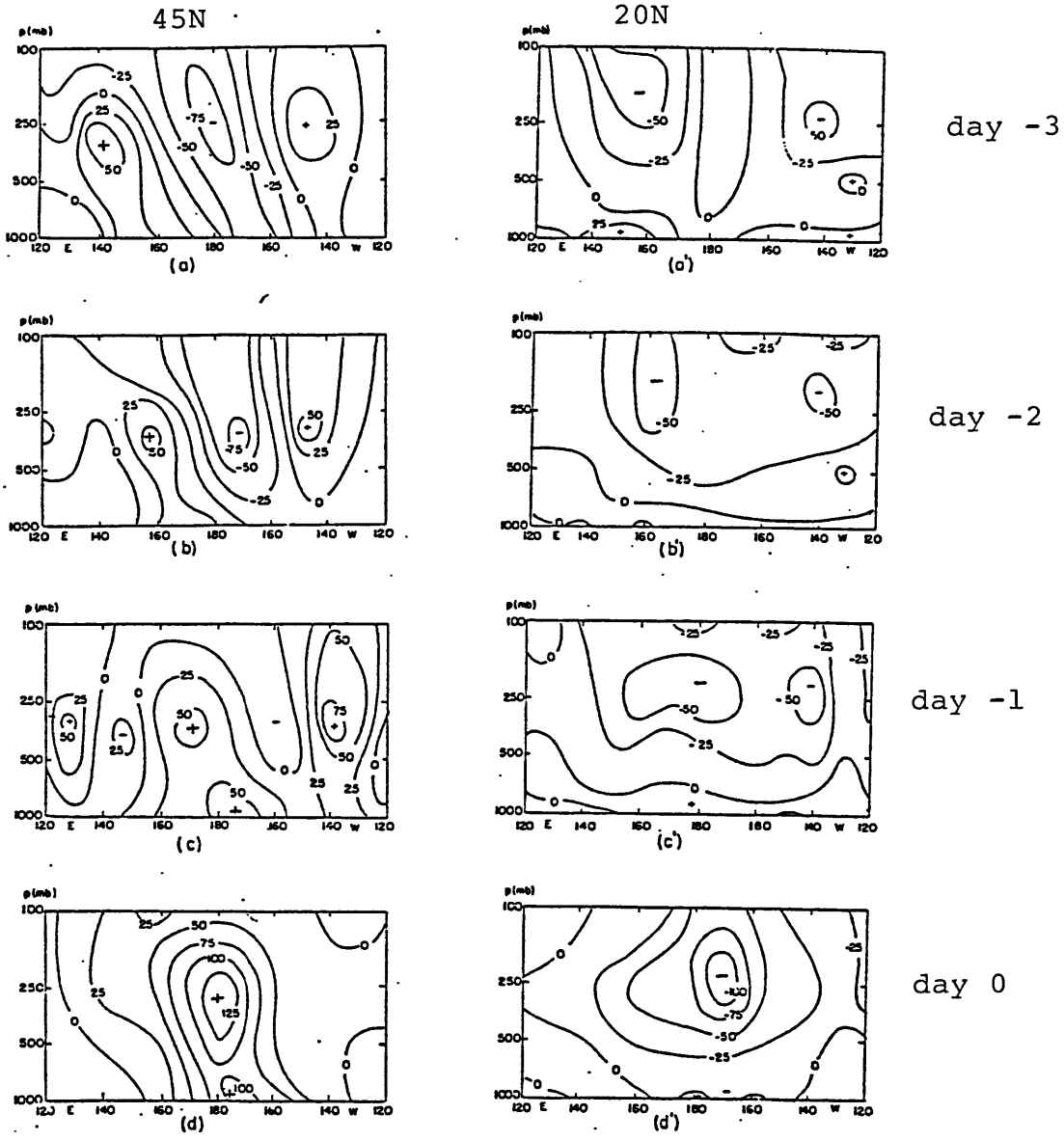

Figure 6.26: Longitude-height cross-section of the composite persistent anomaly evolution for the PAC positive case, at 45N and 20N: a) day -3, b) day -2, c) day -1, and d) day 0 (from Dole, 1982).

changes in stationary wave occur necessary in all longitudes. As mentioned in the last section, there is indication (Weickmann et.al, 1985; Lau et al., 1985) that fluctuation in convection in the maritime continent is accompanied by changes in the flow in the eastern coast of Asia. For such a localized wind change, in the light of the results of this chapter, one expects that changes in stationary waves would occur only downstream of the region where the wind is changing. Preliminary observational work by Black (1989, personal communication) suggests anomalous zonal wind in the eastern coast of Asia prior to the development of the Pacific cases; anomalies in the zonally averaged mean flow are too small to affect the stationary waves in any significant way.

One result that emerges from our calculation is the possibility that the anomalies have a stratospheric continuation. At present there is no available observation of this extension. Such work would help sort out some of the existing theories. Strictly localized theories like modons (McWilliamns,1980) or coherent stationary structures (Malguzzi and Malanotte Rizzoli, 1985a,b,1987) do not predict any significant stratospheric extension.

6.8 Summary and concluding remarks

In this chapter we have extensively examined the effects of wind changes in the subtropics. Concerning the sensitivity of the stationary waves to

such changes we found:

- Shifts in the subtropical jet of only a few degrees ($\approx 5^o$) can produce changes in the topographically forced stationary waves of 120 meters. This difference field is a large scale feature, mainly concentrated downstream of the Tibetan plateau and extending up to Europe. As in Nigam and Lindzen (1989), we find that shifting the jet equatorward increases the stationary wave response in mid- and high-latitudes, as well as in the stratosphere. Conversely, shifting the jet poleward decreases the wave amplitudes in these regions.

- In the subtropics (21N), stationary waves and differences are trapped in the troposphere. In mid-latitudes (47N), the *increased* stationary waves and the difference field reach a maximum amplitude in the troposphere, with very small westward tilts. However, tilts are pronounced above 15 km and there is clear continuation of these disturbances in the stratosphere. These tropospheric trapped disturbances are associated with short meridional scales. In high latitudes (60N), amplitudes have their maximum in the stratosphere and an almost equivalent barotropic structure.

- The sensitivity of thermally forced waves to changes in the subtropical jet is generally smaller than the sensitivity of topographically forced waves, at least in the troposphere. The difference

field has very short meridional scale, and little indication of propagation from the tropics. On the other hand, in the stratosphere the difference field associated with diabatic heating is of the same magnitude as its topographic counterpart. Because there is great uncertainty about the correct magnitude of the thermal forcing in mid latitudes, the exact importance of thermal forcing cannot yet be assessed accurately.

- Consistent with other studies (e.g. Nigam and Lindzen, 1989), in the troposphere the stationary waves downstream of the Tibetan plateau are very sensitive to boundary layer drag. Removing this dissipation altogether increases the amplitude by about 50% in the troposphere; the sensitivity is reduced in the stratosphere. The doubling of Rayleigh damping has the effect of reducing the amplitudes to 80% of their original value, both in the troposphere and in the stratosphere. Critical line dissipation was found to have a negligible effect on our results. For all cases, dissipation leaves the phase of the disturbances pretty much unchanged.

- Dipolar changes of the subtropical jet as the one used in the control run, have the effect of causing a wave train split when the jet is in its equator-most position. This behavior is robust to changes in the amplitude of this dipole, and even to removal of part of the dipole (i.e. monopole change of fig. 6.11b.) This jet split does not fully occur for wind changes in the form of a broad dipole. This is not surprising since wind curvature is the

dominant factor entering the index of refraction definition (see discussion in the end of section 6.3.)

- For this particular zonal wind change, the projection of the difference field in Rossby waves is much smaller than that found with the barotropic model. Thus, Rossby wave excitation is not likely in the time dependent model. The only candidate for excitation is the 16-day wave associated with zonal wavenumber 3. Recall that the subtropical wind shift was chosen because it is the *optimal* wind change that affects stationary waves in mid and high latitudes. As we have seen, this is not the optimal wind change to excite Rossby waves. A search for the best wind change for Rossby wave generation has not been attempted here.

When the wind is allowed to change in a finite time interval, there is a lag until the new stationary solution is established. The main points emerging from this study are:

- The stationary and time dependent models are fairly compatible and instabilities are not likely to play any role in the experiments described here.

- In the troposphere, the effect of changing the subtropical jet is first noted right downstream of the Himalayas and subsequently this *information* propagates eastward and northward. This be-

havior is the same we would get if a vorticity source were specified at the Himalayan region with the wind kept constant. In the stratosphere, the new stationary waves appear to be established without sign of horizontal propagation from the Tibetan plateau. It is indeed indicative of propagation from below.

- The establishment of the new stationary solution is pretty much restricted to lower levels in the first days, and mostly to longitudes just downstream of the Tibetan plateau. This period is followed by vertical propagation. Upward propagation is well defined in the control case (wind shifting equatorward). In the anti-control case (wind shifting poleward), propagation to the stratosphere ceases slowly, leaving the establishment of the new stationary solution there to be dictated by the local dissipation there.

- The transition period does not affect the establishment of stationary waves qualitatively. The parameter τ chiefly determines the rate in which stationary waves are generated; *information* propagates downstream with the group velocity of stationary Rossby waves, irrespective of the value of τ.

The spatial structure of the transients is reminiscent of the difference in the stationary solutions. The transients generated by shifts of the subtropical jet are quasi-stationary and there is no excitation of ultralong Rossby waves. The amplitude of the transients right after

the wind transition period agrees very well with the dissipative limit of the transient efficiency function of chapter 3; the controlling parameter is the ratio of the dissipative time scale by the transition period (τ).

There is a qualitative agreement between the time evolution of our *anomaly* field, and the anomaly field of Dole's(1982): both present features of stationary Rossby waves propagating downstream with the group velocity. The evolution of the vertical structure of the model anomalies also resembles observations: initially there is a eastward tilt with height which decreases as the anomalies evolve. In our model, for almost every tropospheric feature there is a stratospheric continuation. At the moment, there is no observation of Dole persistent anomalies above 100 mb.

Chapter 7

Conclusions

We have studied the evolution of stationary waves from one steady configuration to another. The changes in stationary waves were for the most part associated with changes in the medium (changes in the basic state) rather than changes in the forcing. We have determined the time scale for the establishment of the new stationary waves, the characteristics of their propagation and the transients excited in the process.

To accomplish this goal we used a barotropic and a baroclinic model. In the barotropic calculation we stressed wind changes that cause stationary wave changes of large meridional scales with some structure in the tropics, changes which are favorable for the excitation of ultra-long Rossby waves. In the baroclinic calculation we restricted ourselves to wind changes in the subtropics which have been shown by Nigam

and Lindzen (1989) to be very important for stationary waves in mid- and high-latitudes. For such changes, no excitation of Rossby waves was found. It remains to be seen which wind changes are optimal for excitation of Rossby waves in a baroclinic model.

Despite the limitations of the barotropic model, some aspects of the observed ultralong Rossby waves were present in the calculation. In particular, the dominance of the 16-day waves was suggested. This is simply because changes in stationary waves favor high meridional wavenumbers and wind transition periods of 10-15 days inhibit high meridional wavenumbers more than low meridional wavenumbers. It was also found that topography in the southern hemisphere did not have any impact on excitation of the waves.

Concerning the baroclinic model with wind changes in the subtropics, we found:

- Confirming the results of Nigam and Lindzen (1989), we have found that small changes in the subtropical jet (6 degrees) can cause changes in the stationary wave response of about 120 meters in the troposphere, and of about 200 meters in the stratosphere (25mb). Since our model has a lid at 10mb ($\approx$ 30 km) and a sponge layer from the top extending to about 25mb, it is not altogether clear whether we can trust our results at 25mb. However, Nigam and Lindzen (1989) with a top at 50km, found

stationary wave changes of about 280 meters at 10mb, which is fairly consistent with our results.

- For an equatorward shift of the subtropical jet of only about 6 degrees, occurring in a period of seven days, about 85% of the new stationary wave is already established by the end of the wind transition period. Because of this fast establishment time scale, it is meaningful to regard the steady state stationary waves as actual realizations of the atmosphere. The establishment of the new stationary solution associated with a northward shift of the subtropical jet occurs on a longer time scale in the stratosphere. Due to the reduction in vertical propagation, dissipation rather than Rossby wave propagation determines the time scale for the establishment of the new steady solution.

- The establishment of the new stationary solution is accomplished by horizontal and vertical energy propagation, consistent with tri-dimensional stationary Rossby wave dispersion on the sphere. This characteristic is not dependent on the basic state transition period, which chiefly determines the rate at which stationary waves are being generated.

- After the transition period, transients are always present. Because of the short meridional scale these transients are quasi-stationary and their amplitude at the end of the transition period is mainly determined by dissipation. The dissipative limit of

the transient efficiency function derived in chapter 3 (eq. 3.50) provided a good estimate for the transient amplitudes.

- Comparison of our anomaly field (see section 6.4) with the persistent anomaly composites of Dole (1982) showed many features in common. There is a similar vertical structure in the troposphere[1] and in both studies the time scale for energy propagation is consistent with tri-dimensional stationary Rossby wave dispersion. However, the horizontal structure of our change in stationary waves are global, in contrast to Dole's Pacific cases where anomalies are present only downstream of 180E. The global extension of our response is related to the wind changes considered: for changes in a zonally average basic state, stationary wave changes are expected in all longitudes. In the spirit of the mechanism described here, one can envisage that localized wind changes would behave as localized *diverter* and produce anomalies (stationary wave changes) only downstream of this region[2]. The cooperative effect of the waves themselves on the medium in which they propagate is beyond the scope of this thesis.

Regarding the excitation of ultralong Rossby waves the results of this thesis are not conclusive. The absence of ultralong Rossby waves

[1]Recall that Dole's analysis does not cover the stratosphere.

[2]This notion is not without problems, as local wind changes can be associated with the anomalies themselves. This same criticism can be applied to the zonally averaged wind.

in the transients excited in the baroclinic model may have two causes. First, the wind changes considered (shift of the subtropical jet) produce changes in stationary waves with meridional scales too short to significantly project onto ultralong modes. Second, even for longer meridional scales, there is always the possibility of vertical propagation, implying that an idealized external structure may not capture all of the difference field. In order to address these questions one can formulate the problem in the following terms: *What is the optimal zonal wind change for generating transient ultralong Rossby waves?* This problem can be tackled by trial and error, or more systematically by solving the inverse problem: specifying a change in stationary waves one can then determine the best change in basic state (in a least square sense) that would produce such a change in stationary waves. This will be the subject of future research by the author.

The changes in stationary wave associated with a zonally symmetric basic state does not seem able to fully account for Dole's Pacific persistent anomaly cases. Besides, R. Black (1989, personal communication) has shown that the composite zonally averaged zonal wind during the onset of the Pacific cases is in fact much smaller than that assumed here for the control case. However, local changes of the zonal wind occurs at the eastern coast of Asia, and could possibly result in a split of the wave train excited by the Tibetan plateau. Such change in the wind could be related to fluctuations in convection over Indonesia as have been suggested by Weickmann et al. (1985). The effect

of local changes in wind in our model has not been investigated yet and will constitute an extension of the work presented in this thesis. Furthermore, a comprehensive modeling of these anomalies should include the effects of enhanced (reduced) convection associated with the development of the positive (negative) anomalies, the potential role of nonlinearities, especially the feedback of the waves on the basic state flow. Extension of Dole's analysis above 100mb would help to ascertain whether these anomalies propagate upwards as do stationary Rossby waves or whether they are confined to the troposphere. Within linear theory, there is no support for such tropospheric trapping.

Finally, observational work is needed to assess the role of shifts in the subtropical jet in the interannual variability of stationary waves. In particular, if most of this variability is associated with topographic forcing as this work suggests, one should be able to reproduce this variability with a stationary linear primitive equation model such as the one considered here.

Appendix A

List of Symbols

In this Appendix we present a list of the symbols used in this thesis. They are show by chapters, in order of appearence.

Chapter 3

(x, y)	horizontal geometric coordinates in the (zonal,meridional) directions
t	time
r	linear damping parameter
ψ	quasi-geostrophic streamfunction
f	Coriolis parameter, $f = 2\Omega \sin \phi$
β	meridional gradient of the planetary vorticity, $\beta = df/dy$

U	spatially uniform zonal wind
h_s	topographic height
F	right hand side forcing
(k,ℓ)	wavenumbers in the (x,y) directions
$A_{k\ell}$	streamfunction amplitude for wavenumbers (k,ℓ)
$f_{k\ell}$	forcing amplitude for wavenumbers (k,ℓ)
$\mathcal{L}$	a linear operator containing the dynamics of the system (for both barotropic vorticity eq. and general case)
A_T	amplitude of transients
A_S	amplitude of stationary solution
τ	transition period - time scale for the variation of the zonal flow
A_F	amplitude of the forced solution
$\mathcal{U}_o$	propagator associated with $\mathcal{L}$
c_o	Rossby wave phase speed with respect to the flow
ξ	transient efficiency function
I	identity operator
$\mathbf{x}$	a vector representing the independent variables
$\mathbf{W}$	a vector representing the dependent variables
$\mathbf{W_T}$	traveling component
$\mathbf{W_F}$	quasi-stationary component
$\mathbf{F}$	right-hand-side forcing
s	zonal wavenumber

ℓ	meridional wavenumber
$\mathbf{H}_s^\ell$	ultralong normal mode with (zonal,meridional) wavenumber (s, ℓ)
σ	frequency of the mode
α_n	spectral coefficients of the traveling component
β_n	spectral coefficients of the difference $\Delta \mathbf{W}_S$
ξ^{RW}	transient efficiency function for ultralong Rossby waves
ξ^{dissip}	dissipative limit of the transient efficiency function

Chapter 4

λ	longitude
ϕ	latitude
a	radius of the Earth
Ω	angular speed of rotation of the Earth
g	constant of gravity
U_o	basic state zonal wind
H_o	basic state geopotential height
u	pertubation zonal wind
v	pertubation meridional wind
h	pertubation geopotential height
h_T	thermal forcing

$\mathbf{A, B, C, D}$	matrices related to the linearized shallow water equations
$\Delta\lambda$	mesh size in the zonal direction
$\Delta\phi$	mesh size in the meridional direction
Δt	time step
c_p	specific heat at constant pressure
c_p	specific heat at constant volume
R	gas constant
κ	$= R/c_p$
p	pressure
p_{surf}	pressure at the surface (1013 mb)
p_{top}	pressure at the top of the model (10 mb)
Π	difference in pressure between the top and botton of the model, $\Pi = p_{surf} - p_{top}$
σ	vertical coordinate, $\sigma = (p - p_{top})/\Pi$
T	temperature
θ	potential temperature, $\theta = p^{-\kappa}T$
$\dot{\sigma}$	vertical velocity in σ-coordinates
Φ	geopotential height in σ-coordinates
γ	Newtonian cooling
r	Rayleigh friction
U_o	basic state zonal wind
V_o	basic state meridional wind
Θ_o	basic state potential temperature

$\dot{\Sigma}_o$	basic state vertical velocity
Φ_S	topographic height multiplied by the constant of gravity
H_o	scale height (not to be confused with the depth of the fluid in the shallow water model)
N	Brunt-Vaisala frequency

REFERENCES

AHLQUIST, J. E., 1985: Climatology of normal mode Rossby waves. J. Atmos. Sci., 42, 2059-2068.

———, 1982: Normal mode global Rossby waves: Theory and observations. J. Atmos. Sci., 39, 193-202.

ASSELIN, R.A., 1972: Frequency filter for time integrations. Mon. Wea. Rev., 100, 487-490.

AUGENBAUM, J.M., S.E. COHN, D.P. DEE, E. ISAACSON and D. MARCHESIN, 1985a: A Factored implicit scheme for numerical weather prediction. Comm. Pure Appl. Math., 38 , 503-517.

———, 1985b: A fully implicit scheme for global numerical weather prediction. Seventh Conference on Numerical Weather Prediction, Preprint volume, Amer. Meteor. Soc., Boston.

BENGTSSON, L., M. KANAMITSU, P. KALLBERG and S. UPPALA, 1982: FGGE 4-dimensional data assimilation at ECMWF. Bull. Amer. Meteor. Soc., 63, 29-43.

BRETHERTON, F.P., 1969: Lamb waves in a nearly isothermal atmosphere. Quart. J. Roy. Met. Soc., 95, 754-757.

CHARNEY, J.G. and J.G. DEVORE, 1979: Multiple flow equilibria in the atmosphere and blocking. J. Atmos. Sci., 36, 1205-1216.

CHARNEY,J.G. and P.G. DRAZIN, 1961: Propagation of planetary scale disturbances from the lower into the upper atmosphere. J. Geophys. Res., 66, 83-109.

CHARNEY, J.G. and A. ELIASSEN, 1949: A numerical method for predicting the perturbations of the middle latitude westerlies. Tellus, 1, 38-54.

CHEN, S.-C., and K.E. TRENBERTH, 1988: Orographically forced planetary waves in the northern hemisphere winter: Steady state model with wave- coupled lower boundary formation. J. Atmos. Sci., 45, 657-680.

———, 1988: Forced planetary waves in the northern hemisphere winter: wave-coupled orographic and thermal forcing. J. Atmos. Sci., 45, 682-704.

CODDINGTON, E.A. and N. LEVINSON, 1955: *Theory of Ordinary Differential Equations.* McGraw-Hill, New York.

COHN, S.E., D. DEE, E. ISAACSON, D. MARCHESIN and G. ZWAS, 1985: A Fully implicit scheme for the barotropic primitive equations. Mon. Wea. Rev., 113 , 436-448.

CRUTCHER, H.L. and J.M. MESERVE, 1970: Selected level heights, temperatures and dew points for the Northern Hemisphere. NAVAIR Atlas 50-IC-52, Chief Naval Operations, Washington, D.C. Available through Supt. of Documents, U.S. Govt. Printing Office, Washington, D.C.

DALEY, R., and D.L. WILLIAMSON, 1985: The existence of free Rossby waves during January 1979. J. Atmos. Sci., 42 , 2121-2141.

DA SILVA, A.M., and D.P. DEE, 1985: A subroutine package for computing Hough functions and spectral decomposition. Technical Report no. MAT/19/85, Dept. of Mathematics, PUC/RJ, Rio de Janeiro, CEP22453, BRAZIL.

DEE, D.P., and A.M. DA SILVA, 1986: Using Hough harmonics to validate and assess nonlinear shallow-water models. Mon. Wea. Rev., 114, 2191-2196.

DEROME, J., 1979: Some observations of middle latitude forced planetary waves. In *Dynamical Meteorology and Numerical Weather Prediction*, vol. 1, European Centre for Medium Range Weather Forecasts, 242 pp.

DICKINSON, R.E., 1968: A method of parameterization for infrared cooling between the altitudes of 30 and 70 kilometers. J. Geophys. Res., 78, 4451-4457.

DOLE, R.M., 1982: Persistent anomalies of the extratropical northern hemisphere wintertime circulation. PhD Dissertation, Massachusetts Institute of Technology, Cambridge, MA.

EDMON, H.J., B.J. HOSKINS and M.E. McINTYRE, 1980: Eliassen-Palm cross-sections for the troposphere. J. Atmos. Sci, 37, 2600-2616 and Corrigendum, J. Atmos. Sci., 38, 1115.

ELIASSEN, E., and B. MACHENHAUER, 1965: A study of the fluctuations of the atmospheric planetary flow patterns represented by spherical harmonics. Tellus, 21 , 149-165.

FARRELL, B., 1988: Optimal excitation of neutral Rossby waves. J. Atmos. Sci., 45, 163-172.

FREDERIKSEN, J. and P. J. WEBSTER, 1988: Alternative theories of atmospheric teleconnections and low-frequency fluctuations. To appear.

GARCIA, R.R., and J.E. GEISLER, 1981: Stochastic forcing of small-amplitude oscillations in the stratosphere. J. Atmos. Sci., 38, 2187-2197.

GARCIA, R.R. and M. SALBY, 1987: Transient response to localized episodic heating in the tropics. Part II: Far-field behavior. J.

Atmos. Sci., 44, 499-530.

GROSE, W.L. and B.J. HOSKINS, 1979: On the influence of orography on large-scale atmospheric flow. J. Atmos. Sci., 36, 223-234.

HAMILTON, 1985: A possible relationship between tropical ocean temperatures and the observed amplitude of atmospheric (1,1) Rossby normal mode. J. Geophys., 90 , 8071-8074.

———, 1986: General circulation model simulation of the structure and energetics of atmospheric normal modes, Tellus, ...

HANSEN, A.R. and A. SUTERA, 1984: A comparison of the spectral energy and enstrophy budgets of blocking versus nonblocking periods. Tellus, 36A, 52-63.

HALTINER, G.J. and R.T. WILLIAMS, 1980: *Numerical Prediction and Dynamic Meteorology*, second edition, John Wiley & Sons, New York, 477 pp.

HELD, I.M., 1983: Stationary and quasi-stationary eddies in the extratropical troposphere: theory. In *Large-Scale Dynamical Processes in the Atmosphere*, edited by B.J. Hoskins and R.P. Pearce, Academic Press, London.

———, 1985: Pseudomomentum and the orthogonality of modes in shear flows. J. Atmos. Sci., 42, 2280-2288.

HIROOKA, T., 1986: Influence of normal mode Rossby waves on the mean field: interference with quasi-stationary waves. J. Atmos. Sci., 43 , 2088-2097.

———, and I. HIROTA, 1985: Normal mode Rossby waves in the upper stratosphere. Part II: Second antisymmetric and symmetric modes of zonal wavenumber 1 and 2. J. Atmos. Sci., 42, 536-548.

HIROTA, J., 1971: Excitation of planetary Rossby waves in the winter stratosphere by periodic forcing. J. Met. Soc. Japan, 49, 439-448.

HOSKINS, B.J., and D.J. KAROLY, 1981: The steady linear response of a spherical atmosphere to thermal and orographic forcing. J. Atmos. Sci., 38, 1179-1196.

HOUGH, S., 1898: On the application of harmonic analysis to the dynamical theory of the tides, II. Philos. Trans. R. Soc. London, Ser. A, 191, 139-185.

JACQMIN, D., 1983: The causation and variability of the northern winter quasi-stationary planetary waves. PhD thesis, Harvard University, Cambridge, Mass., 177pp.

JACQMIN, D., and R.S. LINDZEN, 1985: The causation and sensitivity of the northern winter planetary waves. J. Atmos. Sci., 42 , 724-745.

JOHNSON, D.R., and M.-Y. WEI, 1984: The planetary distribution of heat sources and sinks during FGGE. Proc. of the first national

workshop on the Global Weather Experiment: Current Achievements and Future Directions, Vol. 2, Pt. 1, Woods Hole, National Academy of Sciences, 299-316.

JOHNSON, D.R., R.D. TOWNSEND and M.-Y. WEI, 1985: The thermally coupled response of the planetary scale circulation to the global distribution of heat sources and sinks. Tellus, 37A, 106-125.

KAROLY, D.J., and B.J. HOSKINS, 1982: Three dimensional propagation of planetary waves. J. Met. Soc. Japan, 109-122.

KASAHARA, A., 1980: Effect of zonal flows on the free oscillations of a barotropic atmosphere. J. Atmos. Sci., 37 , 917-29. Corrigendum, 1981, J. Atmos. Sci., 38 , 2284-2285.

LAMB, H., 1932: *Hydrodynamics.* 6th ed., Dover, New York.

LAU, N.-C., 1979: The observed structure of tropospheric stationary waves and local balances of vorticity and heat. J. Atmos. Sci., 36, 966-1016.

LAU, N.-C. and J.S. BOYLE, 1987: Tropical and extratropical forcing of the large-scale circulation: A diagnostic study. Mon. Wea. Rev., 115, 400-428.

LIN, B.-D., 1982: The behavior of winter stationary planetary waves forced by topography and diabatic heating. J. Atmos. Sci., 39, 1206-1226; Corrigendum. J. Atmos., Sci., 40, 2321.

LINDZEN, R.S., 1986: Stationary planetary waves, blocking, and interannual variability, in *Anomalous Atmospheric Flows and Blocking*, edited by R. Benzi, B. Saltzman and A. C. Wiin-Nielsen, Adv. in Geophys., vol. 29, Academic Press, Orlando, FL.

———, and D. BLAKE, 1972: Lamb waves in the presence of realistic distributions of temperature and dissipation. J. Geophys. Res., 77, 2166-2176.

———, B. FARRELL, and D. JACQMIN, 1982: Vacillations due to wave interference: applications to the atmosphere and to annulus experiments. J. Atmos. Sci., 39, 14-23.

———, D.M. STRAUS and B. KATZ, 1984: An observational study of large-scale atmospheric Rossby waves during FGGE. J. Atmos. Sci., 41, 1320-1335.

MADDEN, R.A., 1979: Observations of large-scale traveling waves. Rev. Geophys. Space Phys., 17, 1935-1949.

———, 1979: Observations of large scale traveling waves. Rev. Geophys. Space Phys., 17 , 1935-1949.

———, 1983: The effect of the interference of travelling and stationary waves on time variations of the large-scale circulation. J. Atmos. Sci., 40 , 1110-1125.

MALANOTTE-RIZOLLI, P. and P. HANCOCK, 1987: Coherent structures in a baroclinic atmosphere. Part IV: A comparison between

theory and data. J. Atmos. Sci., 44, 2506-2529.

MALGUZZI, P. and P. MALANOTTE-RIZZOLI, 1985a: Nonlinear stationary Rossby waves on nonuniform zonal winds and atmospheric blocking. Part I: The analytical theory. J. Atmos. Sci., 41, 2620-2628.

———, 1985b: Coherent structures in a baroclinic atmosphere. Part II: A truncated model approach. J. Atmos. Sci., 42, 2463-2477.

———, 1987: Coherent structures in a baroclinic atmosphere. Part III: Block formation and eddy forcing. J. Atmos. Sci., 44, 2493-2505.

McWillians, J. C., 1980: An application of equivalent modons to atmospheric blocking., Dyn. Atmos. Oceans, 5, 43-66.

MARCHESIN, D., 1984: Using exact solutions to develop an implicit scheme for the baroclinic primitive equations. Mon. Wea. Rev., 112 , 269-277.

MATSUNO, T., 1970: Vertical propagation of stationary planetary waves in the winter Northern Hemisphere.. J. Atmos. Sci., 27, 871-883.

MUENCH, H.S., 1965: On the structure and behavior of the planetary waves in winter. Proceedings of the (seventh) Stanstead Seminar on the middle atmosphere. Publication in meteorology no. 90, McGill University, 1-7.

NEWELL, R.E., J.W. KIDSON, D.G. VINCENT, and J.G. BOER, 1972: The general circulation of the tropical atmosphere and interactions with extratropical latitudes, 1, 258 pp.; 2, 371 pp. The M.I.T. Press, Cambridge, MA.

NIGAM, S., 1985: On the adequacy of meridional resolution of linear and quasi-linear linear barotropic models. J. Atmos. Sci., 2493-2505.

NIGAM, S., I.M. HELD and S.W. LYONS, 1986: Linear simulation of the stationary eddies in a GCM. Part I: The "No mountain" model. J. Atmos. Sci., 43, 2944-2961.

———, 1988: Linear simulation of the stationary eddies in a GCM. Part II: The "mountain" model. J. Atmos. Sci., 45, 1433-1452.

NIGAM, S. and R.S. LINDZEN, 1989: The sensitivity of stationary waves to variations in the basic state zonal flow. Submitted to J. Atmos. Sci.

PALMER, T., 1981: Diagnostic study of wavenumber 2 stratospheric sudden warming in transformed Eulerian mean formalism. J. Atmos. Sci., 38, 844-855.

PEIXOTO, J.,P., B. SALTZMAN and S. TWELES, 1964: Harmonic analysis of the topography along parallels of the earth. J. Geophys. Res., 69 , 1501.

PIERREHUMBERT, R.T., 1986: The effect of local baroclinic instability on zonal inhomogeneities of vorticity and temperature. in *Anomalous Atmospheric Flows and Blocking*, edited by R. Benzi, B. Saltzman and A.C. Wiin-Nielsen, Adv. in Geophys. vol. 29., Academic Press, Orlando, FL.

PLUMB, R.A., 1985: On the three-dimensional propagation of stationary waves. J. Atmos. Sci., 42, 217-229.

RANDEL, W.J., 1989: The seasonal evolution of planetary waves in the Southern Hemisphere stratosphere and troposphere. Submitted to Quart. J. of Roy. Met. Soc.

REED, M. and B. SIMON, 1975: *Methods of Modern Mathematical Physics, vol. II: Fourier Analysis, Self Adjointness.* Acad. Press, New York.

REX, D.F., 1950: Blocking action in the middle troposphere and its effects on regional climate. II. The climatology of blocking action. Tellus 2, 275-301.

ROSSBY et al., (1939): Relations between variations in the intensity of the zonal circulation of the atmosphere and the displacements of the semipermanent centers of action. J. Mar. Res., 2, 38-55.

SALBY, M.L., 1981a: Rossby normal modes in nonuniform background configuration. Part I: Simple fields. J. Atmos. Sci., 38 , 1803-26.

———, 1981b: Rossby normal modes in nonuniform background configuration. Part II: Equinox and solstice conditions. J. Atmos. Sci., 38 , 1827-1840.

———, 1984a: Survey of planetary-scale transient waves: the state of theory and observations. Rev. Geophys. Space Phys., 22 , 209-236.

———, 1984b: Transient disturbances in the stratosphere: implications for theory and observing systems. J. Atmos. Terr. Phys., 46 , 1009-1047.

——— and R. R. GARCIA, 1987: Transient response to localized episodic heating in the tropics. Part I: Excitation and short-time near-field behavior. J. Atmos. Sci., 44, 458-498.

SANKAR-RAO, M., 1965: Continental elevation influence on the stationary harmonics of the atmospheric motion. Pure Appl. Geophys., 60 , 141-159.

SIMMONS, A.J., J.M. WALLACE and G.W. Branstator, 1983: Barotropic wave propagation and instability, and atmospheric teleconnection patterns. J. Atmos. Sci., 40, 1363-1392.

STRAUS, D.M., R.S.LINDZEN. and A.M. DA SILVA, 1986: The characteristic Rossby frequency. J. Atmos. Sci., 44, 1100-1105.

TUNG, K.-K., 1979: A theory of stationary long waves. Part III: Quasi-normal modes in a singular waveguide. Mon. Wea. Rev.,

107, 751-774.

——— and R.S. LINDZEN, 1979: A theory of stationary long waves. Part I: A simple theory of blocking. Mon. Wea. Rev., 107, 714-734.

——— and R.S. LINDZEN, 1979: A theory of stationary long waves. Part II: Resonant Rossby waves in the presence of realistic vertical shears. Mon. Wea. Rev., 107, 736-750.

van LOON, H., and R.L. Jenne, 1973: Zonal harmonic standing waves. J. Geophys. Res., 78, 4463-4471.

WALLACE, J.M., 1983: The climatological mean stationary waves: Observational evidence. *Large-Scale Dynamical Processes in the Atmosphere*, B.J. Hoskins and R.P. Pearce, Eds., Academic Press, 27-53.

WALLACE, J.M. and D.S. GUTZLER, 1981: Teleconnections in the geopotential height field during the Northern Hemisphere winter. Mon. Wea. Rev., 109, 785-812.

WEICKMANN, K.M., G.R. LUSSKY and J.E. KUTZBACH, 1985: Intraseasonal (30-60 day) fluctuations of outgoing longwave radiation and 250 mb streamfunction during northern winter. Mon. Wea. Rev., 113, 941-961.